Strengthening RC T-beams in Flexure and Shear using New Mechanically-Anchored FRP and Dry Fibre Systems

Amir Mofidi

A Thesis

in

The Department

of

Building, Civil and Environmental Engineering

Presented in Partial Fulfillment of the Requirements

for the Degree of Master of Applied Science (Civil Engineering) at

CONCORDIA UNIVERSITY

Montréal, Québec, Canada

April 2008

© Amir Mofidi, 2008

Concordia University

Library and Archives Canada

Published Heritage Branch

395 Wellington Street
Ottawa ON K1A 0N4
Canada

Bibliothèque et Archives Canada

Direction du Patrimoine de l'édition

395, rue Wellington
Ottawa ON K1A 0N4
Canada

Your file Votre référence
ISBN: 978-0-494-40874-2
Our file Notre référence
ISBN: 978-0-494-40874-2

NOTICE:
The author has granted a non-exclusive license allowing Library and Archives Canada to reproduce, publish, archive, preserve, conserve, communicate to the public by telecommunication or on the Internet, loan, distribute and sell theses worldwide, for commercial or non-commercial purposes, in microform, paper, electronic and/or any other formats.

The author retains copyright ownership and moral rights in this thesis. Neither the thesis nor substantial extracts from it may be printed or otherwise reproduced without the author's permission.

AVIS:
L'auteur a accordé une licence non exclusive permettant à la Bibliothèque et Archives Canada de reproduire, publier, archiver, sauvegarder, conserver, transmettre au public par télécommunication ou par l'Internet, prêter, distribuer et vendre des thèses partout dans le monde, à des fins commerciales ou autres, sur support microforme, papier, électronique et/ou autres formats.

L'auteur conserve la propriété du droit d'auteur et des droits moraux qui protège cette thèse. Ni la thèse ni des extraits substantiels de celle-ci ne doivent être imprimés ou autrement reproduits sans son autorisation.

In compliance with the Canadian Privacy Act some supporting forms may have been removed from this thesis.

While these forms may be included in the document page count, their removal does not represent any loss of content from the thesis.

Conformément à la loi canadienne sur la protection de la vie privée, quelques formulaires secondaires ont été enlevés de cette thèse.

Bien que ces formulaires aient inclus dans la pagination, il n'y aura aucun contenu manquant.

Canada

ABSTRACT

Strengthening RC T-Beams in Flexure and Shear using New Mechanically-Anchored FRP and Dry Fibre Systems

Amir Mofidi

Current conventional strengthening of reinforced concrete (RC) beams using epoxy-bonded fibre-reinforced polymer (FRP) technique requires difficult surface preparation and is susceptible to a brittle form of failure due to peel-off or debonding of the FRP laminate from the beam. This research presents two new mechanically-anchored FRP and dry fibre strengthening systems that can be used to improve the performance of RC beams in flexure and shear, respectively. Unlike conventional FRP-strengthening methods, the proposed systems require less surface preparation and adhesive application, and eliminate peel-off and debonding of FRP sheets. In order to experimentally evaluate the effectiveness of the new strengthening systems, a total of seven half-scale RC T-beams were tested under four-point loading system up to failure.

Three RC T-beams were tested to evaluate the increase in shear capacity using a new FRP strengthening system. One beam was tested as a control beam. One beam was strengthened by using a U-shaped carbon FRP (CFRP) sheet that was externally bonded to the web of the beam. One beam was strengthened by using new anchored U-shaped dry carbon fibre (CF) sheet method. In this method, dry CF sheets are wrapped around and bonded to two steel rods. Then the rods are anchored to the corners of the web-flange intersection of the T-beam with mechanical bolts. The new method relies on utilizing the full mechanical contribution of the dry CF sheets, which will be activated upon development of strain in the RC web, and transferring them through a longitudinal steel rod to the core of the compression web-flange zone by means of mechanical anchors.

Four RC T-beams were tested to evaluate the increase in flexural capacity and ductility using a new FRP strengthening system. One beam was tested as a control beam. One beam was strengthened with conventional epoxy-bonding method. Two beams were strengthened with the new hybrid FRP sheet / ductile anchor system (one with unbonded

CFRP, while the other with bonded CFRP). The proposed system leads to a ductile failure mode by triggering the yield in the steel anchor system (steel links) while avoiding peel-off or debonding of FRP sheets, which is sudden in nature.

The tested beams where modeled to analytically evaluate their performance. The experimental and analytical results indicate that the proposed new retrofitting methods are structurally efficient in enhancing the shear and flexure strengths and ductility of RC T-beams compared to conventional epoxy-bonding methods.

To My Parents

ACKNOWLEDGEMENTS

This is the conclusion of one long journey and the beginning of a new episode in my life. Thanks to God for his presence in my life and allowing me to successfully complete my goals.

There are many people I must thank for their numerous forms of support and appreciation towards me.

First of all, I thank my family. Their love, support and encouragement were essential for the completion of my studies.

I offer my sincere gratitude to my advisor Dr. Khaled Galal. His continuous guidance, support and encouragement led to the completion of this study. His numerous comments were not only of great importance to this study but to my personal development as well.

Thanks to my friends and graduate students, Mona Hassanlou, Navid Sasanian, Hossein Azimi and Nima Farnia who encouraged, helped and supported me during my research. I also thank undergraduate students, Yunke Zhang, Kamal El-Saloussy and Amir Ataei for their valuable help in the structural lab in the summer time.

TABLE OF CONTENTS

LIST OF FIGURES

LIST OF TABLES

LIST OF SYMBOLS

a_g	The specified nominal maximum size of coarse aggregate
A_{frp}	The design area of the FRP sheet
A_{links}	Total cross-section area of the link members at each end
A_v	Total cross-sectional area of stirrups
A_s	Total area of longitudinal steel
b_w	The beam web width
c	Distance from extreme compression fibre to neutral axis
C_c	Compression force in the concrete (kN)
C_s	Compression force in the top longitudinal steel reinforcement (kN)
d	The distance from extreme compression fibre to centroid of longitudinal tension reinforcement
d'	The distance from extreme compression fibre to centroid of longitudinal compression reinforcement
d_{frp}	Effective depth to flexural FRP reinforcement
d_v	The effective shear depth
E_s	The modulus of elasticity of steel reinforcement
E_f	The FRP reinforcement modulus of elasticity
E_{frp}	The FRP reinforcement modulus of elasticity
F-C-O	T-Beam tested in Flexure: COntrol beam
f_c'	Specified compressive strength of concrete (MPa)
F-E-B	T-Beam strengthened in Flexure using externally Epoxy-Bonded FRP
$f_{FRP,u}$	The ultimate tensile strength of the FRP sheets (MPa)
F-M-B	T-beam strengthened in Flexure using Mechanically-anchored epoxy-Bonded FRP sheet
F-M-U	T-beam strengthened in Flexure using Mechanically-anchored Unbonded FRP sheet
f_s	Stress in the bottom steel reinforcement (MPa)
f_s'	Stress in the top steel reinforcement (MPa)
f_y	Specified yield strength of steel reinforcement or anchor steel (MPa)
$f_{y,links}$	The yield stress of the steel link members (MPa)

f_u	Ultimate steel strength (MPa)
h	The overall height of the member
jd	The arm of the tension-compression couple
K_m	Factor for the strain limitation to prevent debonding
l_s	The shear span length
L_1	Steel link member length
L_2	CFRP sheet length
L_e	The FRP effective anchorage length
M_n	The unfactored moment (kN.m)
$M_{n\ orig.}$	Nominal resisting moment (kN.m)
$M_{n\ total}$	The total nominal resisting moment (kN.m)
n	Number of FRP plies
n_e	Number of free ends of the FRP stirrup on the side of the beam
P_{max}	Maximum applied load by hydraulic jack
R	Reduction factor to the ultimate strain of the FRP composite
s	The spacing of shear reinforcement measured parallel to the longitudinal axis of the member
S-C-O	T-Beam tested in Shear: COntrol beam
S-E-B	T-Beam strengthened in Shear using Externally epoxy-Bonded FRP
s_{frp}	The spacing of the FRP shear reinforcement
S-M-D	T-Beam strengthened in Shear using Mechanically-anchored Dry carbon fibre sheet
s_z	Crack spacing parameter dependent on crack control characteristics of longitudinal reinforcement
s_{ze}	The equivalent value of s_z
t_f	Thickness of the FRP sheet
t_{frp}	Thickness of the FRP sheet
T_{frp}	Tension force in the FRP sheet (kN)
T_{link}	Tension force in the steel link member (kN)
T_s	Tension force in the bottom longitudinal steel reinforcement (kN)
T_s'	Tension force in the top longitudinal steel reinforcement (kN)
V_c	Shear resistance provided by tensile stresses in concrete (kN)
V_{frp}	Shear resistance provided by tensile stresses in FRP (kN)

V_n	Nominal shear resistance (kN)
V_s	Shear resistance provided by shear reinforcement (kN)
w_{frp}	The width of the FRP shear reinforcement
α	The reduction coefficient for effective strain
α_1	Ratio of average stress in rectangular compression block to the specified concrete strength
β	The factor accounting for shear resistance of cracked concrete (Clause 6.3.1)
	The angle between inclined FRP sheet and the longitudinal axis of the member (Clause 6.3.2)
β_1	Ratio of depth of rectangular compression block to depth to the neutral axis
Δ_1	Steel link member elongation in the hybrid CFRP / ductile steel anchor
Δ_2	CFRP sheet elongation in the hybrid CFRP / ductile steel anchor
Δ_{eq}	Total elongation of the hybrid CFRP / ductile steel anchor
Δ_{total}	Total elongation of the hybrid CFRP / ductile steel anchor
ΔM	Added moment due to strengthening (kN.m)
θ	The angle of inclination of diagonal compressive stresses to the longitudinal axis of the member
λ	Factor to account for low-density concrete
ε_c	The strain at the extreme concrete compression fibre
ε_{eq_1}	Equivalent strain at yield
ε_{eq_2}	Equivalent strain at strain hardening point
ε_{eq_3}	Equivalent strain at ultimate strain
ε_{frp}	The strain in FRP reinforcement
ε_{frpe}	The effective strain in the FRP reinforcement
ε_{frp_u}	The ultimate strain in the CFRP sheet
ε_s	The steel strain in the bottom longitudinal steel reinforcement
ε_s'	The steel strain in the top longitudinal steel reinforcement
ε_{sh}	The steel strain at strain hardening point
ε_x	The longitudinal strain at mid-depth of the member due to factored loads

ε_y	The steel strain at yield
ρ_{frp}	FRP shear reinforcement ratio
ρ	Ratio of tension steel reinforcement
ρ_{FRP}	CFRP reinforcement ratio
σ_{eq_1}	Equivalent stress at yield point
σ_{eq_2}	Equivalent stress at strain hardening point
σ_{eq_3}	Equivalent stress at ultimate strain
σ_{frp_u}	The ultimate stress in the CFRP sheet

CHAPTER 1

INTRODUCTION

1.1 Background and Problem Definition

Deterioration of the ageing civil infrastructure has been well documented worldwide. In the United States and Canada, nearly 50 percent of the bridges were built before the 1940s or the 1950s. A large number of these are known to be structurally deficient at the present time. Mirza and Haider (2003) estimated that the cost of Canada's infrastructure deficit as well as the overall state of repair is roughly comparable to that of the US. The size of the deficit is roughly $125 billion for 30 million Canadians vs. US$ 1.3 trillion for 280 million Americans. According to the study, deterioration is the key determining factor in the infrastructure deficit. Three decades of deferred maintenance work have created a situation where if the deterioration is not halted, the associated costs will escalate exponentially. Structural deficiencies in bridge girders are usually the result of deterioration caused by ageing, exposure to harsh environments, and higher traffic demands. Common structural deficiencies of deteriorated bridge girders are their inadequate shear strength or their low flexural and displacement ductility capacities. As a result, a large number of concrete highway bridges are in need for rehabilitation or replacement. Similar to the consequences of deterioration of bridges, there exist many RC beams in need for upgrade or strengthening in older buildings, due to ageing, increase in load, or deterioration.

Historically, concrete members have been repaired by post-tensioning or jacketing with new concrete in conjunction with a surface adhesive (Klaiber et al. 1987). Since the mid 1960s epoxy-bonded steel plates have been used to retrofit flexural members (Dussek 1980). Steel plates have a durability problem pertinent to this technique, because corrosion may occur along the adhesive interface. This type of corrosion adversely affects the bond at the steel plate/concrete interface and is difficult to monitor during routine inspection. Additionally, special equipment is necessary to install the heavy plates. As a result, Fibre-reinforced polymer (FRP) composites have emerged as alternatives to traditional materials and techniques (externally bonded steel plates, steel or concrete jackets, and external post-tensioning). The advantages of using composites are mainly due to their high modulus of elasticity, lightness, corrosion resistance, and adaptable electromagnetic properties. To date, various FRP rehabilitation methods are being put in the practice in strengthening and improvement of RC concrete beams. The majority of these methods rely on incorporating the FRP to the original concrete element through chemical bonding.

1.2 Objectives and Scope of work

The main objectives of this research program is to develop innovative techniques that utilize anchored fibre-reinforced polymer sheets for strengthening reinforced concrete T-beams in shear and flexure and to evaluate their effectiveness experimentally and analytically. The process of development of the proposed strengthening techniques involves considerations for optimizing the use of the FRP material, the speed in the

application of the strengthening system, and the durability of the strengthening system by counting on anchorage to concrete whilst maintaining ductile behaviour.

In order to achieve the study objectives, the scope of the research is as follows:

1. Develop and design a strengthening technique for increasing the shear capacity of RC T-beams using mechanically-anchored unbonded dry Carbon Fibre (CF) sheets.
2. Conduct a testing program on three simply-support reinforced concrete T-beams to evaluate the effectiveness of the proposed mechanically-anchored unbonded CF sheets strengthening technique compared to conventional epoxy-bonded FRP wraps in increasing the shear capacity of RC T-beams.
3. Develop and design a strengthening technique for increasing the flexural capacity and ductility of RC beams using hybrid FRP sheet / ductile anchor system.
4. Conduct a testing program on four simply-support reinforced concrete T-beams with two column stubs to evaluate the effectiveness of the proposed hybrid FRP sheet / ductile anchor strengthening system compared to conventional epoxy-bonded FRP sheets in increasing the flexural capacity and ductility of RC beams.
5. Develop a numerical / analytical procedure that is capable of predicting the behaviour of the tested RC beams.

1.3 Configuration of the Thesis

The research work in this study is reported in seven chapters. Chapter 1 provides a brief introduction and discusses the objectives and scope of the research work. Chapter 2 provides a literature review of the previous research topics related to the current work.

Chapter 3 describes the experimental phase. Chapters 4 and 5 report the structural behaviours observed from experimental testing on the RC T-beams strengthened in shear and flexure, respectively. Chapter 6 discusses the analytical modeling of the tested beams and comparisons with the experimental results. Chapter 7 includes the conclusions drawn from this research and recommended research extensions.

CHAPTER 2

LITERATURE REVIEW

2.1 General

The last decade has witnessed increasing demand for strengthening or rehabilitation of existing reinforced concrete (RC) bridges and buildings. This is mainly due to ageing, deterioration, increase in loads, corrosion of steel reinforcement, or advancement in the design codes and knowledge. There exist many beams that were designed based on the pre-1970s codes (e.g. ACI 1968; AASHO 1965). Several researchers pointed out that previous design provisions did not have a comprehensive understanding of the shear behaviour (e.g. Higgins 2007). As the result, pre-1970s designs might be deficient in shear according to current codes. For example, AASHO provisions prior to 1965 (AASHO 1965) for shear design of RC bridges used allowable stress design and counted on the concrete to endure a recommended serviceability stress at service load levels. After the collapse of two storehouses in 1955 and 1956, significant investigational research work was done to advance the understanding of shear behaviour. Research pointed out that previous design provisions overestimated the concrete share in the shear capacity and the permissible concrete stresses were decreased in the early 1960s to be $1.1\sqrt{f_c'}$ (ACI 1963) and is currently $0.95\sqrt{f_c'}$ in AASHTO (2002) in SI units (Higgins 2007). Such deficient beams, would fail in a non-ductile manner once their shear capacity is reached. Also extensive inspections showed that cracks near the mid-height of large girders were significantly wider than at the level of the flexural

reinforcement, also resulted in the use of skin reinforcement that was not normally present in bridge girders designed and constructed prior to 1960s. In addition, construction materials were changing substantially. The AASHO bridge design provisions did not necessitate modern deformed reinforcing bars until 1949, and explicit bond specifications for deformed bars were not announced until 1953. Awareness of proper anchorage and development of flexural reinforcement was unclear. As a result, many existing bridges designed before 1960s would have smaller cross-sectional sizes, smaller dimensions for stirrups or farther and wider spaced shear reinforcement, and decreased requirements for flexural bond stresses.

Despite the fact that actual truck load extents and the quantity of truck traffic have intensified over time, the 17th edition of the standard specification (AASHTO 2002) uses the HS20-44 truck, which is, surprisingly, the same truck load model H20-S16-44 that was used in older editions of the code.

Furthermore, the infrastructure of transportation built facilities is now getting to a crucial age with escalating signs of deterioration and diminished functionality (Karbhari 2001). In case of old bridges which are showing signs of aging, including corrosion of steel and spalling of concrete another reason of this type of degradation could be high usage of deicing salt (Deniaud 2003).

Since replacement of too many deficient structures requires huge investments, strengthening has become the suitable way of improving their load carrying capacity and prolonging their service age. Over the past two decades many bridges have been strengthened in North America and world wide.

2.2 Shear Strengthening of Beams

2.2.1 Chemically bonded methods

Most of the research activities on the use of FRP in strengthening RC beams directed to enhancing their flexural capacity. For the few researches that have been done in strengthening RC beams in shear, most of the researches were conducted on RC rectangular sections (Bousselham and Chaallal 2004), which is not representative of the fact that most RC beams would have a T-section due to the presence of top slab.

Al-Sulaimani et al. (1994) investigated the possibility of using glass fiber reinforced polymer (GFRP) sheets to rehabilitate weak concrete beams in shear. A series of small-scale rectangular RC beams deficient in shear were cast. The specimens were loaded until the first visible cracks appeared, then rehabilitated with glass-fiber sheets. Even when the beams were designed to yield at flexural capacity of 1.5 times the shear capacity before repair, some beams still failed due to bending, and the full potential of FRP shear strengthening could not be reached. Similar concrete beam specimens without stirrups were also tested by other researchers (Chajes et al. 1995; Triantafillou 1998), but both studies concluded that full-scale tests and tests with internal shear reinforcement should be conducted.

To date, most of the research conducted on strengthening RC T-beams in shear focused on, to the author's knowledge, enhancing the shear strength of the beam by utilizing the contribution of the FRP through bond with the exterior sides of the beam. Cao et al. (2005) categorized different shear strengthening techniques using FRP as: complete FRP wraps covering the whole cross section (i.e., complete wrapping, valid only for rectangular sections, Figure 2.1), and FRP U-jackets covering the two sides and

the tension face (i.e., U-jacketing as shown in Figure 2.2). Most of the design guidelines such as, ACI-440 (2004), FIB (2001) and ISIS (2001), endorsed design formulas for the shear strength contribution from FRP that is bonded to the web as U-jacketing. Previous studies have established clearly that such strengthened beams fail in shear mainly in one of the two modes: tensile rupture of the FRP and debonding of the FRP from the sides of the RC beam, depending on how the beam is strengthened. Although not widely applicable, available experimental data indicates that almost all beams strengthened by complete wrapping (referred to as FRP-wrapped beams) failed due to FRP rupture. On the other hand, almost all beams strengthened by side bonding only, and most of the ones strengthened by U-jacketing, failed due to FRP debonding (Cao et al. 2005; Bousselham and Chaallal 2004). With the goal of improving bond in mind, Khalifa et al. (1999) investigated a form of bonded anchored U-jacketing FRP application (Figure 2.3). The anchor was an embedded bent portion of the end of the FRP reinforcement into preformed groove in concrete. No FRP debonding was observed at ultimate due to anchorage.

2.2.2. Unbonded anchored methods

Prior to this study, there has been no research regarding the strengthening of RC beams with unbonded methods using FRP material. Most of the previous researches in this area were focused on different types of externally chemically bonded FRP sheets or laminates to strengthen RC beams in shear. Using an unbonded dry FRP material to strengthening RC beams is proposed for the first time in this research.

2.2.3. Mode of failure in FRP-strengthened beams in shear

Previous studies have established clearly that such strengthened beams fail in shear mainly in one of the two modes: tensile rupture of the FRP and debonding of the FRP from the sides of the RC beam, depending on how the beam is strengthened. Although not widely applicable, available experimental data indicates that almost all beams strengthened by complete wrapping (referred to as FRP-wrapped beams) failed due to FRP rupture. On the other hand, as it can be seen in Table 2.1, almost all beams strengthened by side bonding, and most of the ones strengthened by U-jacketing, failed due to FRP debonding (Cao et al. 2005; Bousselham and Chaallal 2004).

2.3. Flexural Strengthening of Beams

2.3.1. Chemically bonded methods

The oldest and mostly used method using FRP in the practice is the epoxy-bonded FRP. Since the 1990s, externally bonded FRP sheets/strips have been successfully applied to strengthen concrete structures in flexure (Meier 1992; Nanni 1995).

The FRP epoxy bonding method is capable of increasing the strength and stiffness of RC beams, conditional upon several of variables, such as FRP type, number of layers, stiffness, etc. (Ritchie et al. 1991; Fanning and Kelly 2001). Although externally bonded FRP reinforcement performs well in the service stage, failure due to premature debonding (Figure 2.4) was observed and identified by many researchers (e.g. Saadatmanesh and Ehsani 1989; Sharif et al. 1994). In fact, beams strengthened using FRP epoxy-bonding method are mostly susceptible to fail suddenly and without any precautions in a brittle manner due to debonding of the FRP sheet or laminate (Ritchie et al. 1991; Fanning and

Kelly 2001; among others). A number of researchers suggested the application of several different end-anchors (Figure 2.5) to guarantee that the rehabilitated beam can reach its full capacity (Sharif et al. 1994; Bencardino et al. 2002). Several details were proposed to avoid this type of failure, which is unacceptable from the point of view of structural safety (Swamy and Mukhopadhyaya 1999).

With the goal of improving bond in mind, near-surface mounted FRP was proposed. Use of near surface mounted FRP rods and strips can preclude delamination-type failures, frequently observed by using externally bonded reinforcement. Blaschko and Zilch (1999) carried out bond tests on carbon FRP (CFRP) strips inserted inside grooves (Figure 2.6). Bond tests were conducted on double shear specimens. Test results showed that strengthening using near surface mounted CFRP strips has a greater anchoring capacity compared to externally bonded CFRP strips. De Lorenzis and Nanni (2001) investigated the structural performance of simply supported reinforced concrete beams strengthened with near surface mounted glass FRP (GFRP) and CFRP rods. Both flexural and shear strengthening were examined. Test results showed that the use of near surface mounted FRP rods is an effective technique to enhance flexural and shear capacity of reinforced concrete beams (Hassan and Rizkalla 2003).

Additionally, near-surface mounted applications showed higher fracture energy at failure, leading to higher resistance to end peel, more ductile behaviour at failure, and higher endurance against fire, vandalism, and impact than that of externally bonded applications (Täljsten 2003).

It has been recommended that in tension controlled members, still, debonding is an anticipated failure mode (De Lorenzis et al. 2002). This method also needs a

complicated surface preparation to prepare an appropriate groove in the concrete to install and epoxy the FRP strip in the groove.

2.3.2. Unbonded anchored methods

A more recent application of FRP for flexural strengthening of reinforced concrete beams used mechanical anchors as bonding technique (Figure 2.7 and 2.8). Unlike externally epoxy bonded strengthening system, mechanically-anchored unbonded FRP strengthening system does not require surface preparation, adhesive application, or skilled labours. One method of application of mechanically anchored unbonded FRP, referred to as powder-actuated, fastener-applied uses a powder-actuated fastener gun to install mechanical fasteners and fender washers through holes in the FRP predrilled into the concrete substrate, "nailing" the FRP in place (Lamanna et al. 2001). Little work has been done on the performance of RC beams strengthened with mechanically-anchored unbonded FRP strengthening systems. Nevertheless, results from preliminary studies indicate that significant strength increase is possible through the use of mechanically-anchored unbonded FRP strengthening system in specimens tested under monotonic conditions (Borowicz 2002). Some notable disadvantages of this method have been observed, including scale effects, greater initial cracking induced by the impact of fasteners in higher-strength concrete and less-effective stress transfer between the FRP and the concrete because of discrete attachment points. However, failure modes in these specimens are more ductile than failures associated with the externally epoxy bonded method. In cases where speed and ease of installation are major concerns, mechanically anchored FRP method is a viable option (Borowicz 2002). Soudki et al. (2005)

investigated the structural performance of reinforced concrete T-beams strengthened with mechanically-anchored unbonded system which was compared to that of T-beams strengthened with externally epoxy bonded system. The anchor used to attach the CFRP strip to the bottom soffit of the specimen was a steel plate, which was placed below the CFRP strip and held in place using four bolts. The results showed that mechanically-anchored unbonded strengthening system was effective in upgrading the T-beam strength but the strength gain was less than that obtained by the use of externally epoxy bonded strengthening system.

2.3.3. Mode of failure in FRP strengthened beams in flexure

In FRP strengthening methods, it is desirable to have a mode of failure where the FRP sheets reach their maximum tensile capacity. Having the FRP sheets ruptured before the failure of the beam guarantees the full utilization of the maximum possible flexural capacity of an FRP-strengthened beam (Figure 2.9). In conventional FRP rehabilitation methods, the FRP rupture mode of failure does not occur very often since in most cases other failure mode occur prior to FRP rupture. The failure varies depending on the strengthening method used and it fails in a lower load than the failure load corresponding to the FRP rupture mode.

In externally epoxy-bonded FRP method, higher failure loads and desirable failure behaviour in strengthened RC beams are both highly dependent on the effective transmission of bond stresses between the FRP sheet and the RC beam via the adjacent connecting layers of the FRP sheet, epoxy and cover concrete (which is not confined by the stirrups). High-bond stresses finally cause failure of one of these layers. In such

rehabilitation method, more than one debonding mode of failure has been reported in the literature. Mainly, there are two debonding failure modes: end debonding and midspan debonding. End debonding is the failure that begins near the FRP sheet end and propagates in the concrete either along the longitudinal steel reinforcement (end cover separation) or near the bond line (end interfacial delamination). Inclined and horizontal cracks form in the cover concrete layer causing it to disconnect from the beam while remaining strongly attached to the FRP sheet (Figure 2.10). This mode has been inspected experimentally and analytically by many researchers (Jones et al. 1988; Roberts 1989; Oehlers and Moran 1990; Zhang et al. 1995; Brosens and Van Gemert 1997; Saadatmanesh and Malek 1997; Rabinovich and Frostig 2000). The stresses responsible for end peel mode of failure appear from the offset in position along the beam between the zero moment locations (supports) and the ends of the FRP sheets (Sebastian 2001). This mode of failure only takes place when a large flexural crack is present (Figure 2.11). This occurs when the beam is lightly reinforced or when there is a sudden change in the beam cross-section, such as by notching or corrosion of tension reinforcement (Al-Mahaidi 2004). Whereas end peel debonding includes the full depth of cover concrete and propagates from the ends of the plates inwards, another debonding mode exists that fractures only a part of the depth of cover concrete and begins at the toes of flexural cracks in the midspan area of the beam with propagation out to the ends of the FRP sheet (Figure 2.12). This latter mode is termed midspan debonding (Sebastian 2001). Midspan debonding is the failure that initiates either from a flexural crack (flexure crack delamination) or an inclined flexure-shear crack (shear crack delamination). The failure then propagates to the FRP sheets' ends parallel to the epoxy/concrete interface. The

shear crack delamination has been found to be the most serious as a result of the brittleness of the failure (Al-Mahaidi 2004). Such a failure is more likely in members with large shear span-to-depth ratios and also where the FRP has been terminated close to the end support in a low-moment region (Sebastian 2001; Aidoo et al. 2004).

The recently studied mechanically anchored methods (Lammana et al. 2001; Borowicz 2002; Soudki et al. 2005) mostly have less-effective transfer of force between the FRP and the concrete due to splitting and crushing of the FRP around the anchors. Additionally, the mechanically anchored methods require a small amount of relative movement, or slip, between the FRP and the concrete to engage the shear transfer mechanism, the fasteners (Figure 2.13). This slip reduces the efficiency of the retrofit, resulting in lower strength gains and greater displacement ductility than observed for the fully bonded retrofit systems.

Table 2.1. Experimental data on shear strengthening with FRP (Chaallal 2004)

Specimen	b_w, m	d, m	Section	f_c, MPa	Fiber	Config-uration	ρ_{FRP}, 10^{-3}	E_{FRP}, GPa	ε_{fu}, 10^{-3}	β, degrees	ρ_s, %	ρ_w, %	E_s	a/d	FRP at failure	V_{FRP}, kN	V_{total}, kN
B(3)	0.114	0.085	Rec.*	42.9	G	Ct-S	11	16.8	20.5	45	0	2.61	200	3.53	Debonded	15.1	62.5
B(4)	0.114	0.085	Rec.	42.9	G	Ct-S	27	16.8	20.5	45	0	2.61	200	3.53	Debonded	31.5	78.9
U(3)	0.1	0.17	Rec.	24.6	C	Ct-W	1.94	230	11.5	90	0	2.36	200	2.5	Fracture	34.5	59.5
U(5)	0.1	0.17	Rec.	24.6	C	Ct-S	1.94	230	11.5	90	0	2.36	200	2.5	Debonded	20.5	45.5
U(6)	0.1	0.17	Rec.	27.4	C	Ct-S	1.94	230	11.5	56	0	2.36	200	2.5	Debonded	33	58
U(7)	0.1	0.17	Rec.	27.4	C	Ct-S	3.9	230	11.5	90	0	2.36	200	2.5	Debonded	20.5	45.5
AS(WO)	0.15	0.113	Rec.	37.7	G	Ct-S	40	16	12.5	90	0.19	2	200	3.54	Debonded	7	41.5
AS(SO)	0.15	0.113	Rec.	37.7	G	St-S	16	16	12.5	90	0.19	2	200	3.54	Debonded	7.5	42
CJ(A)	0.063	0.152	T-	46	A	Ct-U	33	11	22.5	90	0	2.05	200	2.7	No fracture	15.6	34.4
CJ(E)	0.063	0.152	T-	46	G	Ct-U	15	14.3	13.4	90	0	2.05	200	2.7	Fracture	16.6	35.4
CJ(G)	0.063	0.152	T-	46	C	Ct-U	18	21	9.5	90	0	2.05	200	2.7	Fracture	17.1	35.9
CJ(45G)	0.063	0.152	T-	46	C	Ct-U	18	21	9.5	45	0	2.05	200	2.7	Fracture	23.6	42.4
SU(S2)	0.2	0.26	Rec.	45.2	C	St-U	0.6	230	15.1	90	0	3.3	180	2.7	Debonded	68.4	160.5
SU(S3)	0.2	0.26	Rec.	41.3	C	St-S	0.6	230	15.1	90	0	3.3	180	2.7	Debonded	110	202.1
SU(S4)	0.2	0.26	Rec.	37.5	C	Ct-S	1.2	230	15.1	90	0	3.3	180	2.7	Debonded	64.2	156.3
SU(S5)	0.2	0.26	Rec.	39.7	C	Ct-U	1.2	230	15.1	90	0	3.3	180	2.7	Debonded	106.1	198.2
MI(AN-1/5 Z-3)	0.125	0.165	Rec.	35.1	C	St-W	0.35	230	15.1	90	0	4.76	200	3	Fracture	18.75	75.2
MI(AN-1/2 Z-3)	0.125	0.165	Rec.	32.4	C	St-W	0.88	230	15.1	90	0	4.76	200	3	Fracture	29.5	86
MI(CN-1/L Z-2)	0.125	0.165	Rec.	39.1	C	St-W	0.88	230	15.1	90	0	2.75	200	2	Fracture	34.55	93.1
TK(BS2)	0.2	0.42	Rec.	35.1	C	St-U	0.14	280	12.5	90	0.14	2.24	200	3	Debonded	41.2	247.5
TK(BS5)	0.2	0.42	Rec.	36.8	C	St-U	0.14	280	12.5	90	0.07	2.24	200	3	Debonded	33.4	170
TK(BS6)	0.2	0.42	Rec.	35.8	C	St-U	0.14	280	12.5	90	0.07	2.24	200	3	Debonded	30.1	166.7
TK(BS7)	0.2	0.42	Rec.	34.7	C	St-W	0.28	280	12.5	90	0.07	2.24	200	3	No fracture	98.9	235.5
SUK(2)	0.15	0.24	T-	35.7	C	Ct-U	1.48	230	15.1	90	0.42	5.63	183	2.5	Debonded	24	223
SUK(3)	0.15	0.24	T-	35.3	C	Ct-U	1.48	230	15.1	90	0.42	5.63	183	2.5	Debonded	65	264
UF(CS1)	0.3	0.257	Rec.	40.5	C	Ct-W	0.74	244	17.5	90	0.48	1.09	200	3	No fracture	87	214
UF(CS2)	0.3	0.257	Rec.	40.5	C	St-W	0.37	244	17.5	90	0.48	1.09	200	3	Fracture	32	159
UF(CS3)	0.15	0.272	Rec.	44.8	C	St-W	0.47	244	17.5	90	0.96	1.03	200	3	No fracture	52	116
UF(AS1)	0.15	0.272	Rec.	43	A	Ct-W	0.587	73	37	90	0.96	1.02	200	3	No fracture	27.5	91.2
UF(AS2)	0.15	0.272	Rec.	43	A	St-W	0.293	73	37	90	0.96	1.02	200	3	Fracture	26	89.7
UF(AS3)	0.15	0.272	Rec.	44.8	A	Ct-W	1.17	73	37	90	0.96	1.02	200	3	No fracture	50	114
UF(AB1)	0.15	0.253	Rec.	41.9	A	Ct-W	0.587	73	37	90	0.96	2.19	200	3	No fracture	64	110
UF(AB2)	0.3	0.253	Rec.	45.6	A	Ct-W	0.293	73	37	90	0.48	2.19	200	3	No fracture	46	173
UF(AB3)	0.3	0.253	Rec.	41.9	A	Ct-W	0.587	73	37	90	0.48	2.19	200	3	No fracture	82	209
UF(AB4)	0.3	0.253	Rec.	41.9	A	Ct-W	0.587	73	37	90	0.48	2.19	200	3	No fracture	97	224
UF(AB5)	0.3	0.253	Rec.	42.7	A	Ct-W	0.96	73	37	90	0.48	2.19	200	3	No fracture	127	254
UF(AB8)	0.6	0.253	Rec.	43.5	A	Ct-W	0.48	73	37	90	0.24	2.19	200	3	No fracture	140	424
UF(AB9)	0.45	0.39	Rec.	39.9	A	Ct-W	0.64	73	37	90	0.32	2.24	200	3	No fracture	163	379
UF(AB10)	0.55	0.49	Rec.	39.9	A	Ct-W	0.53	73	37	90	0.26	2.05	200	3	Fracture	294	569
UF(AB11)	0.55	0.49	Rec.	40.6	A	Ct-W	1.05	73	37	90	0.26	2.05	200	3	No fracture	387	662
FS(S-2)	0.6	0.51	Rec.	30	C	Ct-W	0.56	240	16	90	0.13	3.63	200	2.5	Fracture	242	691
FS(S-3)	0.6	0.51	Rec.	30	C	Ct-W	1.1	240	16	90	0.13	3.63	200	2.5	Fracture	346	795
FS(S-4)	0.6	0.51	Rec.	30	C	Ct-W	1.67	240	16	90	0.13	3.63	200	2.5	No fracture	493	942
AM(CF045)	0.2	0.34	Rec.	24.8	C	St-W	0.26	230	15.1	90	0.19	2.84	188	1.5	No fracture	35	236
AM(CF064)	0.2	0.34	Rec.	24.9	C	St-W	0.45	230	15.1	90	0.19	2.84	188	1.5	No fracture	61	262
AM(CF097)	0.2	0.34	Rec.	25.2	C	St-W	0.77	230	15.1	90	0.19	2.84	188	1.5	No fracture	106	307
AM(CF131)	0.2	0.34	Rec.	25.4	C	Ct-W	1.1	230	15.1	90	0.19	2.84	188	1.5	No fracture	157	358
AM(CF243)	0.2	0.34	Rec.	25.6	C	Ct-W	2.2	230	15.1	90	0.19	2.84	188	1.5	No fracture	206	407
AM(AF060)	0.2	0.34	Rec.	25.8	A	St-W	0.59	87	28.1	90	0.19	2.84	188	1.5	No fracture	36	237
AM(AF090)	0.2	0.34	Rec.	25.9	A	St-W	1	87	28.1	90	0.19	2.84	188	1.5	No fracture	58	259
AM(AF120)	0.2	0.34	Rec.	26.1	A	Ct-W	1.4	87	28.1	90	0.19	2.84	188	1.5	No fracture	111	312
T(S4)	0.18	0.46	Rec.	48.5	C	Ct-S	8.9	70.8	10	45	0	1.94	200	2.6	Fracture	211	331
T(SR1)	0.18	0.46	Rec.	53.8	C	St-S	4.4	70.8	10	45	0	1.94	200	3.5	Debonded	89	195
T(SR2)	0.18	0.46	Rec.	52.7	C	Ct-S	8.9	70.8	10	45	0	1.94	200	2.6	Debonded	123	243

Table 2.1. (cont.) Experimental data on shear strengthening with FRP (Chaallal 2004)

Specimen	b_w, m	d, m	Section	f_c, MPa	Fiber	Config-uration	ρ_{FRP}, 10^{-3}	E_{FRP}, GPa	ε_{fu}, 10^{-3}	β, degrees	ρ_s, %	ρ_w, %	E_s	a/d	FRP at failure	V_{FRP}, kN	V_{total}, kN
MT(A)	0.15	0.22	Rec.*	28.5	C	Ct-W	3.7	230	15	90	0.26	1.2	200	1.14	Fracture	40.2	134.4
MT(B)	0.15	0.22	Rec.	28.5	C	Ct-W	3.7	230	15	90	0.26	1.2	200	1.14	Fracture	43.2	137.3
MT(C)	0.15	0.22	Rec.	28.5	C	Ct-W	3.7	230	15	90	0.26	1.2	200	1.14	Fracture	34.5	128.5
MT(D)	0.15	0.22	Rec.	28.5	C	Ct-W	3.7	230	15	90	0.26	1.2	200	1.59	Fracture	55.4	126.5
MT(E)	0.15	0.22	Rec.	28.5	C	Ct-W	3.7	230	15	90	0.26	1.2	200	1.59	Fracture	38	108.9
MT(F)	0.15	0.22	Rec.	28.5	C	Ct-W	3.7	230	15	90	0.26	1.2	200	1.59	Fracture	18	88.8
TR(S1a)	0.07	0.1	Rec.	30	C	St-S	2.2	235	14	90	0	1.44	200	3.2	Debonded	13.55	21.75
TR(S1b)	0.07	0.1	Rec.	30	C	St-S	2.2	235	14	90	0	1.44	200	3.2	Debonded	11.25	19.45
TR(S2a)	0.07	0.1	Rec.	30	C	St-S	3.3	235	14	90	0	1.44	200	3.2	Debonded	15.85	24.05
TR(S2b)	0.07	0.1	Rec.	30	C	St-S	3.3	235	14	90	0	1.44	200	3.2	Debonded	12.9	21.1
TR(S3a)	0.07	0.1	Rec.	30	C	St-S	4.4	235	14	90	0	1.44	200	3.2	Debonded	13.2	21.4
TR(S3b)	0.07	0.1	Rec.	30	C	St-S	4.4	235	14	90	0	1.44	200	3.2	Debonded	10.55	18.75
TR(S1-45)	0.07	0.1	Rec.	30	C	St-S	2.2	235	14	45	0	1.44	200	3.2	Debonded	14.05	22.25
TR(S2-45)	0.07	0.1	Rec.	30	C	St-S	3.3	235	14	45	0	1.44	200	3.2	Debonded	15.45	23.65
TR(S3-45)	0.07	0.1	Rec.	30	C	St-S	4.4	235	14	45	0	1.44	200	3.2	Debonded	12.5	20.35
CH1(RS90)	0.15	0.22	Rec.	35	C	St-S	6.7	150	14	90	0.19	1.82	200	2.5	Debonded	76	182.5
CH1(RS135)	0.15	0.22	Rec.	35	C	St-S	6.7	150	14	135	0.19	1.82	200	2.5	Debonded	87	193.5
KH3(SO3-2)	0.15	0.26	Rec.	27.5	C	St-U	0.88	228	16	90	0	4.2	200	3	Debonded	54	131
KH3(SO3-3)	0.15	0.26	Rec.	27.5	C	St-U	1.32	228	16	90	0	4.2	200	3	Debonded	56.5	133.5
KH3(SO3-4)	0.15	0.26	Rec.	27.5	C	Ct-U	2.2	228	16	90	0	4.2	200	3	Debonded	67.5	144.5
KH3(SO4-2)	0.15	0.26	Rec.	27.5	C	St-U	0.88	228	16	90	0	4.2	200	4	Debonded	62.5	127.5
KH1(CO2)	0.15	0.26	Rec.	20.5	C	St-U	0.88	228	16	90	0	4	200	3.6	Debonded	40	88
KH1(CO3)	0.15	0.26	Rec.	20.5	C	Ct-U	2.2	228	16	90	0	4	200	3.6	Debonded	65	113
KH2(BT2)	0.15	0.36	T-	35	C	Ct-U	2.2	228	16	90	0	2.28	200	3	Debonded	65	155
KH2(BT3)	0.15	0.36	T-	35	C	Ct-U	4.4	228	16	90	0	2.28	200	3	Debonded	67.5	157.5
KH2(BT4)	0.15	0.36	T-	35	C	St-U	0.88	228	16	90	0	2.28	200	3	Debonded	72	162
KH2(BT5)	0.15	0.36	T-	35	C	St-S	0.88	228	16	90	0	2.28	200	3	Debonded	31.5	121.5
DE(T6NS-C45)	0.14	0.54	T-	44.1	C	St-U	26	230	15	45	0	2.81	200	2.9	Debonded	103.5	213.6
DE(T6S4-C90)	0.14	0.54	T-	44.1	C	St-U	0.8	230	15	90	0.1	2.81	200	2.9	Debonded	85.25	272.8
DE(T6S4-G90)	0.14	0.54	T-	44.1	G	Ct-U	26	17.7	15	90	0.1	2.81	200	2.9	Debonded	109.9	297.45
DE(T6S4-Tri)	0.14	0.54	T-	44.1	G	Ct-U	30	8.1	15	45	0.1	2.81	200	2.9	Debonded	129.2	316.7
DE(T4NS-G90)	0.14	0.34	T-	29	G	Ct-U	26	17.7	15	90	0	4.46	200	3.2	Debonded	43.6	159
DE(T4S4-G90)	0.14	0.34	T-	29	G	Ct-U	26	17.7	15	90	0.1	4.46	200	3.2	Debonded	48.65	205.6
DE(T4S2-C45)	0.14	0.34	T-	29	C	St-U	0.8	230	15	45	0.2	4.46	200	3.2	Debonded	17.8	219.05
DE(T4S2-G90)	0.14	0.34	T-	29	G	Ct-U	26	17.7	15	90	0.2	4.46	200	3.2	Debonded	24.35	225.6
DE(T4S2-Tri)	0.14	0.34	T-	29	G	Ct-U	30	8.1	15	45	0.2	4.46	200	3.2	Debonded	41.4	242.5
CH2(G5.5-1L)	0.092	0.343	T-	37.9	C	Ct-U	2.37	231	16	90	1.1	3.6	203	2	Fracture	31.15	320.23
CH2(G5.5-2L)	0.092	0.343	T-	37.9	C	Ct-U	4.75	231	16	90	1.1	3.6	203	2	Fracture	53.4	342.51
CH2(G8-1L)	0.092	0.343	T-	37.9	C	Ct-U	2.37	231	16	90	0.76	3.6	203	2	Fracture	31.15	298
CH2(G8-2L)	0.092	0.343	T-	37.9	C	Ct-U	4.75	231	16	90	0.76	3.6	203	2	Fracture	62.3	329.2
CH2(G8-3L)	0.092	0.343	T-	37.9	C	Ct-U	7.12	231	16	90	0.76	3.6	203	2	Fracture	84.55	351.41
CH2(G16-1L)	0.092	0.343	T-	37.9	C	Ct-U	2.37	231	16	90	0.38	3.6	203	2	Fracture	40.05	275.8
CH2(G16-2L)	0.092	0.343	T-	37.9	C	Ct-U	4.75	231	16	90	0.38	3.6	203	2	Fracture	84.55	320.3
CH2(G24-1L)	0.092	0.343	T-	37.9	C	Ct-U	2.37	231	16	90	0.25	3.6	203	2	Fracture	53.4	258
CH2(G24-2L)	0.092	0.343	T-	37.9	C	Ct-U	4.75	231	16	90	0.25	3.6	203	2	Fracture	48.95	253.6
CH2(G24-3L)	0.092	0.343	T-	37.9	C	Ct-U	7.12	231	16	90	0.25	3.6	203	2	Fracture	53.4	258

*Rec. = rectangular.
Note: B = Berset (1992); U = Uji (1992); AS = Al-Sulaimani (1994); CJ = Chajes (1995); Su = Sato (1996); MI = Miyachi (1997); TK = Taerwe (1997); SUK = Sato (1997); UF = Umezu (1997); FS = Funakawa (1997); AM = Araki (1997); T = Täljsten (1997); MT = Mitsui (1998); TR = Triantafillou (1998); CH1 = Chaallal (1998); KH1 = Khalifa (1999); KH2 = Khalifa (2000); KH3 = Khalifa (2002); DE = Deniaud (2001); and CH2 = Chaallal (2002).
A = aramid; C = carbon; G = glass; Ct = continuous; St = strips; S = on sides shapes; U = U-shape; W = wrapped around: Fracture = fractured at shear failure; No fracture = fractured after shear failure.

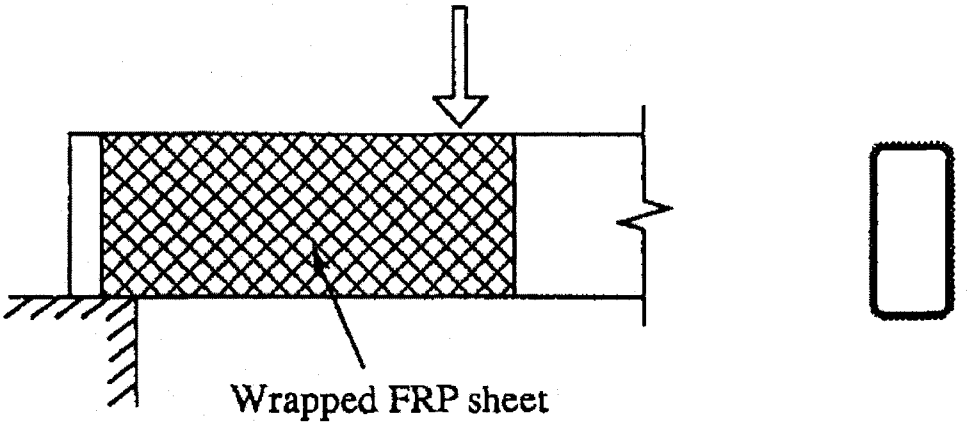

Figure 2.1. Complete FRP wraps covering the whole cross section (Triantafillou 2002)

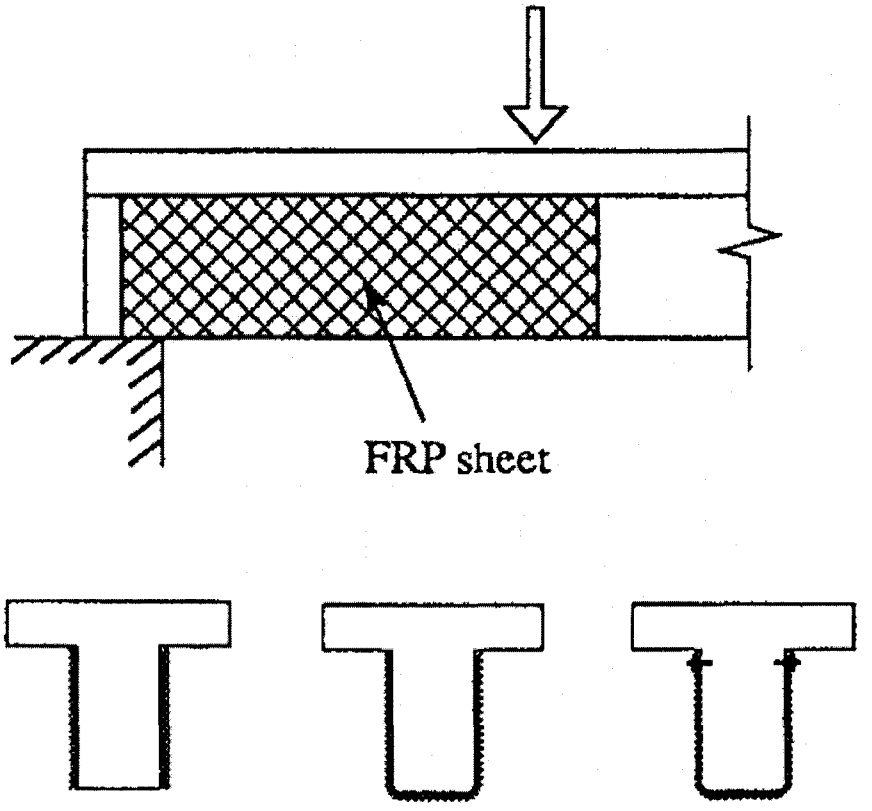

Figure 2.2. FRP U-jackets covering the two sides and the tension face (Triantafillou 2002)

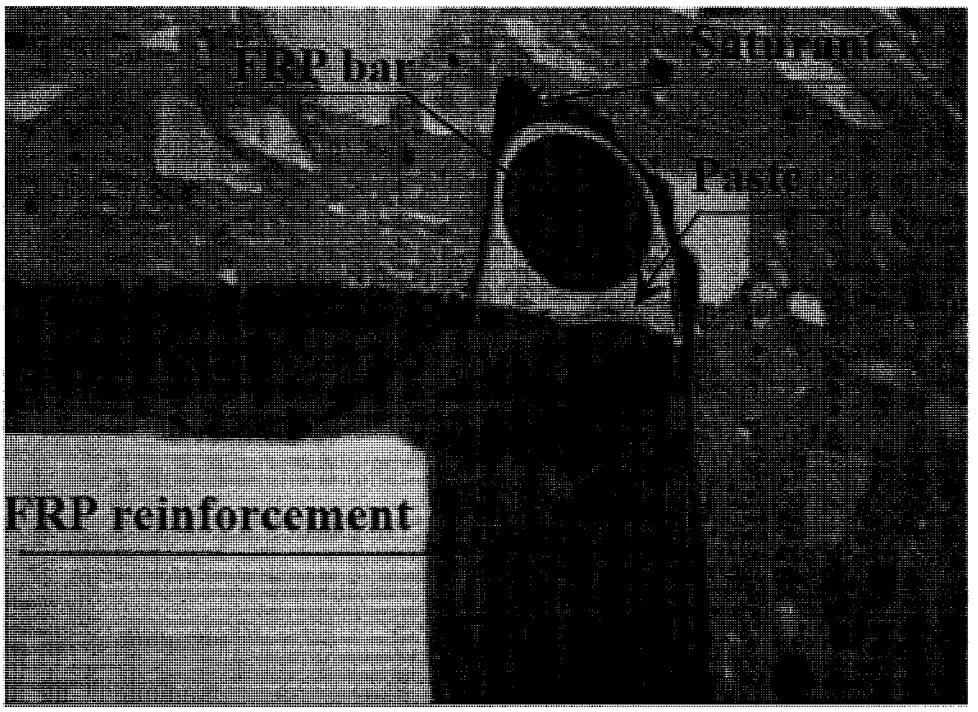

Figure 2.3. Anchorage of surface mounted FRP sheet (Khalifa 1999)

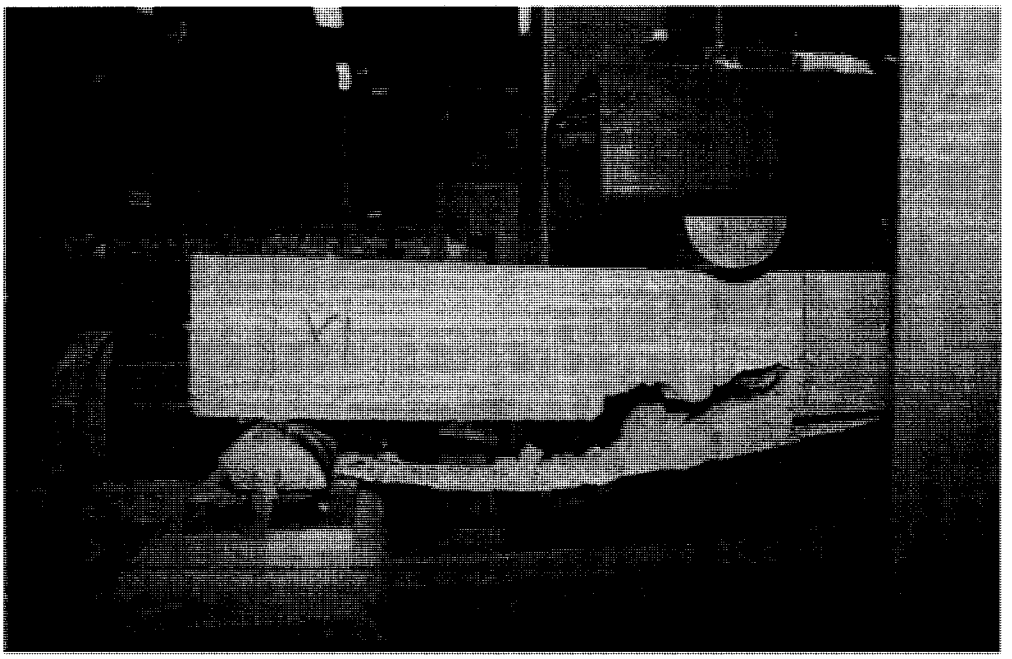

Figure 2.4. Premature debonding failure in externally bonded FRP strip (Lamanna 2002)

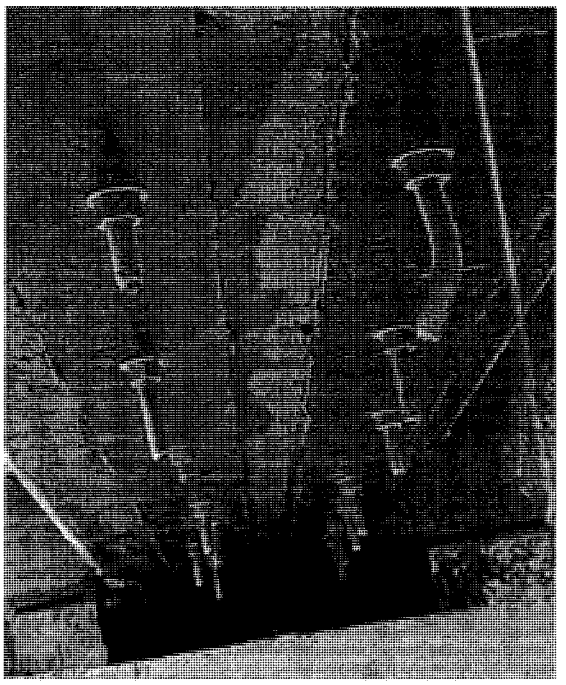

Figure 2.5. Application of end-anchors to prevent FRP debonding (Shahrooz 2002)

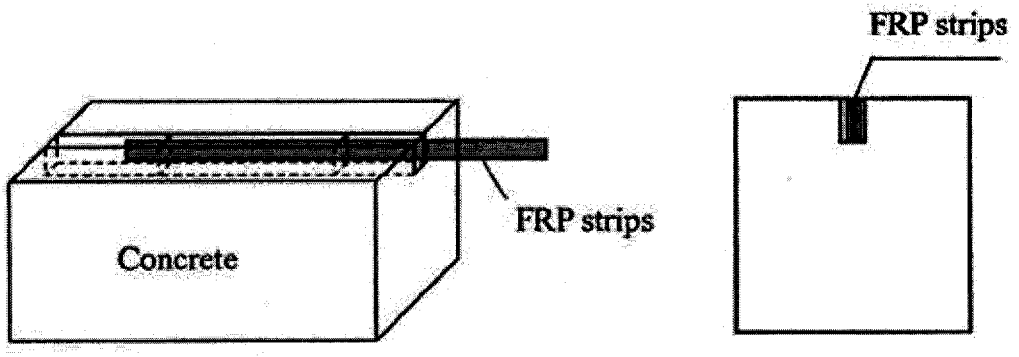

Figure 2.6. Near surface mounted FRP strip application (Teng et al. 2006)

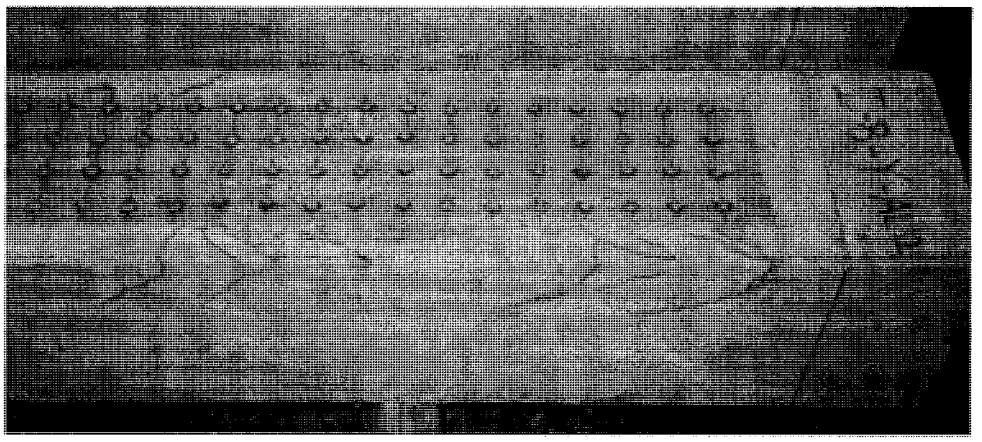

Figure 2.7. Mechanically anchored FRP strip application (Lamanna 2002)

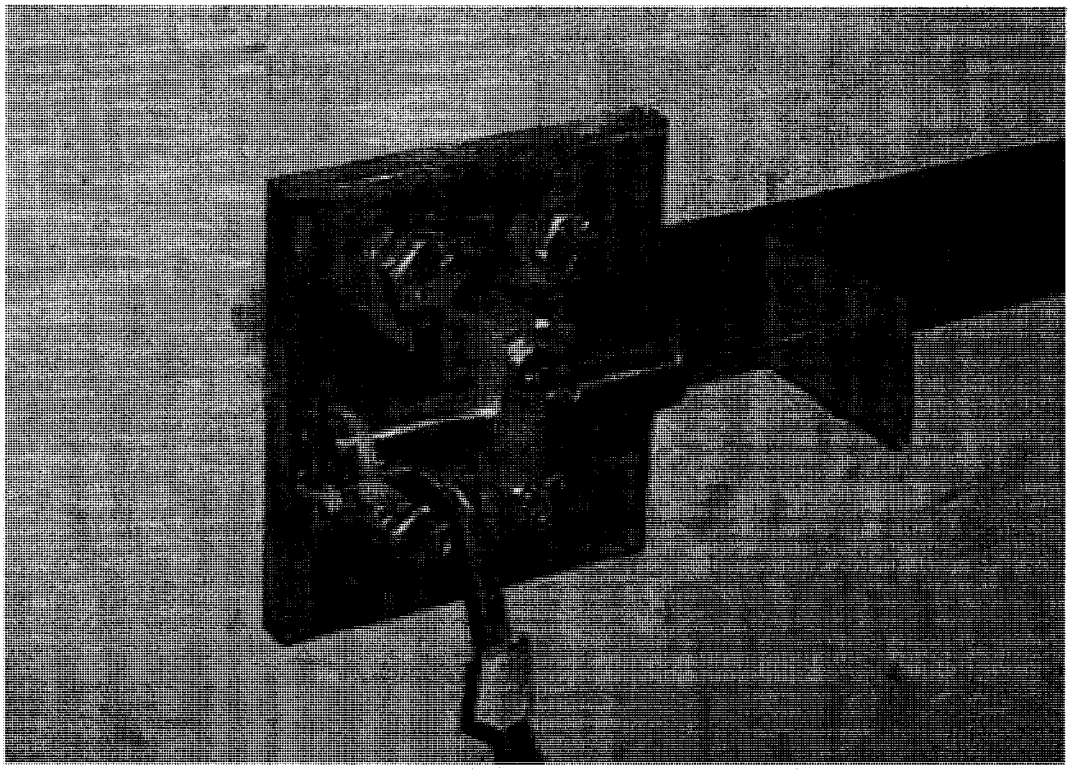

Figure 2.8. Mechanically end-anchored FRP strip application (Soudki 2005)

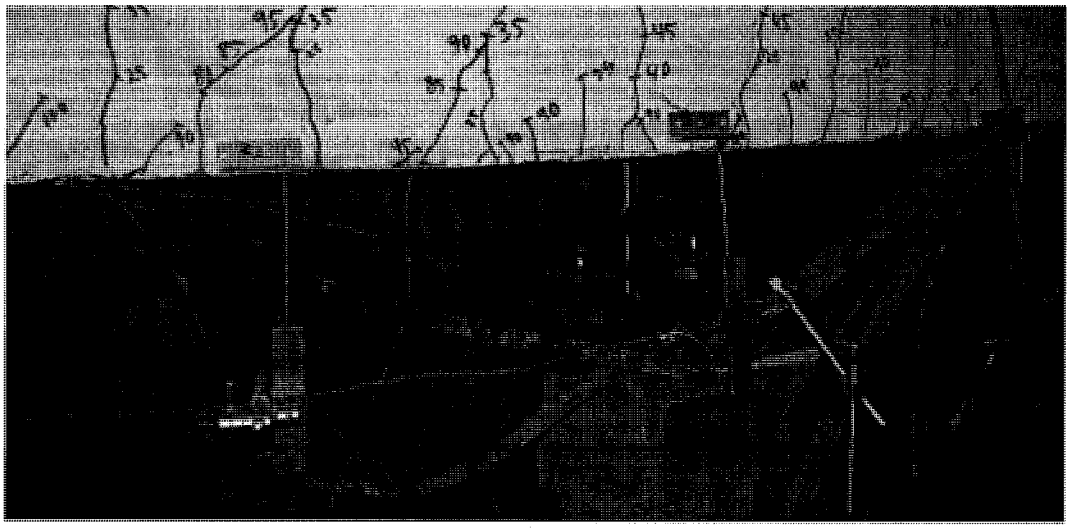

Figure 2.9. FRP sheet rupture failure mode

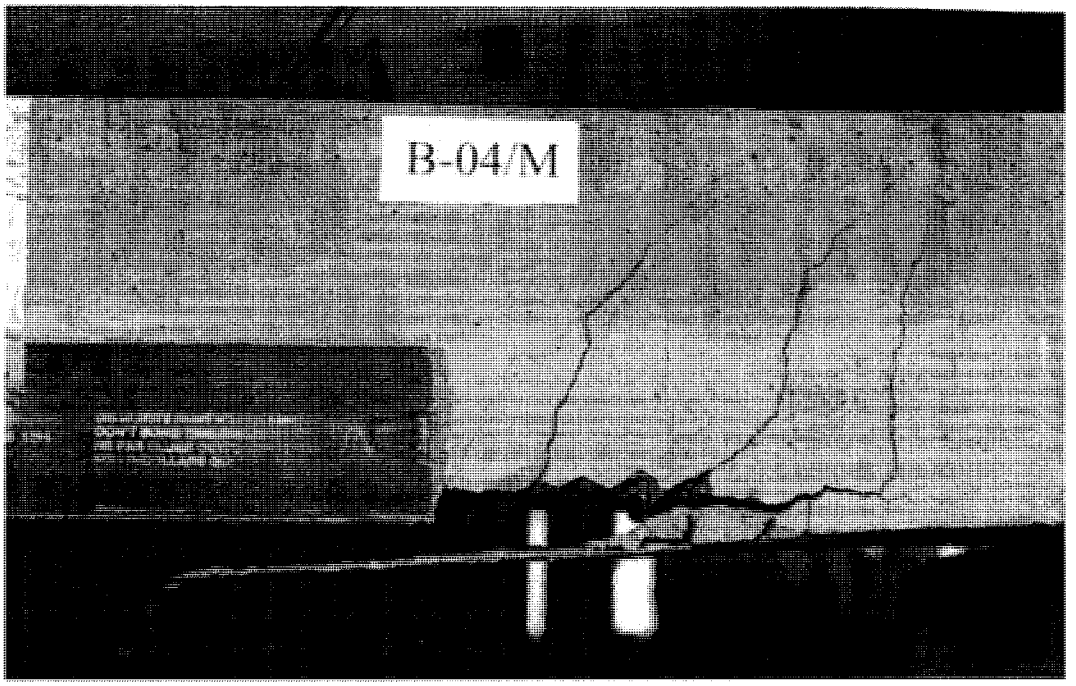

Figure 2.10. FRP strip end debonding failure mode (Kotynia 2005)

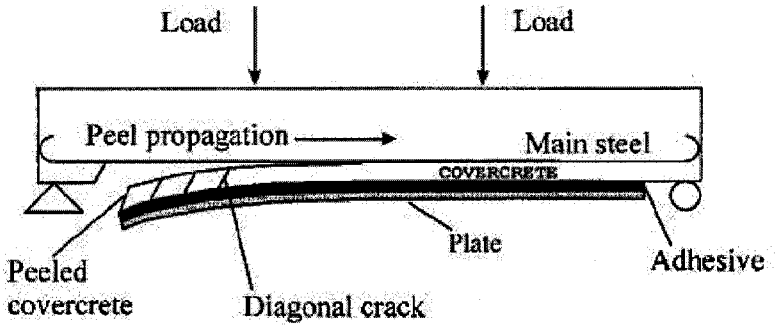

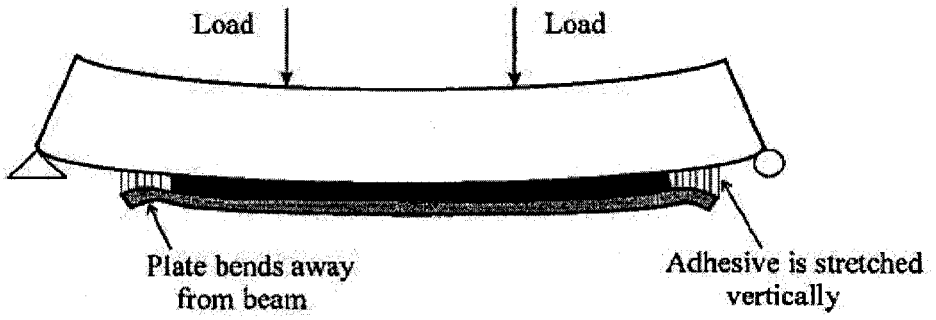

Figure 2.11. FRP strip end debonding failure mode (Sebastian 2001)

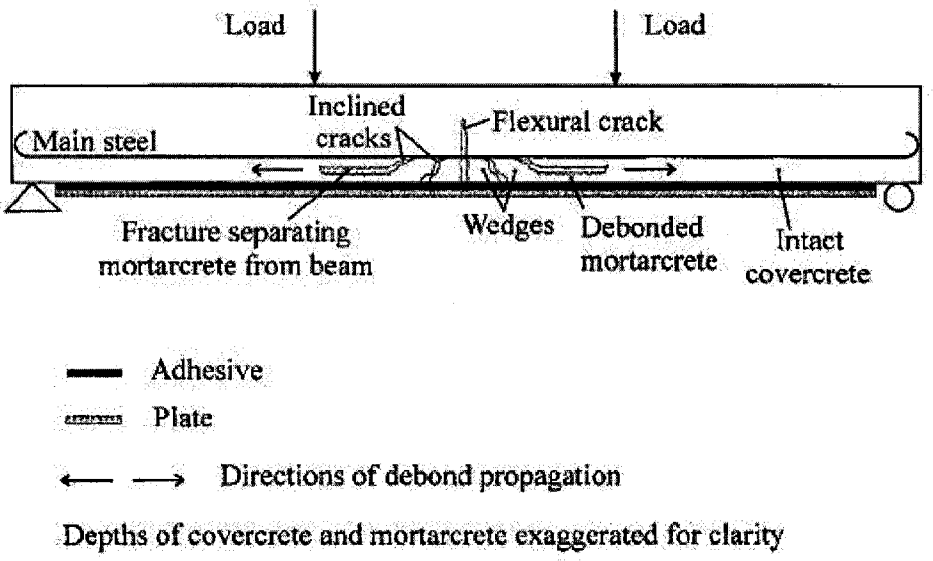

Figure 2.12. FRP strip mid-span failure mode (Sebastian 2001)

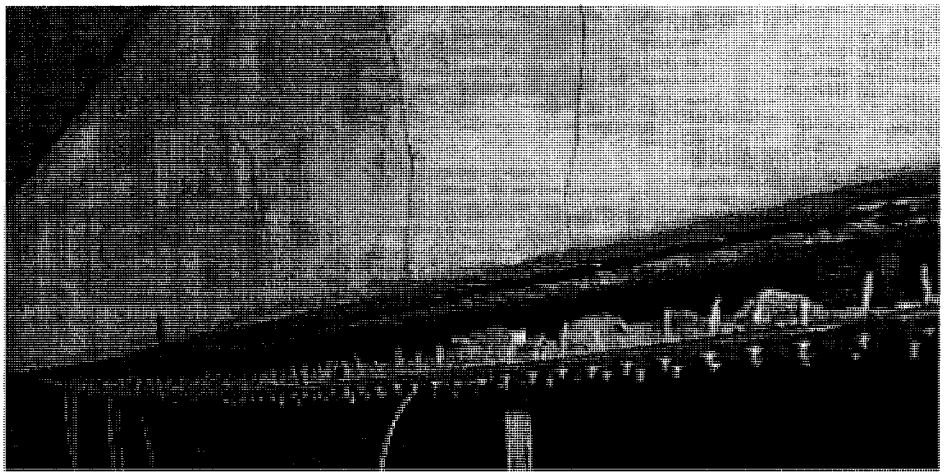

Figure 2.13. Mechanically anchored FRP strip failure mode (Borowicz 2002)

CHAPTER 3

Experimental Work

3.1. Test program for beams strengthened in Shear

3.1.1 Anchored U-shaped dry Caron Fibre (CF) sheet proposed method

Figure 3.1 shows a schematic diagram of the anchored U-shaped dry Carbon Fibre (CF) sheet proposed method for shear strengthening of RC T-beams. The method relies on utilizing the full mechanical contribution of the dry CF sheets, which will be activated upon widening of the shear cracks and development of strain in the RC web, and transferring them through a longitudinal steel rod to the core of the compression web-flange zone by means of mechanical anchors. In order to keep the attractive feature of corrosion-resistance of CF, it is recommended that the steel rod and anchors are made of a non-corrosive alloy. It is anticipated that the proposed method will be less time consuming and consequently cost-effective compared to conventional epoxy-bonding methods. Also, using mechanical anchors, rather than epoxy-based materials, is expected to have more uniform and predictable behaviour and performance of the CF rehabilitation system with time. It is recommended to provide a protection to the dry CF sheets against possible vandalism of the dry fibre sheets.

In order to evaluate the relative shear enhancement of epoxy-bonded and the proposed rehabilitation techniques, three half-scale RC T-beams were tested up to failure. The term S- represents that the beams were to be strengthened in Shear; C-O is for the

Control Original beam; E-B is for the beam strengthened using Epoxy-Bonding technique; and M-D is for the new Mechanical-anchored Dry CF technique. S-C-O was designed to have flexural capacity that is approximately 1.7 times higher than the shear resistance, in order to guarantee a shear failure in the T-beam. To reinforce the T-shape beams in flexure, two 25M bars with a 27.6 mm nominal diameter were used to provide the targeted flexural capacity. The beams were tested in four-point bending. The total length of the beams was 2.4 meters, with shear-spans of 575 mm, which results in a shear-span-to-depth ratio of 2.0. 10M U-shaped stirrups (with 11.3 mm nominal diameter) at a spacing of 250 mm were used as shear reinforcement. The yield strength of the longitudinal reinforcement and stirrups was 462 MPa. Figure 3.2 shows a typical cross section of the control T-beam and the layout of the reinforcement. The beams were cast with ready-mix concrete. The concrete compressive strength at 28 days for the three specimens is shown in Table 3.1. Also, the three tested T-beams were strengthened in the web area using 5/32 inch thick steel plates bolted to the beams' web above the support location in both sides by 4 medium duty 3/8 inch bolts to prevent any possibility of local failures above the supports.

3.1.2. Test Setup

The test setup shown in Figure 3.3 consisted of a four-point loading system that created a zone of constant moment at mid-span. All three beams were tested under the four-point loading over the span of 1900 mm up to failure. The shear span on each side equaled 575 mm and the distance between the two loads was 750 mm. The shear-span-to-depth ratio was approximately 2.0. The strains in longitudinal reinforcement stirrups and

several locations of CFRP were monitored and recorded during the test. Also deflections were measured at the mid-span and the loading point's locations. The crack opening and propagation were checked by visual inspection during the test.

3.1.3. Test Specimens

3.1.3.1. Beam S-C-O

Beam S-C-O is the control beam. The tested beam represented a ½-scale prototype of RC T-beam. The beam was simply supported over the span of 1900 mm with a height of 280 mm, flange width of 420 mm, flange height of 80 mm and web width of 155 mm. The longitudinal bottom reinforcement was identical for all tested beams. Two 25M bars (ρ = 2.5 %) were used for the flexural reinforcement, while two layers of a mesh of 102 $\times$102 18/18 with area of steel equal to 107 mm^2 were used for the compression zone in the flange. U-shaped stirrups made of 10M rebars were used for transverse reinforcement. The beam was designed to guarantee a shear failure. Therefore, minimum acceptable shear reinforcement by the code was used. The corresponding shear force for the maximum nominal resisting moment of the T-beam's cross-section was 70% bigger than the maximum nominal shear resistance of the cross-section. The cross-section was still designed as an under-reinforced beam in flexural design.

3.1.3.2. Beam S-E-B

Beam S-E-B had the same dimensions and internal reinforcement as beam S-C-O, yet it was strengthened using U-shaped bonded CFRP jackets in its shear spans as external shear reinforcement. Figure 3.4 shows strengthened beam S-E-B in elevation and

cross section. The jackets were made of single CFRP sheet with the fiber in the direction perpendicular to the longitudinal axis of the beam. In this case, the CFRP sheets were wrapped around the web sides and extended below the two flanges to provide a minimum anchorage length of 100 mm. Before bonding the FRP sheets to the web and the bottom of the flange of the beam, composite sheets were cut to the required length. The type of FRP that was used to externally strengthen the T-beams was uniaxial carbon fiber (Tyfo SCH-11UP, Fyfe 2006). The CFRP sheets were bonded to the test beam according to the instructions provided by the manufacturer (Fyfe 2006). The two components of the epoxy were carefully mixed using a mixing paddle and electric drill motor. A thin coat of epoxy was applied to the area where sheets were to be applied on the RC T-beam, as well as both sides of the composite sheets using roller. The sheets were then applied to the epoxy-coated concrete beam surface and rolled out with a roller to release the confined air and ensure proper bonding. (Figure 3.2) shows the externally bonded CFRP sheet after its application. Tables 3.3 to 3.5 show the properties of CFRP sheets (Tyfo SCH-11UP) and epoxy adhesive (Tyfo S Epoxy) used for bonding process, respectively. Figure 3.5 shows the strengthened zone of the beam S-E-B.

3.1.3.3. Beam S-M-D

Beam S-M-D had the same dimensions and internal reinforcement as beam S-C-O, yet it was strengthened by the anchored U-shaped dry CF sheet system. Dry CF sheets were wrapped around and bonded to two round steel rods with 1 inch diameter using Tyfo S Epoxy which is the same adhesive epoxy that was used to bond the CFRP sheets in the beam S-E-B (Figure 3.6). Then the concrete and the steel rods were drilled in

specific locations in the two corners of web-flange intersection of the T-beam. The locations of the anchors were designed such that the rod does not fail before the dry CF sheet reaches its ultimate capacity. The two end rods were anchored to the T-beam in the drilled points with heavy duty HSL-3 M10 Hilti bolts (Hilti 2007) to create a U-shaped dry CF jacket around the shear span zone (Figure 3.7). In both beams, S-E-B and S-M-D, the bottom corners of the web were chamfered at a radius of 10 mm in order to avoid stress concentration and premature rupture of carbon fibres.

3.2. Test program for beams strengthened in Flexure

3.2.1. Proposed system for increasing flexural strength and ductility capacities

The proposed flexural strengthening system is mainly composed of an FRP sheet(s) that could be bonded (or not) to the soffit of the RC beam. The FRP sheets are wrapped around two steel plates at its ends (i.e. with a 180°) and then epoxy-bonded (through an overlap) to the original FRP sheet. The steel plates have rounded corners in order not to have stress concentration and rupture of FRP sheets. The overlap is to avoid debonding between the FRP sheets (usually > 150 mm). The steel plate is then linked to an angle that is anchored to the beam-support corner, through two steel link members (one at each side of the beam). The steel link member (looks like a conventional tensile test coupon sample) is linked to the steel plate and the anchored angle by means of high tensile threaded steel rods. According to this setup, the steel link members will always have axial tensile forces with no moments in them. The total cross-sectional area of the steel link members at one side of the beam are designed to have a yield stress that is less

than the ultimate strength of the total FRP sheets. As such, the FRP sheets will transfer the stresses to the link members, than would yield before FRP ruptures. The total cross-sectional area of the steel link members, and consequently the total area of FRP, should be designed to achieve the targeted increase in the strength of the beam. Also, in order to keep the attractive feature of corrosion resistance of FRP, it is recommended that the steel mechanism and anchors are made of non-corrosive alloy. Figure 3.8 shows the details of the proposed strengthening system. Figure 3.9 shows the expected (designed) contribution of the strengthening system to the flexural capacity and ductility of the RC beams. Table 3.6 shows the details of the test variables in the experimental program.

In order to evaluate the relative flexural performance enhancement of epoxy bonded and the proposed rehabilitation technique, four half-scale RC T-beams with two column stubs were cast, with the main flexural steel reinforcement ratio selected to ensure under-reinforced behaviour (i.e. tension-controlled section) with a reinforcement ratio of 0.92%. Figure 3.10 shows the dimensions and details of reinforcement of the four tested beams. The flexural tension reinforcement consisted of two 15M rebars. A mesh of 102×102 18/18 was used in the flange of the T-beam to represent typical slab reinforcement. The stirrups used were 10M U-shaped rebars spaced at 165 mm. The beams were overdesigned in shear (shear capacity is > 200 % higher than flexural capacity) to avoid a brittle shear failure. The column stubs were reinforced with four 20M rebars as longitudinal reinforcement enclosed by 10M ties.

All four beams were tested under four-point loading, where the variation amongst the beams was the strengthening method. The strains in longitudinal reinforcement, several locations of CFRP sheet, and steel link members (whenever applicable) were

monitored and recorded during the tests. Also deflections were measured at the mid-span and the loading points and the mid point of the shear span locations. The crack opening and propagation were checked by visual inspection and marked on the beams during the tests.

3.2.2. Test Setup

All T-beams were tested under four point bending with a span of 3000 mm and a shear span of 1100 mm. The beams were tested under an increasing monotonic load up to failure, or after reaching the end of the stroke of the actuator which is 100 mm. The T-beams were connected to two column stubs that were simply supported using hinge and roller supports, 3000 mm apart. One linear variable differential transducer (LVDT) was placed under the mid-point of the T-beam to measure the vertical deflection while a calibrated load cell was used to record the load. Four other LVDTs measured the vertical deflection at the loading points and the mid point of the shear span locations.

Eight strain gauges were mounted on critical locations along the length of the two longitudinal bars, two at the mid-span, four at the loading points and two at the mid point of the shear span as shown in Figure 3.11. In addition, five strain gauges were installed on the flexural strengthening CFRP sheets of the T-beams, at the mid-span and the loading points and the mid point of the shear span. These strain gauges were attached to the CFRP sheets on the beams F-E-B, F-M-U, and F-M-B and oriented along the fibre direction as shown in Figure 3.11.

3.2.3. Test Specimens

All tested beams in flexural strengthening were identical in size and proportion, with similar longitudinal and transverse reinforcement. Beam F-C-O was tested as a control beam without any strengthening systems. Beam F-E-B was strengthened with conventional epoxy-bonded FRP sheets. Beam F-M-U was strengthened with the new unbonded hybrid FRP sheet / ductile anchor system. In this beam, epoxy was applied to the FRP sheet, yet the FRP was not bonded to the beam. Beam F-M-B was strengthened using the same anchorage system of beam F-M-U, yet the FRP sheet was bonded to the soffit of the beam by epoxy. The three strengthened beams were strengthened using one layer of carbon FRP (CFRP) sheet.

3.2.3.1. Beam F-C-O

The tested beam represented a ½-scale prototype of RC T-beam. The beam was simply supported over the span of 3000 mm with a height of 280 mm, flange width of 420 mm, flange height of 80 mm and web width of 155 mm. The control beam was designed to satisfy the requirements of the CSA Standard A23.3-04 (2004) Design of concrete structures. The longitudinal bottom reinforcement was identical for all tested beams. Two 15M bars (ρ = 1%) were used for the flexural reinforcement, while two layers of a mesh of 102×102 18/18 with area of steel equal to 107 mm^2 were used for compression zone in the flange. U-shaped stirrups made of 10 mm diameter bars were used for transverse reinforcement. The column stubs were reinforced with four 20M rebars as longitudinal reinforcement surrounded by 10M ties. Figure 3.12 shows beam F-C-O before test.

3.2.3.2. Beam F-E-B

This specimen is strengthened in flexure using externally epoxy-bonded FRP method. Before bonding the FRP sheets to the soffit of the beam, composite sheets were cut to the required length. The CFRP sheets, Tyfo® SCH-11UP carbon fibre sheets (Fyfe 2006), were bonded to the test beam according to the instructions provided by the manufacturer (Fyfe 2006). The two components of the epoxy were thoroughly mixed using a mixing paddle and electric drill motor. A thin coat of epoxy was applied to the soffit of the RC T-beam in the area where sheets were to be applied, as well as to the both sides of the composite sheets using roller. The sheets were then applied to the epoxy-coated concrete beam surface and rolled out with a roller to ensure proper bonding. Figure 3.13 shows beam F-E-B before test.

3.2.3.3. Beam F-M-U

Specimen F-M-U was strengthened using hybrid FRP/ductile steel anchorage system to mechanically strengthen the RC T-beam in flexure. The ductile anchor that holds the CFRP sheet under the soffit of the specimen consisted of one steel plates, 160×40×13 mm having two threaded 3/8" holes in its thickness, one steel angle, L 64×64×13 mm having one hole in the middle and two threaded 3/8" holes in its thickness (the angle is 160 mm long), two steel tensile link members (typical coupon samples for steel tension test), four high tensile 3/8" threaded rods (f_y = 724 MPa and f_u = 862 MPa) and one heavy duty HSL-3 M 24/60 Hilti bolt (Hilti 2007) at each end. The steel angle was fastened by the heavy duty Hilti bolt with 45° inclination located in the pre-drilled hole at the middle of the intersection point of the T-beam's soffit and the

column stub. The two tensile steel link members connected the angle to the steel plate via high tensile 3/8" rods which located in the holes in the thickness of both angle and the plate and it was fastened using nuts. A photo of the anchorage system is shown in Figure 3.14.

3.2.3.4. Beam F-M-B

Specimen F-M-B was strengthened with one externally-bonded CFRP sheet that is anchored at its ends using the hybrid FRP / ductile anchorage system. The CFRP sheet was bonded to the test beam according to the instructions provided by the manufacturer (Fyfe 2006). At the same time, the two ends of the CFRP sheet were wrapped around the hybrid FRP / ductile anchors. While the epoxy was curing, two HSL-3 M 24/60 Hilti bolts were fastened to the pre-drilled holes. This caused the FRP sheet to stay firm while the epoxy is hardening. The hybrid FRP / ductile anchorage system along with the externally bonded FRP method were meant to act like a safety net in case if the CFRP sheet debonded. In this manner, after the FRP sheet debonds, the hybrid FRP / ductile anchorage system comes into action and the load transfer will be through the mechanical end anchorage and not through shear transfer provided by epoxy bonding.

On the other hand, there is another possible behaviour in which the presence of the hybrid FRP / ductile anchorage system prevents the debonding of the CFRP sheet, and in this case the failure mode will be through the FRP rupture. This mode of failure could be a desirable failure mode. Also, as it will allow the utilization of the full capacity CFRP sheet, which in turn increases the flexural capacity of the strengthened beam.

3.3. Materials

This section describes the properties of the materials used in constructing and strengthening the seven half-scale RC T-beams strengthened in shear and flexure.

3.3.1. Concrete

Ready mix concrete supplied by a local vendor for the construction of all of the T-beams was poured in the formworks in two separate sessions for shear test beams and flexural test beams. Concrete with 28^{th} day compressive strength of $f_c' = 30$ MPa with maximum aggregate size of 10 mm and slump of 110 mm was ordered from the ready mix plant. The concrete slump provided proper concrete workability during the concrete casting in the formworks (See Figure 3.15). While pouring concrete, a total of 18 concrete cylinders (100 mm×200 mm) were cast and cured in the same circumstances as the test specimens. The curing procedure consisted of moist curing by covering the whole beam with burlap. Three cylinders were tested after 3, 7, and 28 days. Another six were tested on the day of testing of the beams leaving 2 cylinders per beam. Also three cylindrical specimens were used to test the tensile strength of used concrete on the 28^{th} day. Table 3.2 and 3.3 show the results for the concrete compressive and tensile strengths in different ages from casting the beams for both beams strengthened in shear and flexure.

3.3.2. Steel reinforcement

The beams were designed according to CSA A23.3-04 (2004). The beams strengthened in flexure were highly reinforced in shear in order to prevent shear mode of

failure. Vice versa, the beams that were strengthened in shear were relatively over designed in flexure to make sure that the beams will fail in shear. In both cases, the condition of under reinforcement of the beams in flexure was respected and area of steel which was designed in shear and flexure rebars was within the limit of minimum and maximum allowable amount according to CSA A23.3-04 (2004). In specimens strengthened in flexure, the longitudinal reinforcement used was 15M (15.96 mm nominal diameter) with cross-sectional area of 200 mm^2 deformed steel rebars. In the specimens strengthened in shear 25M (15.96 mm nominal diameter) with cross-sectional area of 500 mm^2 was used as longitudinal rebars. 10M rebars (11.3 mm nominal diameter) with cross-sectional area of 100 mm^2 were used for stirrups in both types of specimens. Also steel meshes of 102×102 18/18 were used as the top reinforcement (flange reinforcement) in all beams.

Samples of the rebars were tested to obtain their tensile stress-strain relationship. The tested rebars had an average yield strain of 2310 microstrain, yield stress of 462 MPa, modulus of elasticity of 200 GPa and tensile strength of 571 MPa with the maximum elongation of 16.9%. The stirrups were made of steel with the same mechanical properties.

3.3.3. CFRP strengthening sheets

The CF sheet that is used in this program is carbon hybrid sheet with a vinylester resin. The beams is strengthened using Tyfo® SCH-11UP unidirectional carbon fibre sheets (Fyfe 2006) which comes in $24" \times 300'$ roll and a two-component epoxy resin to be mixed and applied to the fibres to form the composite material, used in the cases of wet

FRP. The carbon fibres are characterized by a very high tensile strength, a linearly elastic stress-strain relationship up to failure, and a modulus of elasticity slightly higher than that of steel. Researchers in the manufacturers company determined the sheet properties through tensile testing of the composite. Table 3.3 shows the typical dry fibre properties while Table 3.4 shows the composite gross laminate properties as provided by the supplier (Fyfe 2006). Also Table 3.5 shows the characteristics of the used two component epoxy. Comparing the results of the tensile characteristics of the dry CF and wet CFRP, it could be seen that dry CF has significantly higher tensile characteristics.

3.3.4. Fasteners

Hilti mechanical anchors were used to attach the designated steel parts to RC T-beams for each test. For the beams strengthened in flexure, Hilti HSL-3 22M were used to fasten the hybrid FRP / ductile anchors to the T-beam and column stubs connection. The Hilti HSL-3 heavy duty sleeve anchor is a torque-controlled expansion bolted designed for high performance in static and dynamic application including the tension zone of concrete structures where cracking can be expected. These heavy duty bolts are also corrosion resistant due to their zinc plating carbon steel. This type of Hilti bolts have force-controlled expansion which allows for follow-up expansion.

For the beams strengthened in shear, Hilti HSL-3 10M was used to connect 1 inch steel rod (U-shaped dry CF jackets) to the intersection of the flange and the web in the RC T-beams. Furthermore Hilti HLC 3/8 inch was used to fasten, shear-strengthening 5/32 inch steel plates in the support area and out of the shear span. Figure 3.16 shows photos of the bolts used in this research.

3.4. Construction of T-Beams

The construction of T-beams involved wooden formwork preparation, steel rebar cage assembly, installation of the strain gauges, casting and curing concrete, and finally stripping the formwork.

3.4.1. Preparation of formworks

The formworks were manufactured in two different sessions for each of the shear test specimens and flexural test specimens using 3/4 inch plywood. To prevent any undesired lateral movement or change in dimensions during casting, the formworks were braced using the T-shaped wooden endings at the two ends and the U-shaped pieces of wood on the top. The interior sides of the wood sheets were coated by 3 thin layers of wax oil paint to ease their removal after hardening of the concrete (Figure 3.17 and 3.18).

3.4.2. Preparation of steel rebar cages

All the rebars were cut and bent to the designed dimensions by a local supplier. Before assembling the steel cage, electrical strain gauges were installed in the specified locations on the flexural reinforcement and stirrups.

Figures 3.19 to 3.21 show the wooden forms with steel cage before pouring concrete.

3.4.3. Casting and curing concrete

The slump of the concrete mix was 110 mm, which provided adequate concrete workability during the concrete casting in the forms. No segregation or honeycombs in

the cast concrete were noticed. Electric vibrator was used to vibrate the concrete into proper position. The top surface was then trowelled to a smooth surface (Figures 3.22 and 3.23). Eighteen cylinders (100 mm×200mm) were cast simultaneously with each specimen and were cured along the side of the specimens to determine the concrete compressive strength at different ages of the concrete and at the time of testing. After the concrete had set, specimens and cylinders were covered with burlap and moistened regularly. Figure 3.24 shows specimens after pouring concrete. The forms were removed after the beams were cured for seven days.

3.5. Beam Instrumentations

The strain in the flexural rebars and stirrups in different locations and also the strain in the CFRP sheets were monitored using 120 Ω quarter bridge electrical resistance strain gauges with a 5 mm gauge length. Deflections were also measured at various locations using Linear Variable Displacement Transducers (LVDT). During each loading test, load, displacement and strain readings were recorded simultaneously using a data acquisition system at rate of one scan per second. The high-capacity hydraulic jack was used to apply vertical force on the top of the T-beams.

3.5.1. Deflections

The beams were tested under an increasing monotonic load up to failure, or after reaching the end of the stroke which is 100 mm. The vertical displacement was recorded using three vertical linear variable differential transformers (LVDT), each with a gauge length of 100 mm. One linear variable differential transducer (LVDT) was placed under

the mid-point of the T-beam to measure the vertical deflection while a calibrated load cell was used to record the load. Four other LVDTs measured the vertical deflection at the loading points and the mid point of the shear span locations. The readings of the strain gauges, LVDTs and the load cell were scanned and recorded using a data acquisition system.

Each specimen in shear strengthening test was instrumented with 3 LVDT ranging from 50 mm to 100 mm capacity depending on the monitored location. Vertical deflections were measured at various locations along the span using these LVDTs as shown in the Figure 3.25.

3.5.2. Strains

The strains in longitudinal reinforcement, several locations of CFRP sheet, and steel link members (where ever applicable) were monitored and recorded during the tests. Each beam strengthened in shear had 18 strain gauges embedded in concrete, out of which 8 were placed on the longitudinal reinforcement at the centre and at $1/4^{th}$ positions. Ten strain gauges were put on the stirrups to trace their strain in the shear span of the beams. In addition, eight strain gauges were installed on the CFRP sheets on the shear spans of the T-beams. These strain gauges were attached to the FRP on one side of the beams S-E-B and S-M-D and oriented along the fibre direction. Strain gauges were mounted such that they would capture the high strains resulting from the shear cracks as observed when testing the control beam S-C-O. The strain gauges positions are shown in Figures 3.25.

Table 3.1. Results of concrete cylinder tests for beams strengthened in shear (in MPa)

Compression tests (MPa)			Tension test (MPa) after 28 days
3 days	7 days	28 days	
14.53	19.11	34.3	3.16

Table 3.2. Results of concrete cylinder tests for beams strengthened in flexure (in MPa)

Compression tests (MPa)			Tension test (MPa) after 28 days
3 days	7 days	28 days	
20.51	24.97	32.10	3.36

Table 3.3. Properties of dry carbon fibre sheet SCH-11UP (as provided by the supplier Fyfe 2006)

Typical dry fibre properties	Value
Tensile Strength	3.79 GPa
Tensile Modulus	230 GPa
Ultimate elongation	1.70 %
Density	1.74 $\frac{gr}{cm^3}$
Weight per sq. meter	298 $\frac{gr}{m^2}$
Fibre thickness	0.127 mm

Table 3.4. Properties of composite gross laminate SCH-11UP (as provided by the supplier Fyfe 2006)

Composite gross laminate properties	Value
Ultimate tensile strength in primary fibre direction	903 MPa
Elongation at Break	1.05 %
Tensile Modulus	86.9 GPa
Laminate thickness	0.25 mm

Table 3.5. Properties of epoxy adhesive Tyfo S (as provided by the supplier Fyfe 2006)

Epoxy adhesive properties	Value
Tensile Strength	72.4 MPa
Tensile Modulus	3.18 Gpa
Elongation Percent	5.00 %
Flexural Strength	123.4 MPa
Flexural Modulus	3.12 GPa

Table 3.6. Test variables for beams strengthened in flexure

Beam	Concrete compressive strength (MPa)	CFRP sheet condition	Number of layers	Direction of fibre alignment	External anchorage
F-C-O	33.0	--	--	--	--
F-E-B	37.1	Wet-bonded	1	horizontal	--
F-M-U	39.0	Wet-unbonded	1	horizontal	Hybrid CFRP/steel ductile anchor
F-M-B	39.2	Wet-bonded	1	horizontal	Hybrid CFRP/steel ductile anchor

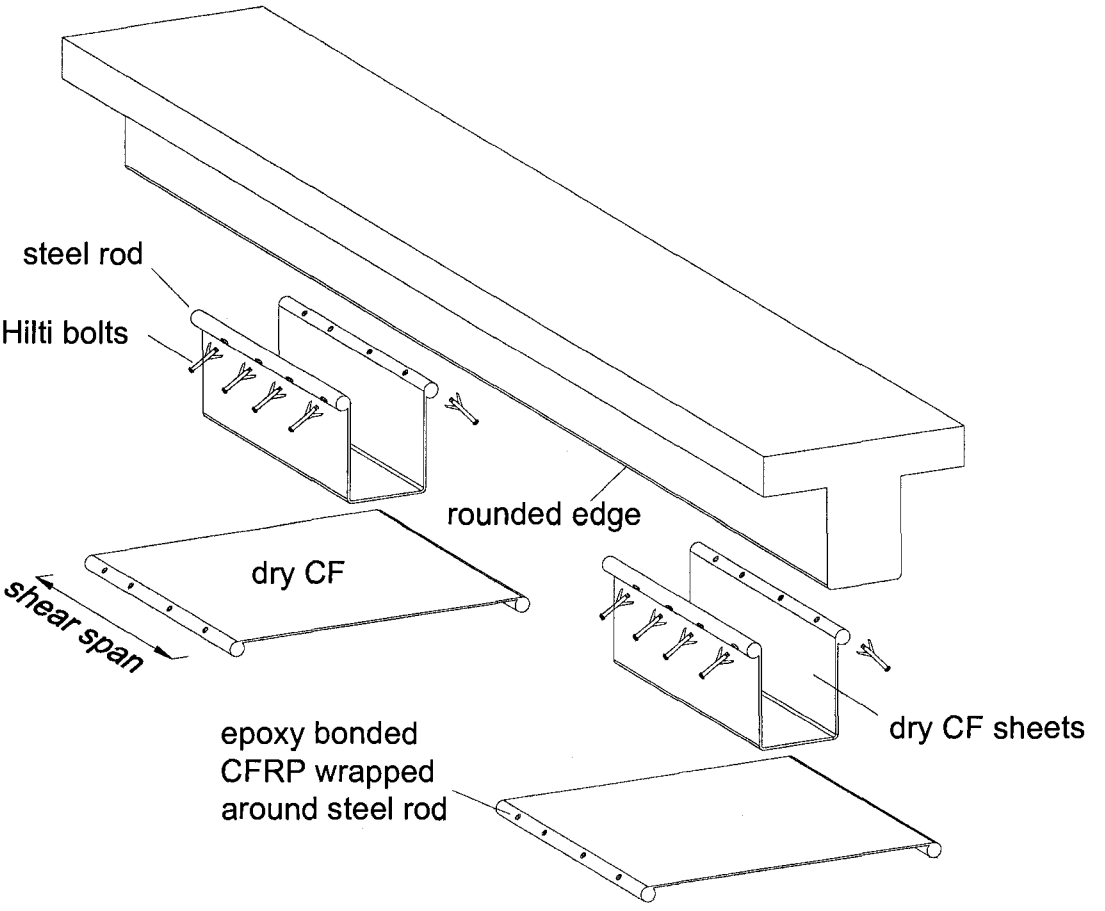

Figure 3.1. Detailed view of the U-shaped dry CF anchorage system

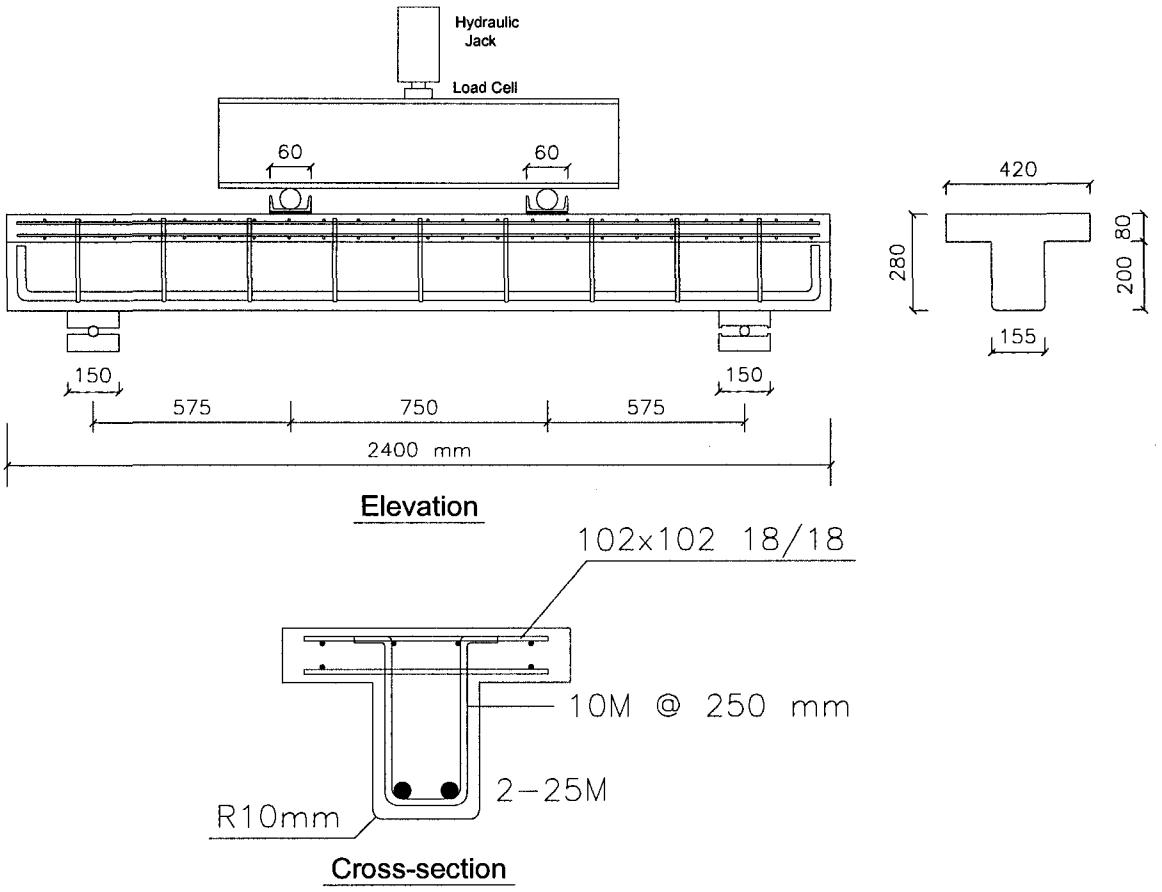

Figure 3.2. Dimensions and details of reinforcement of the three shear-critical tested beams

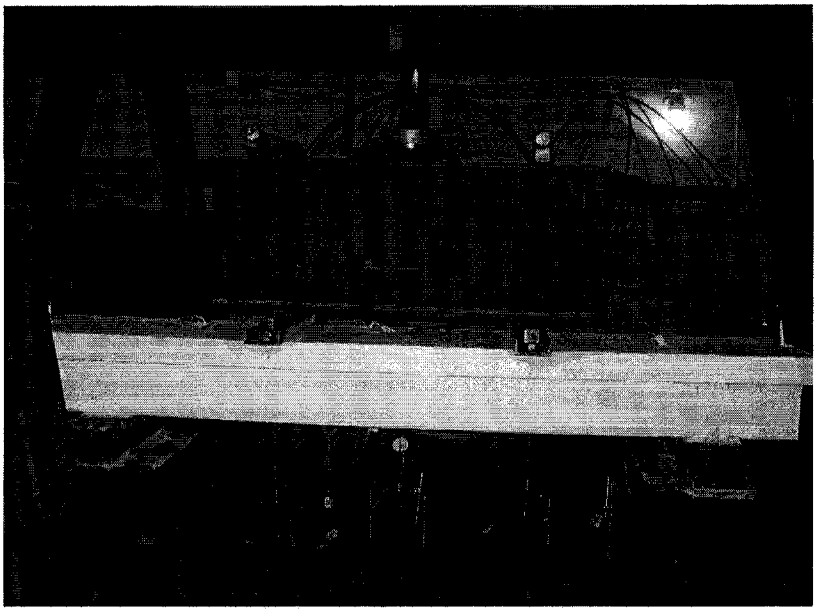

Figure 3.3. Beam S-C-O before test

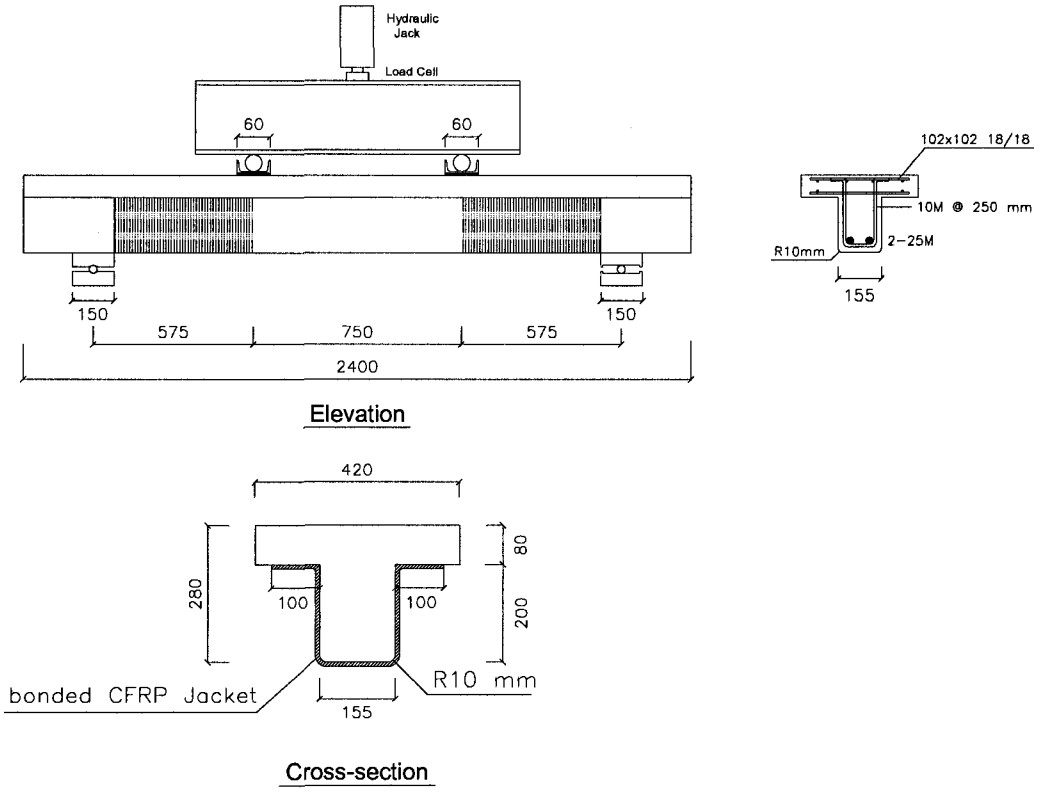

Figure 3.4. Layout of beam S-E-B strengthened with externally–bonded CFRP sheet

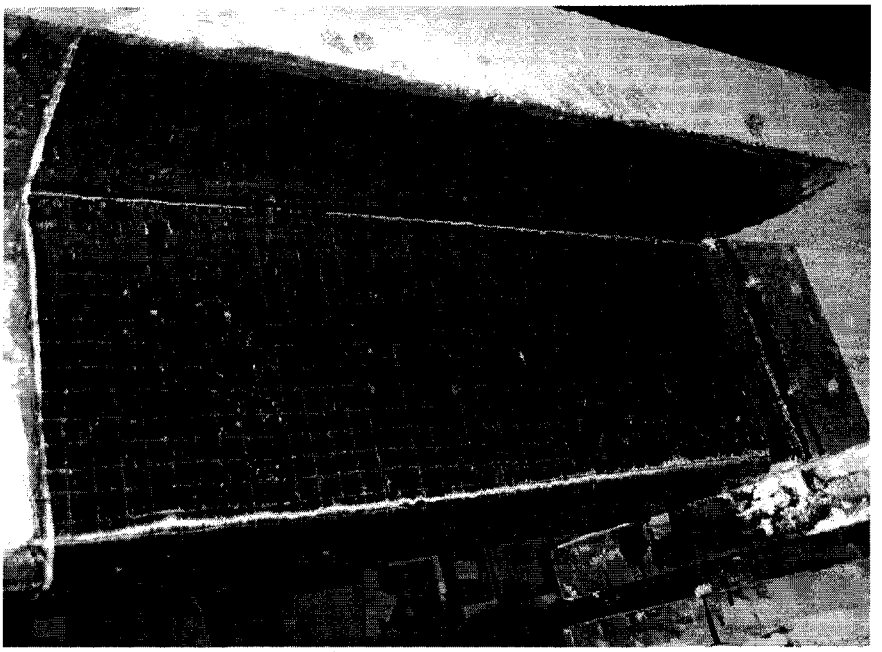

Figure 3.5. Beam S-E-B before test

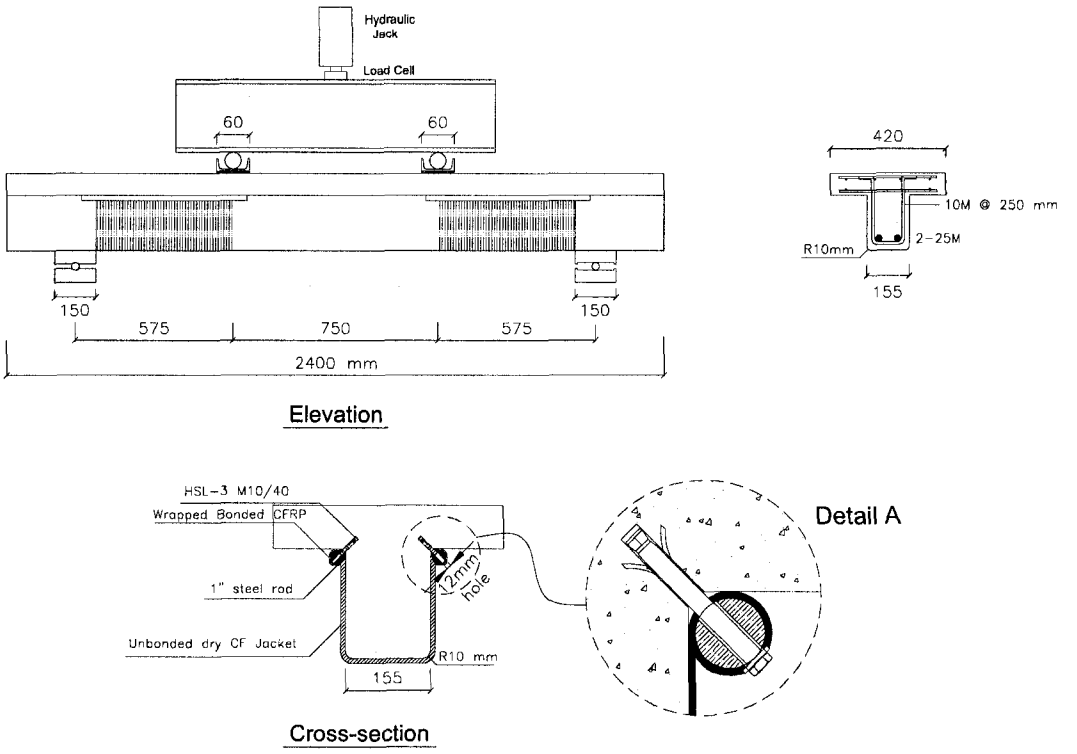

Figure 3.6. Layout of beam S-M-D strengthened using the anchored U-shaped dry CF jacket

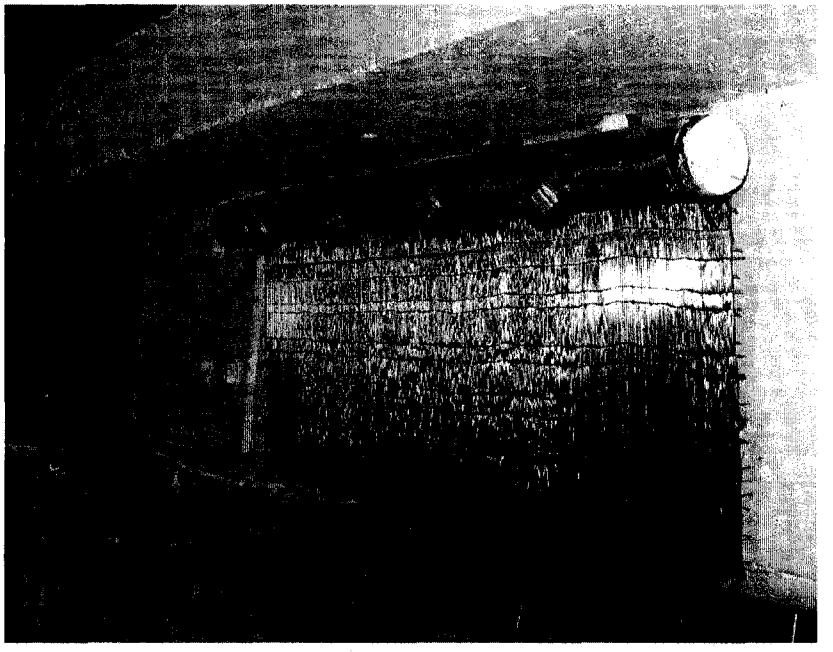

Figure 3.7. U-shaped dry CF jacket around the shear span zone of beam S-M-D

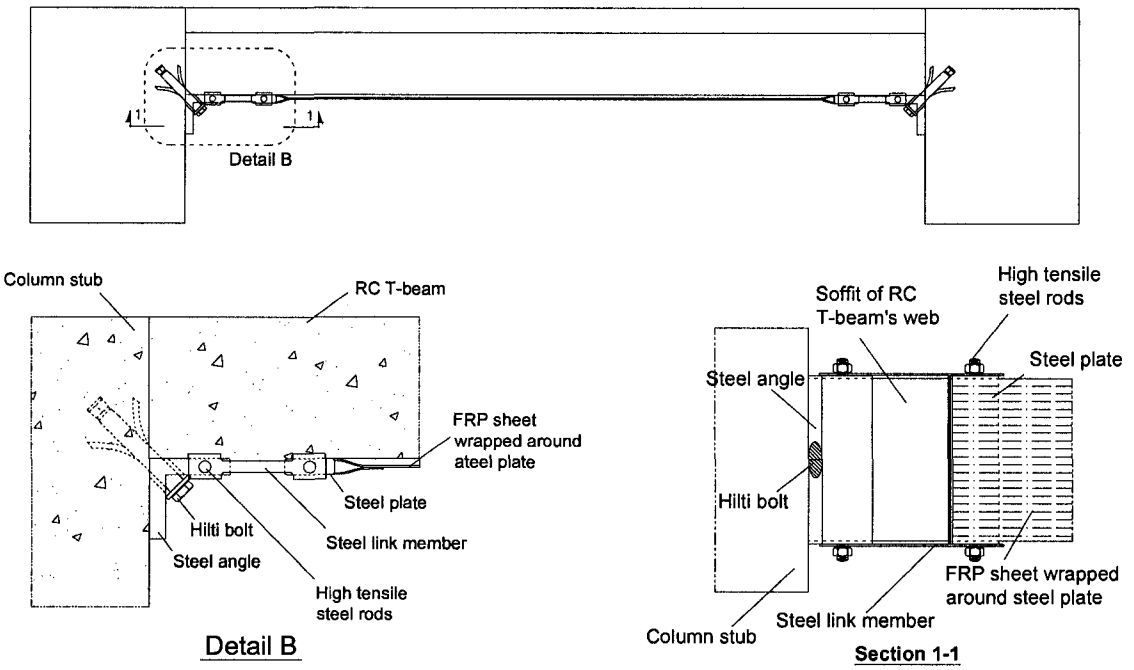

Figure 3.8. Proposed Hybrid FRP / ductile steel anchor system

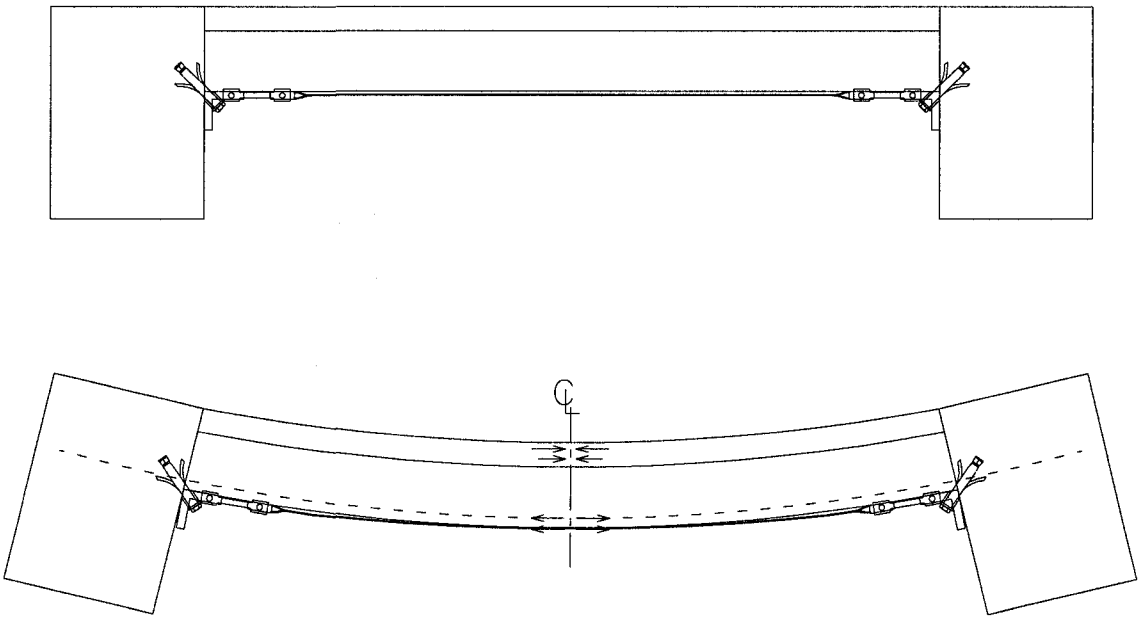

Figure 3.9. Behaviour of beams strengthened with the proposed hybrid FRP / ductile steel anchor system

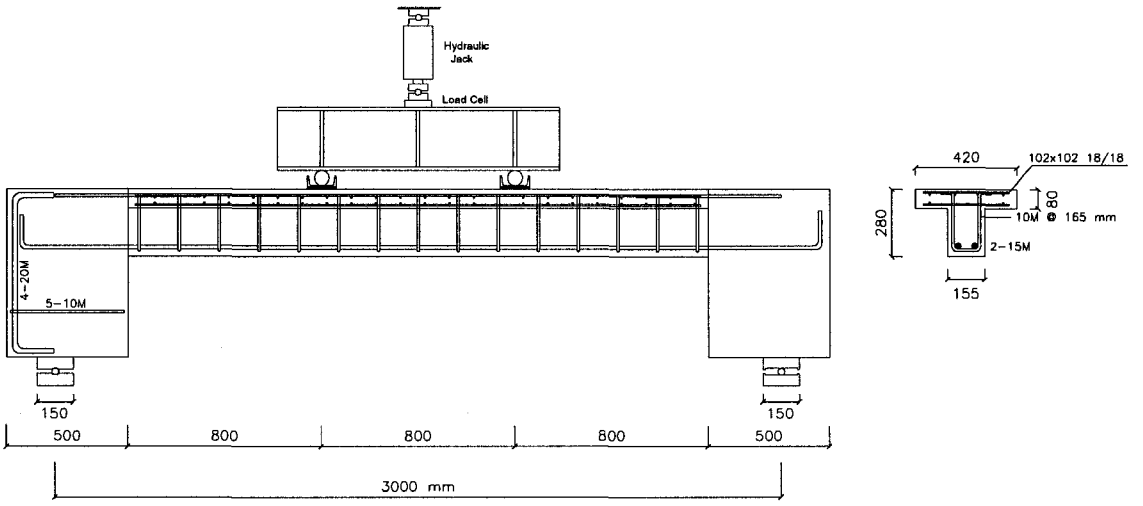

Figure 3.10. Dimensions and details of reinforcement of the four beams strengthened in flexure

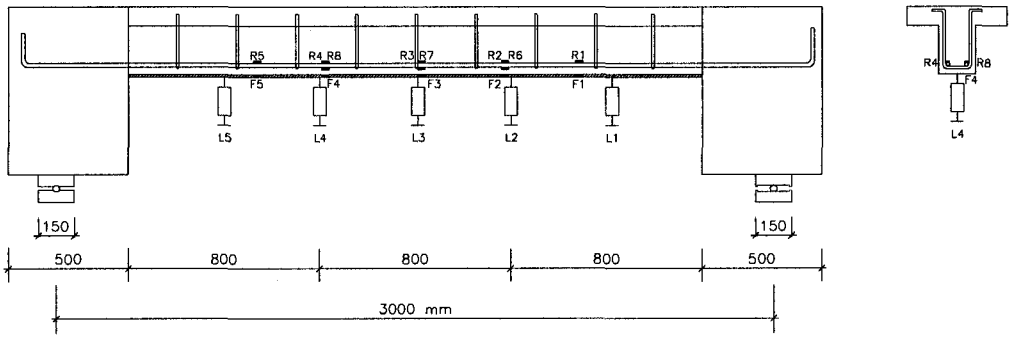

Figure 3.11. Test setup and instrumentation of the T-beams strengthened in flexure

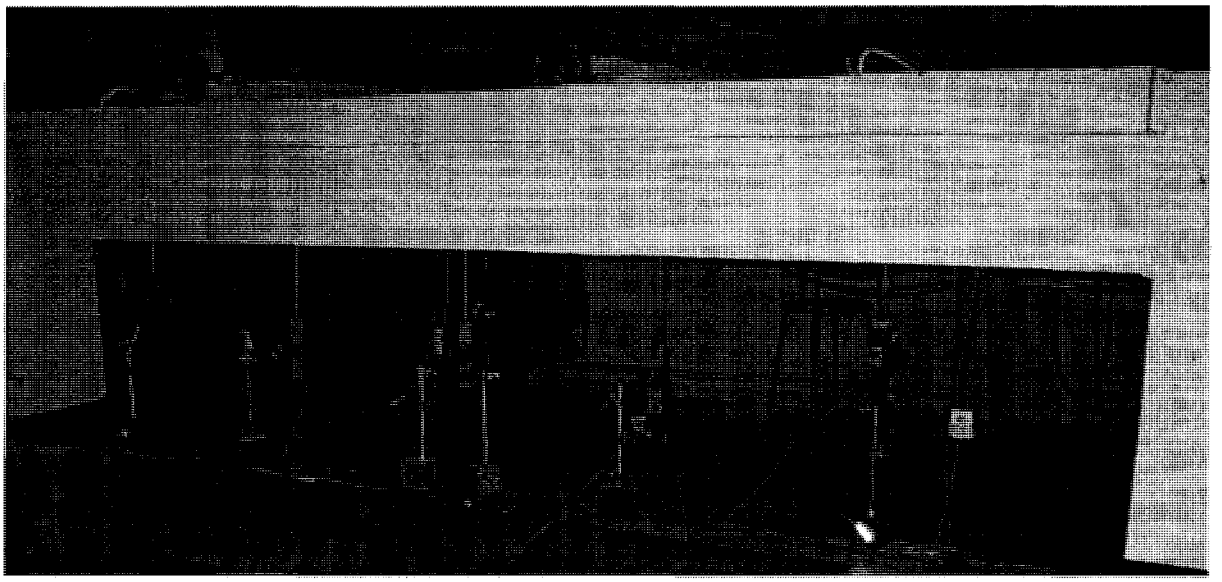

Figure 3.12. Beam F-C-O before test

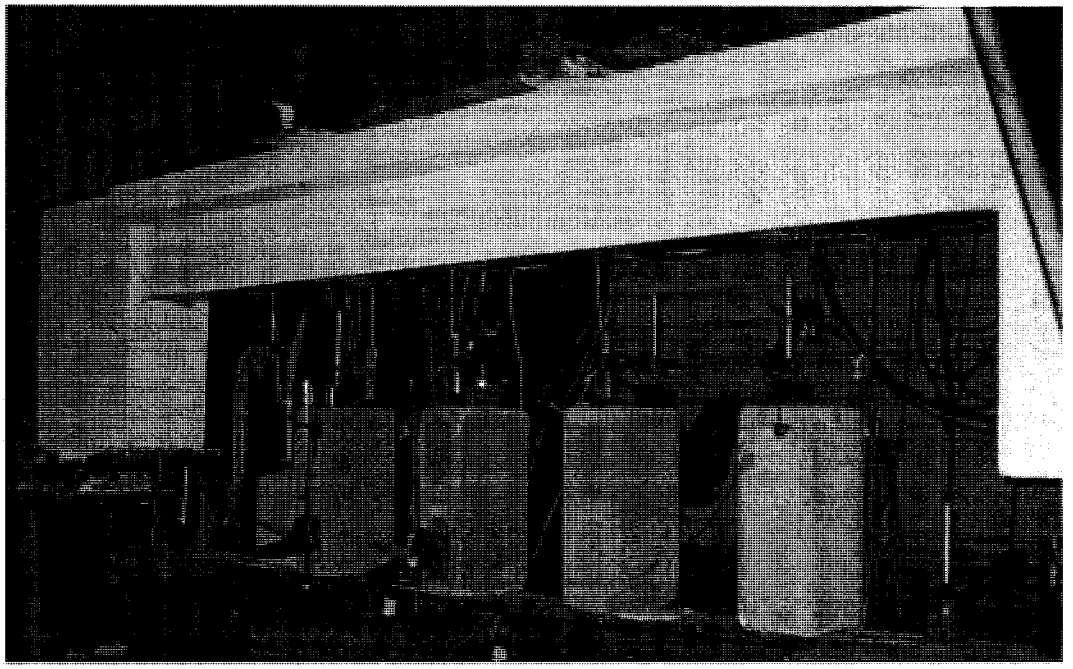

Figure 3.13. Beam F-E-B (strengthened using one layer of epoxy-bonded CFRP sheet) before test

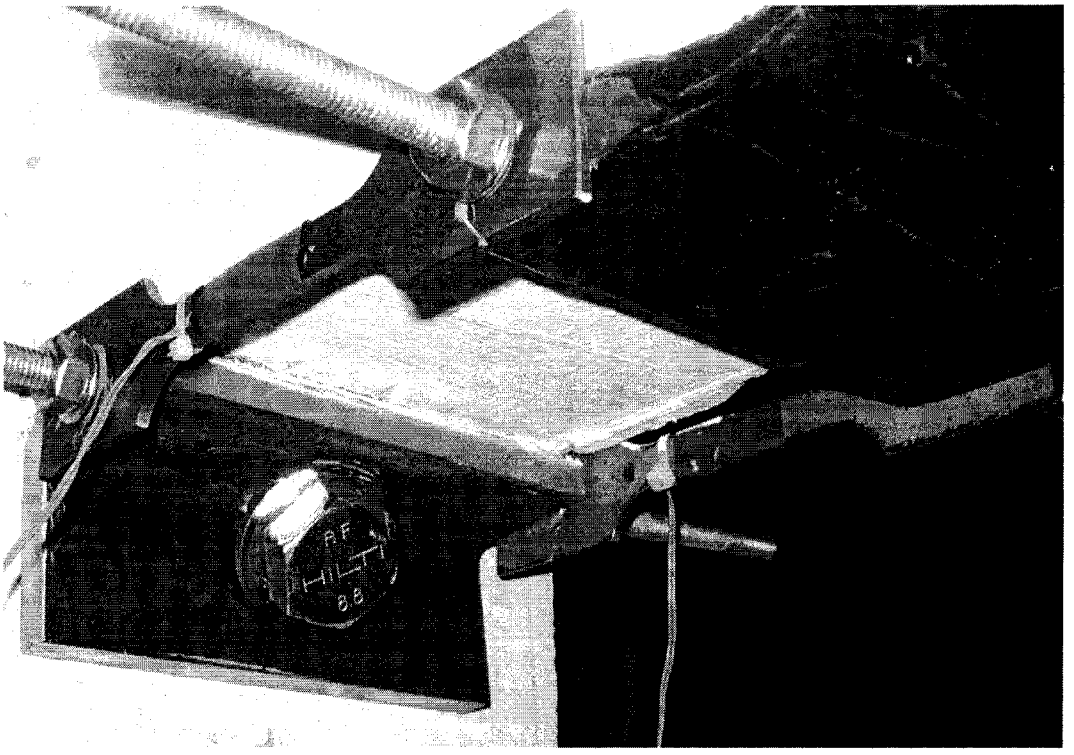

Figure 3.14. Ductile anchor system used in strengthening beams F-M-U and F-M-B

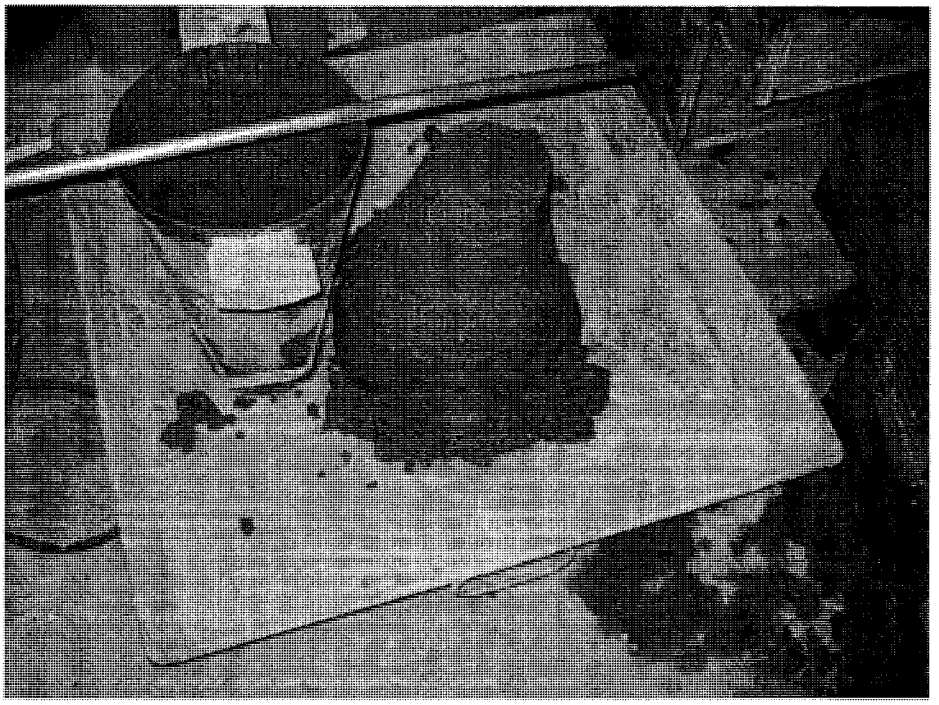

Figure 3.15. Slump test result

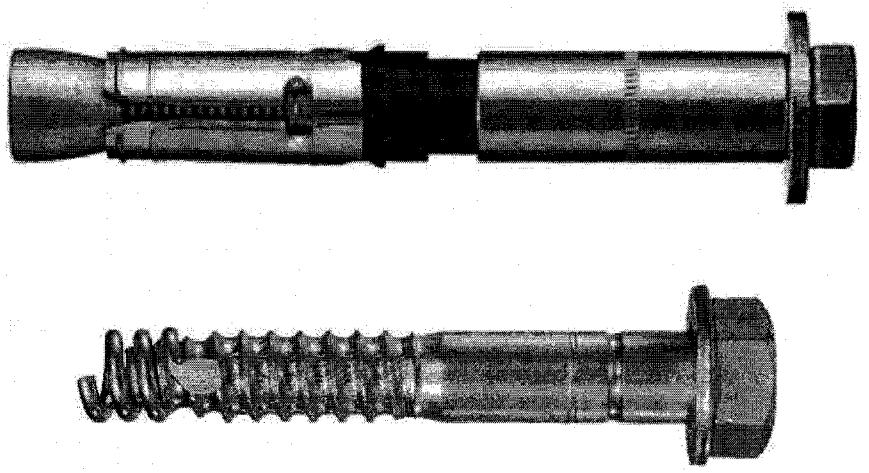

Figure 3.16. HSL-3 (top) and HLC (bottom) Hilti bolts used in the research

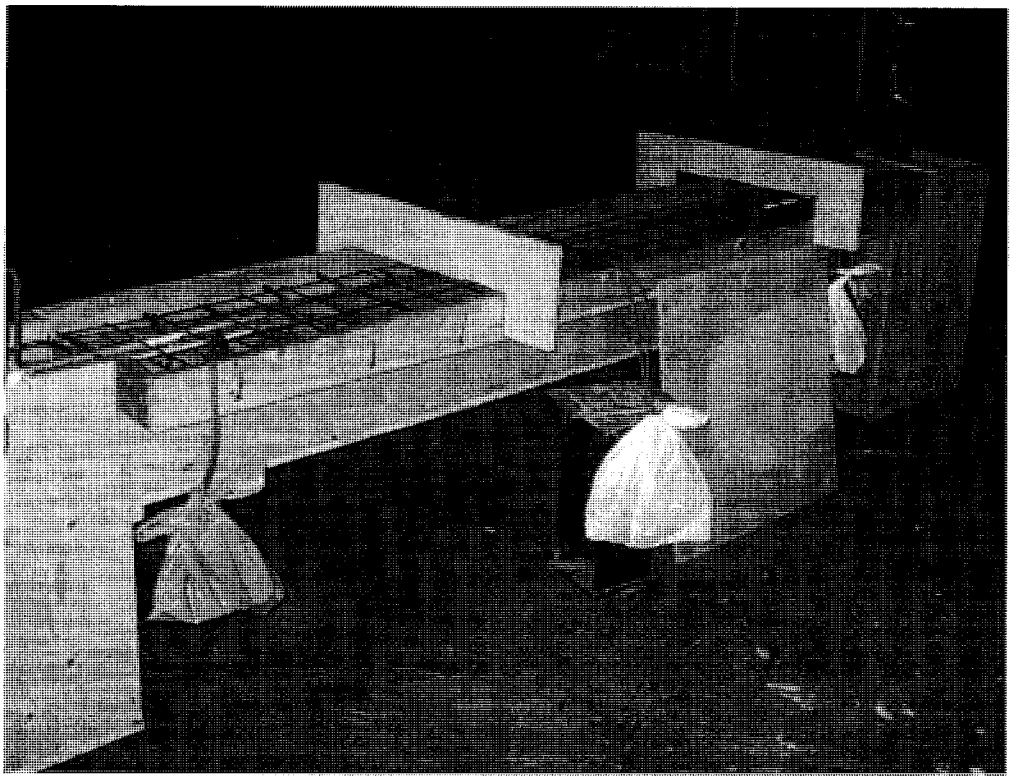

Figure 3.17. Wooden formwork of the beams strengthened in flexure

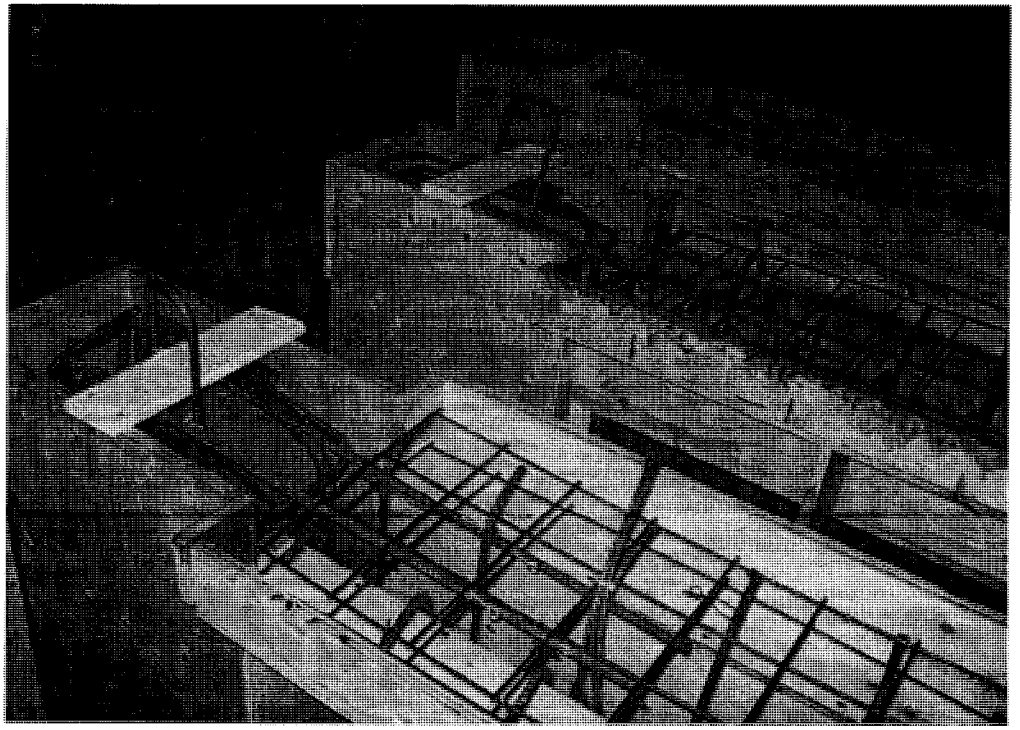

Figure 3.18. Wooden formwork of the T-beams connected to column stubs

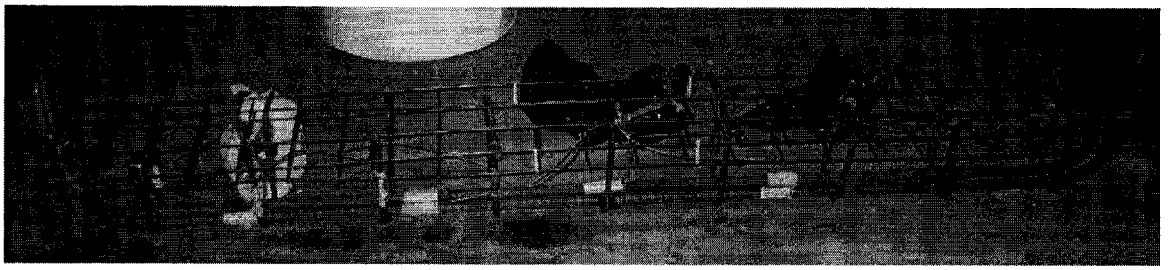

Figure 3.19. Typical reinforcement steel in the specimens strengthened in shear

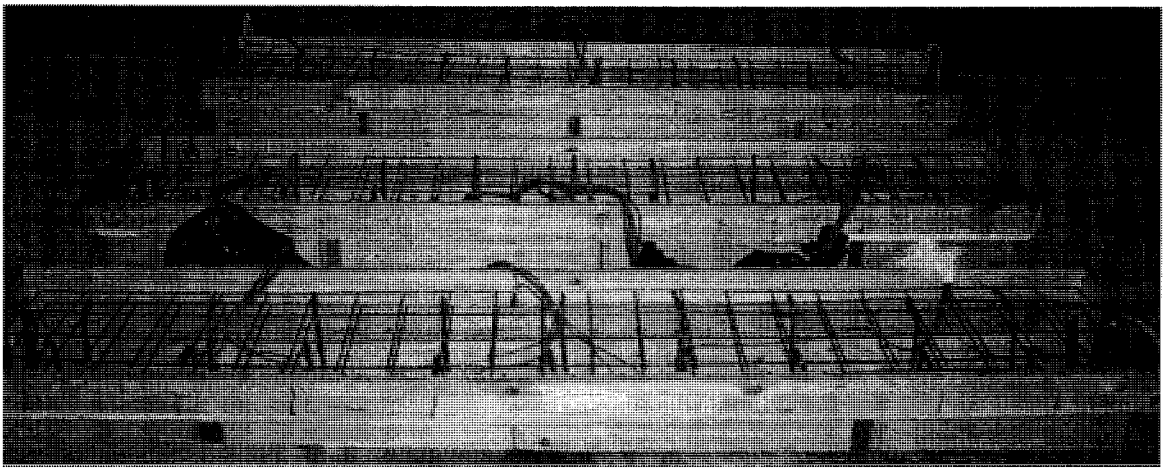

Figure 3.20. Reinforcement steel cage in the formwork for the beams strengthened in shear

Figure 3.21. Reinforcement steel cage in the formwork on the plastic rounded support

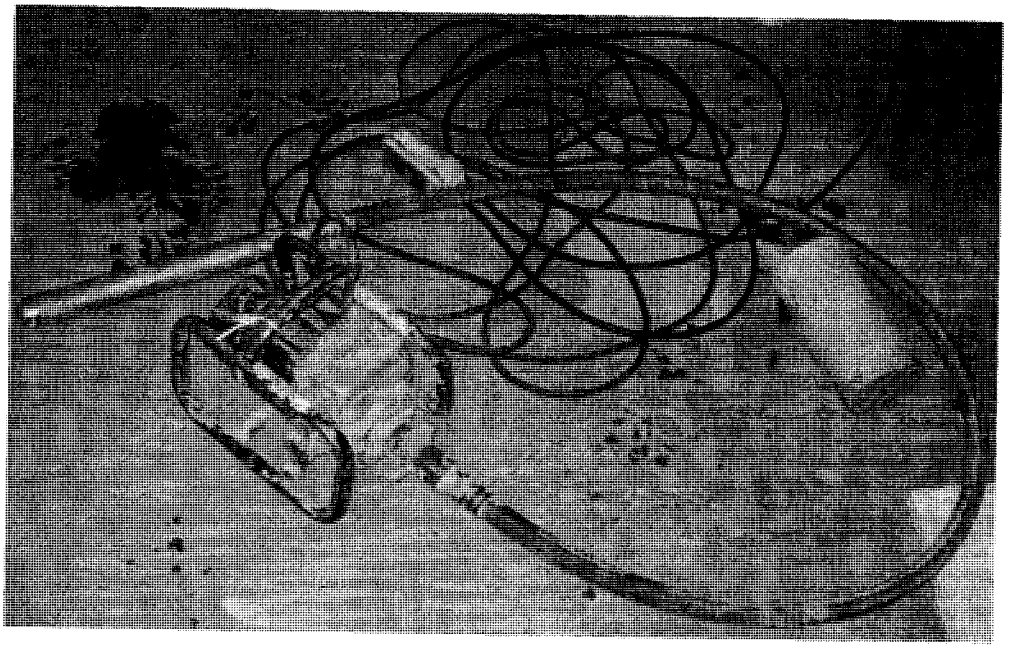

Figure 3.22. Electrical concrete vibrator used in the research

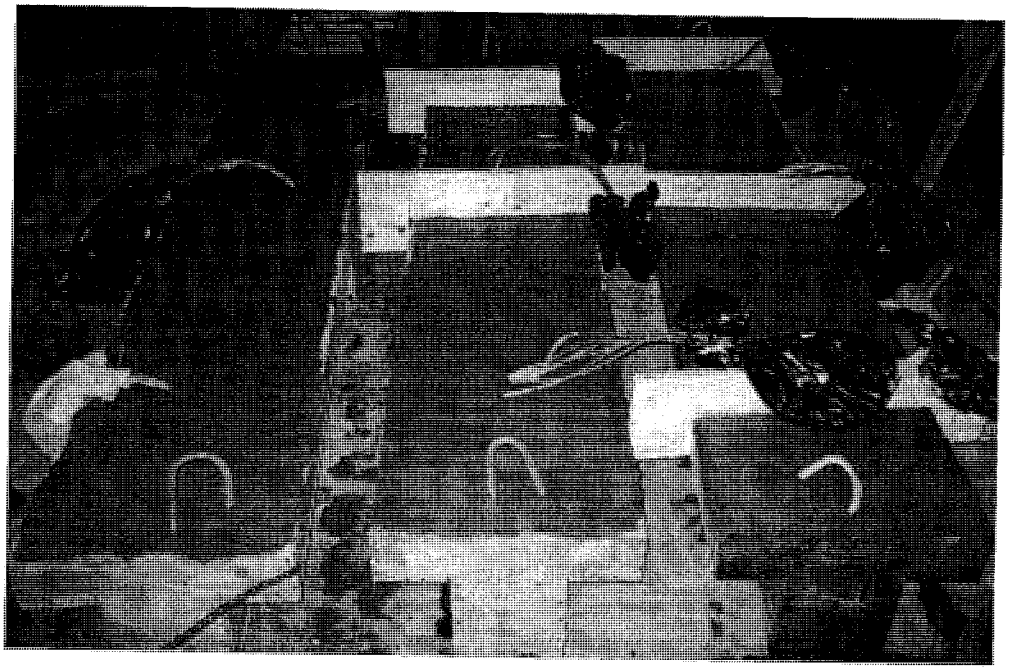

Figure 3.23. Wet concrete in the formwork finished with a float

Figure 3.24. Concrete covered with burlap and moistened regularly

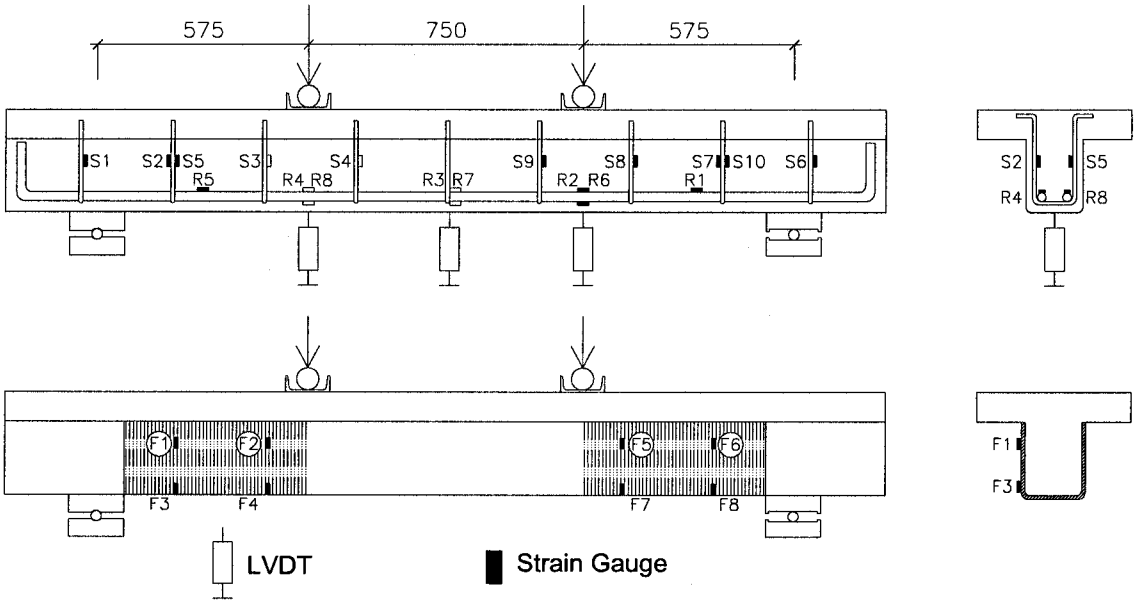

Figure 3.25. Instrumentation of the T-beams strengthened in shear

CHAPTER 4

EXPERIMENTAL RESULTS FOR BEAMS STRENGTHENED IN SHEAR

4.1. General

Three reinforced concrete (RC) T-beams were tested to study the efficiency of using anchored U-shaped dry carbon fibre (CF) sheet in increasing the shear capacity of RC T-beams. The RC T-beams were tested under 4-point loading system and subjected to incremental increase of the load up to failure. During the test, the complete behaviour of each T-beam was monitored, including the strains in the steel reinforcements and in the CFRP sheet. In addition, the deflection at different locations along the T-beams was recorded by LVDT. The crack patterns were manually traced. In this chapter, the test data and the experimental results are discussed. The experimental results include the load-deflection relationships and the strain along the CFRP sheets.

All three beams failed in shear as there were initially designed to. Table 4.1 shows the ultimate failure loads, and the failure modes for all beams. Figures 4.1 to 4.3 show failure modes of all the test beams.

4.2. Behaviour of control beam S-C-O

Upon loading of the beam S-C-O, diagonal shear cracks were visible at a load of 145 kN. At this point, two main shear cracks were detected within each shear span, as shown in Figure 4.1. The shear cracks were initiated at the middle of both shear spans simultaneously. As the load increased, the major crack started to extend and propagated

upward through the flange close to the loading point leading to a brittle failure at an ultimate load of 202 kN.

4.2.1 Strain in steel rebars

Figure 4.4 shows the longitudinal strain in longitudinal reinforcement at mid-span for the beam S-C-O. This specimen did not show yielding of the longitudinal reinforcement and eventually failed in shear with a brittle manner.

From the Figure 4.5, it can be seen that the beam S-C-O had the highest amount of vertical strain in its stirrup in the early stages of load application (Load = 50 kN). Vertical strain increased gradually in the steel stirrup of the beam S-C-O until it reaches to its maximum shear capacity and it fails at the load 202 kN. A sudden increment of the vertical strain can been seen in the stirrup after the load passes 200 kN (Figure 4.5). The stirrup with the maximum vertical strain in the beam S-C-O has noticeably higher values in comparison with the stirrup with the maximum vertical strain in the other beams.

4.2.2. Load-deflection relationship

The primary objective of testing this beam was to have a baseline for comparing the strengthening RC beams in shear using different methods of CFRP sheet bonding. Figure 4.6 shows the load-mid span deflection of the control specimen S-C-O. From this figure, it can be seen that the control specimen S-C-O failed in a non-ductile manner in shear. The first diagonal shear cracks were observed at 115 kN. No horizontal cracks were formed between the two loading points. More minor cracks developed along the beam due to the increase in loading. Web shear cracks stopped progressing and cracks

under the loading plates started to widen. At around 202 kN, T-beam failed due to shear failure with a maximum deflection of 6 mm.

4.3. Behaviour of beam S-E-B

While the beam S-E-B was being loaded, failure started by debonding of the CFRP sheets over the major shear crack in the same location observed in the beam S-C-O; though, subsequent to the web shear cracks, a vertical crack was created on the top of the flange near the support, and then spread descending. The bonded CFRP eventually unzipped vertically, as shown in Figure 4.2. This effect can be explained by the strain compatibility between the flange and the web. When the concrete strut formed in the web, it created a secondary effect in the top flange. As the applied load increased, the bottom of the beam close to the support attempted to rotate, but the large, wide flange restrained the movement. This led to, horizontal tensile strains in the top part of the flange near the loading point. Finally, these strains acquired the ultimate tensile strength of the concrete. A vertical crack was then produced from the top of the flange and propagated downward throughout the flange's thickness up to where it reached the web and the CFRP sheets, causing a vertical tearing of the fibres. This resulted in a sudden drop of the load in the load-deflection curve for the beam S-E-B in Figure 4.6, leading to shear failure. The same failure mode was reported by Khalifa (2000), Adhikary (2001), Deniaud et al. (2003) and Cao (2005). The load carrying capacity of the beam S-E-B was 256 kN with a 27% increase in the shear capacity compared to the control beam S-C-O. If debonding could be restrained, a more effective utilization of the strengthening material

and as a result a higher increase in shear capacity of the RC beam would have been achieved.

4.3.1. Strain in steel rebars

Figure 4.4 shows the longitudinal strain in longitudinal reinforcement at mid-span for the beam S-E-B. This specimen did not show yielding of longitudinal reinforcement and eventually failed in shear with a brittle manner.

The behaviour of the stirrups during the loading process was monitored using several strain gauges on the stirrups located in the shear spans. Figure 4.5 shows that the strain on the stirrup with the maximum strain was low in the early stages of the loading (Force = 100 kN). In comparison with the strain at the same load in the specimen S-C-O, the presence of the FRP shear contribution (V_{FRP}) was the reason that the strain in the stirrup decreased extensively. Only after the load passes 100 kN, the strain started to increase significantly in the stirrups. When the load passed 250 kN and the CFRP debonded, the strain suddenly increased in the stirrup until it led to the ultimate failure of the specimen S-E-B.

4.3.2. Strain in FRP

Figure 4.7 shows the maximum vertical strains observed in the CFRP sheets among the locations where the strain gauges were placed in the shear span just before the failure of the beams. It is to be noted that, although these strain gauges are installed in the shear constant zone where the maximum shear forces and strains in FRP occur, these strain gauges may not necessarily show the maximum values developed in the sheet;

rather, they show the strains where the gauges were attached. In order not to alter the strength of CFRP sheets, the amount of the strain gauges were limited, since surface preparation on the dry CF to install strain gauges may influence the strength of the material. Therefore, the measured strains shown in Figure 4.7 represent those only at the instrumented fibre bands. It can be seen that the strain was very small prior to the diagonal cracks. However, once the beams developed diagonal cracks, there was a rapid increase in strain. The strain in the bonded CFRP sheets of the S-E-B specimen increased until the CFRP debonded and the beam failed at 256 kN. The beam S-E-B developed a strain of 1402 microstrains in the sheet, which is about 13% of the ultimate strain for the CFRP (1.05%; maximum elongation for the wet CFRP) used in this study. This value is not the absolute maximum value because it greatly depends on the location of the strain gauge with respect to a crack since there might have been higher strains in some fibres with no strain gauges. The load versus vertical strain in the CFRP sheets relationship for the specimen S-E-B is shown in Figure 4.7.

The beam S-E-B benefits from the contribution of concrete (V_c), steel stirrup (V_s) and the CFRP sheet (V_{FRP}) in the shear resistance comparing to the beam S-C-O which only takes advantage of V_c and V_s for shear resistance. Therefore, the difference between these values of strain in the stirrups of the beams S-C-O and S-E-B can be explained as the bonded CFRP contribution in shear resistance of the RC beam.

After load passes 250 kN, the CFRP sheets debond completely and the beam S-E-B loses the V_{FRP} contribution completely. A sudden drop can be seen in the strain of the CFRP sheet after 250 kN.

4.3.3. Load-deflection relationship

Figure 4.6 shows the load versus mid-span deflection of the specimen S-E-B. From the figure, it can be seen that the specimen S-E-B failed in a non-ductile manner in shear. The specimen S-E-B had a mid-span displacement of 8 mm when it reached its peak load capacity of 256 kN. It is observed that the beam S-E-B strengthened by the bonded CFRP sheets showed relatively lower stiffness compared to the beam S-E-B strengthened by the mechanically anchored dry CF sheet. Also, beam S-E-B experienced less ductility than the beam S-M-D. The beam S-E-B exhibited brittle behaviour due to the CFRP sheet debonding, a sudden drop can be observed in the load-displacement curves after the peak load.

4.4. Behaviour of beam S-M-D

As a result of the use of the newly proposed mechanical hybrid end-anchors, a significant increase in the shear capacity was achieved in the beam S-M-D without bonding the CF sheet to the web, relying only on the end-anchor strength. Although the reinforcement and strengthening of the beam S-M-D were designed such that the contribution of the CF strengthening system could be quantified before reaching the yielding strength of the beam, yet the flexural steel started yielding and gained some ductility to the specimen before the failure. Due to the usage of the U-shaped dry CF sheet, the vertical fibers were able to bridge the diagonal shear cracks. As such, the abrupt debonding of the CFRP sheet used in the strengthening of specimen S-E-B was successfully prevented. Failure of the beam S-M-D occurred due to major shear crack in the concrete beam. The load carrying capacity of the beam S-M-D was 298 KN which

represents an increase in the shear capacity of 48% compared to the control beam S-C-O and 16% higher ultimate failure load over the CFRP bonded specimen S-E-B. It is anticipated that the contribution of the new U-shaped dry CF sheet strengthening system would have been higher if the beam S-M-D did not reach yielding of the longitudinal rebars.

4.4.1. Strain in steel rebars

Figure 4.4 shows the longitudinal strain in longitudinal reinforcement at mid-span for the beam S-M-D. The beam S-M-D partly showed yielding of longitudinal reinforcement at the maximum moment region, which enabled the beam to exhibit a very slight ductile behaviour; even though it ultimately failed in shear.

The stirrup with the maximum vertical strain in the beam S-C-O and that in the beam S-M-D follow a similar pattern until the load passes 150 kN. This shows that the U-anchored dry CF did not fully come into action immediately after the loading starts. In this manner, the contribution from U-shaped dry CF sheet is activated at relatively higher load levels. After the load passes 150 kN the strain in the stirrup of the beam S-M-D increases until the force reaches 280 kN. A significant drop in the vertical strain of the steel stirrups of the beam S-M-D can be seen in the Figure 4.5 while the force reaches 290 kN. At the same force level there is a significant increment in the strains of the U-shaped dry CF sheet (Figure 4.7). This shows the anchored U-shaped dry CF sheet fully contributes to shear resistance and releases a large amount of force from the stirrups.

4.4.2. Strain in FRP

As it was mentioned earlier, the U-anchored dry CF sheets did not fully come into action immediately after the loading started. This fact can be seen in the Figure 4.7 that shows the maximum strain in the CF sheet versus the load applied to the specimen. As such, although the dry CF sheet was activated in the service stage, it kept most of its capacity for the higher force levels where the contribution of the CF was more required. After the load passed 150 kN, the strain in the stirrup of the beam S-M-D slightly grew until the force reached 280 kN. A significant increase can be seen in the strain of the U-shaped dry CF sheet (Figure 4.7) when the force reached 290 kN, at the same force level a significant drop can be observed in the vertical strain of the steel stirrups of the beam S-M-D (Figure 4.5). At this load, the anchored U-shaped dry CF sheet fully contributed to the shear resistance and released a part of forces from the stirrups.

Figure 4.7 shows the maximum vertical strains observed in the CF sheets among the locations where the strain gauges were installed in the shear span in the S-M-D specimen. As mentioned earlier, it is to be noted, that these values may not necessarily be the maximum values of the strain developed in the CF sheet; rather, they show the strains at places where the gauges were installed. It is to be noted, that although these strain gauges are installed in the shear constant zone, where the maximum shear force is applied and as a result the maximum strain in the CF occurs, these strain gauges may not necessarily show the maximum values developed in the sheet; rather, they show the strains at points where the gauges were attached. The number of strain gauges that could be installed was limited, in order not to reduce the strength capacity of the dry CF sheet, since surface preparation on the dry CF to install strain gauges may influence the strength

of the material. Therefore, strain in selected fibres could be measured and for the rest there was no measurement. The CF strain shown in the Figure 4.7 is the behaviour of a selected group of fibres. Since the used CF is uniaxial and there is no significant load transfer perpendicular to the major axis, the behaviour of the fibres could be greatly independent from each other. The only element that helped the fibres bridge the shear cracks and transfer the contribution of the CF in shear was the 1-inch steel rod at the end of the U-jacket. The strain in the CF increased gradually from the beginning of the loading in the beam S-M-D. Prior to the failure, the strain increased highly in the CF until it eventually failed at 298 kN. The beam S-M-D showed relatively higher strains indicating the maximum utilization of the strengthening sheet before the failure. The measured local maximum vertical strain of the hybrid CF U-jacket was in the range of 4200 or 25% of ultimate strain (1.7%; maximum elongation for dry CF). This value is not the absolute maximum value because it greatly dependant on the location of the strain gauge with respect to a crack since there might be higher strains in other fibers with no strain gauges attached.

Although a continuous carbon fibre sheet was used in strengthening beam S-M-D, yet during the test it has been observed that the dry carbon fibres were significantly stretched in middle of the spacing of the internal steel stirrups in comparison to the fibres in other locations. This could be interpreted that the dry CF sheets are contributing to the shear capacity of the beam through the formation of a truss pattern, where the highest tensile stresses occurs at the middle of the spacing of the stirrups. This resulted in the formation of CF strips every 200 mm (at the middle of the spacing of the internal stirrups) each of them with approximately 48 mm width, based on test observations (Figures 4.8 and 4.9).

4.4.3. Load-deflection relationship

The load-mid span deflection of the specimen S-M-D is shown in Figure 4.6. The beam S-M-D exhibited a slight ductile behaviour. It is observed that the beam S-M-D strengthened by the mechanically anchored CF sheets showed relatively higher stiffness compared to the beam S-E-B strengthened by the bonded CFRP sheets. Also, beam S-M-D experienced more ductility than the beams S-E-B and S-C-O. The supplemental ductility was gained from the flexural steel yielding. The beam S-M-D had a mid-span displacement of 14 mm when it reached its peak load capacity of 298 kN.

4.5. Performance comparison of T-Beams strengthened in Shear

The U-shaped dry CF sheet attached to the reinforced concrete T-beams with mechanically anchored fasteners was more effective than the traditional method of bonding the sheets to beams, as seen with the beam S-M-D. The new method provided increased shear capacity over the bonded method. Table 4.1 summarizes the structural test results.

From the behaviour of RC T-beams strengthened in shear, the following was observed:

1. All the beams excluding the beam S-M-D exhibited brittle behaviour resulted by a shear failure, a sudden drop can be observed in the load-deflection curves after the peak load (Figure 4.6).
2. The installation of U-shaped dry CF sheet anchorage system on the predrilled and prepared T-beam is faster and has less interruption to the vicinity of the beam compared to the application of epoxy-bonded FRP.

3. Using anchored U-shaped dry CF sheet is effective in increasing the shear capacity of the RC T-beams.
4. Figure 4.6 shows that beam S-M-D experienced more ductility compared to the beam S-E-B. The supplemental ductility was gained from the flexural steel yielding. The mid-span deflection of the beam S-M-D just prior to failure was 1.21 times (8.5mm at load 298 kN/7mm at 256 kN) the deflection of the beam S-E-B at failure, whereas the beam S-C-O had the smallest deflection (5mm at 202 kN). All the beams excluding beam S-M-D exhibited brittle behavior, a sudden drop can be observed in the load-displacement curves after the peak load. Beam S-M-D slightly behaved in a ductile manner before it suddenly failed in shear.
5. The ultimate load of the specimen strengthened by the U-shaped dry CF sheet anchorage method (S-M-D) was about 16% higher than that of the specimen that was strengthened with the epoxy-bonded CFRP sheet (S-E-B) and 48% higher than that of the control beam (S-C-O).

Table 4.1. Experimental results of the beams strengthened in shear

Beam	Shear strength (kN)	Increase (%)	Failure mode
S-C-O	202	0	Diagonal shear
S-E-B	256	27	Shear crushing + CFRP sheet debonding
S-M-D	298	48	Shear crushing + horizontal cracks at top face

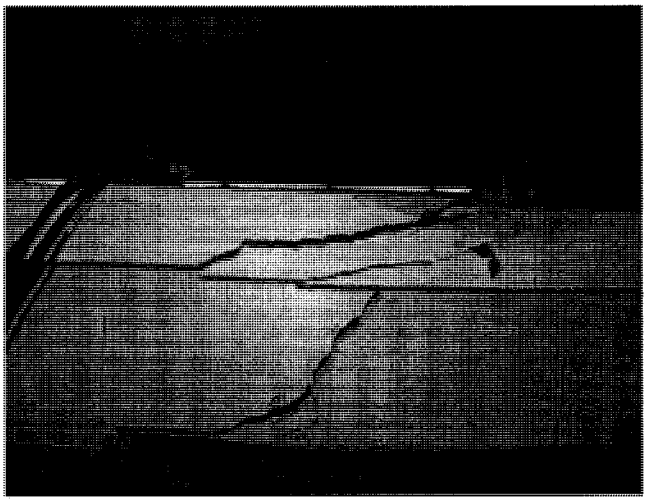

Figure 4.1. Cracking and failure pattern of beam S-C-O

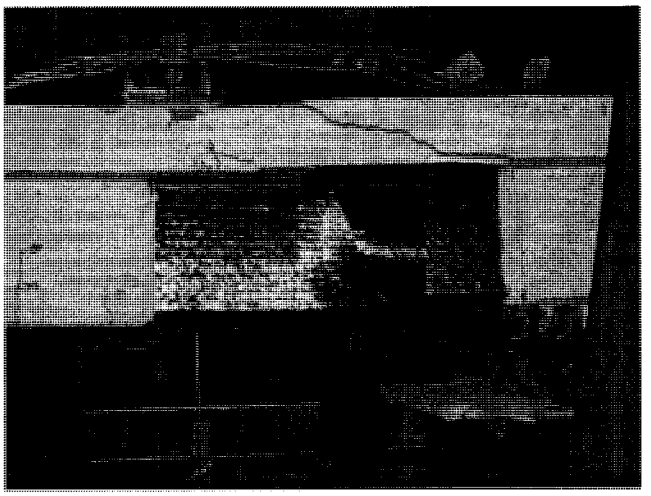

Figure 4.2. Cracking and failure pattern of beam S-E-B

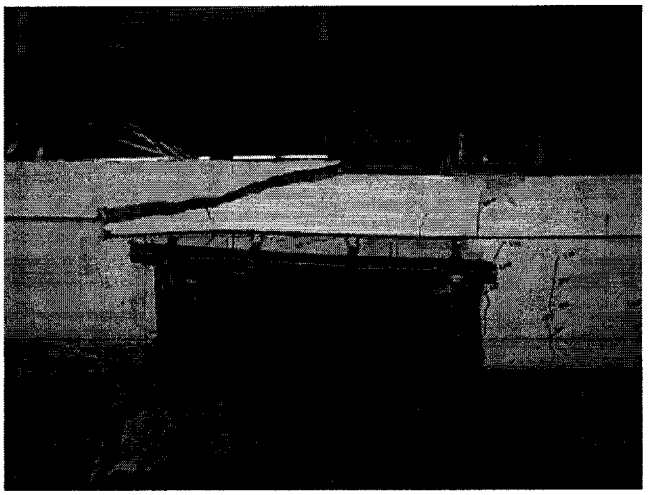

Figure 4.3. Cracking and failure pattern of beam S-M-D

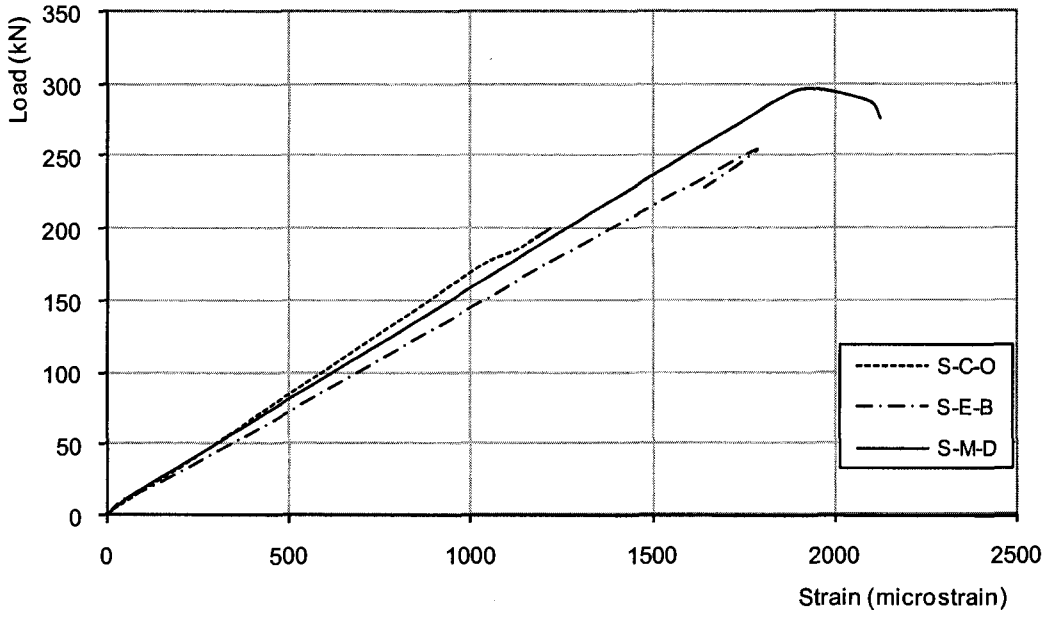

Figure 4.4. Load versus strain in flexural reinforcement of all the beams strengthened in shear

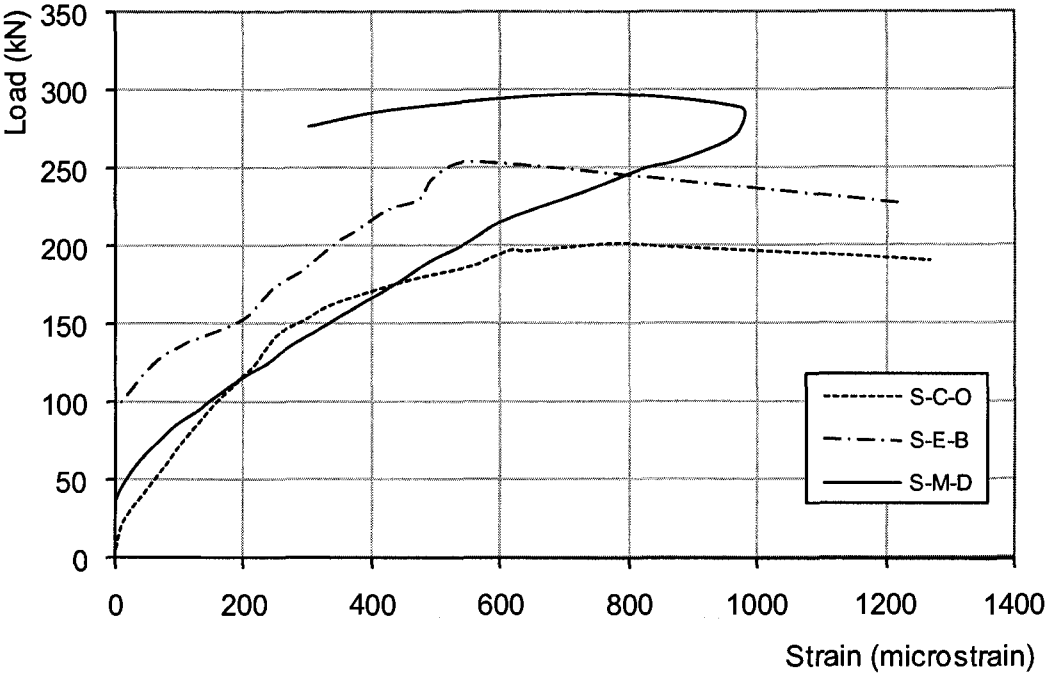

Figure 4.5. Load versus vertical strain in steel stirrup of all the beams strengthened in shear

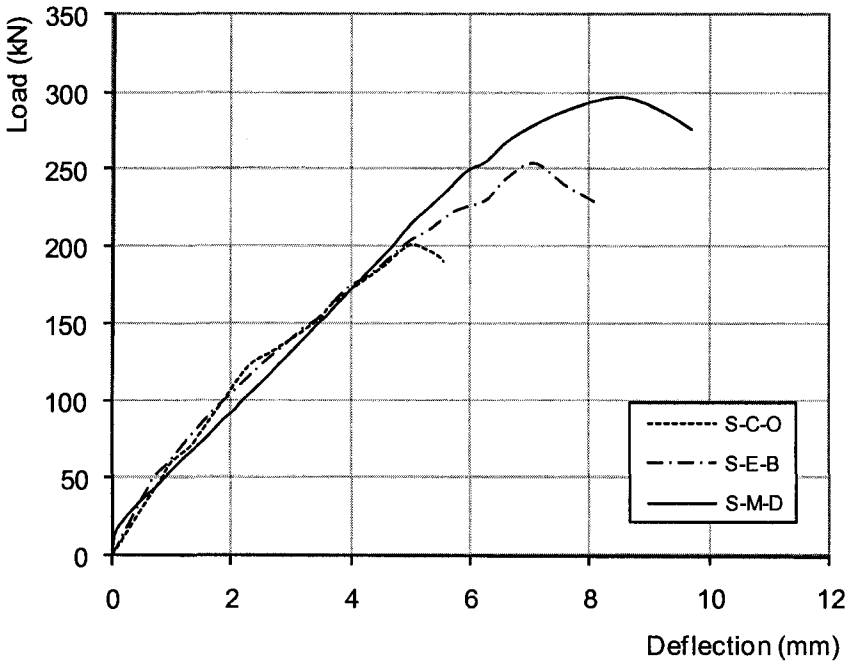

Figure 4.6. Load versus mid-span deflection of all the beams strengthened in shear

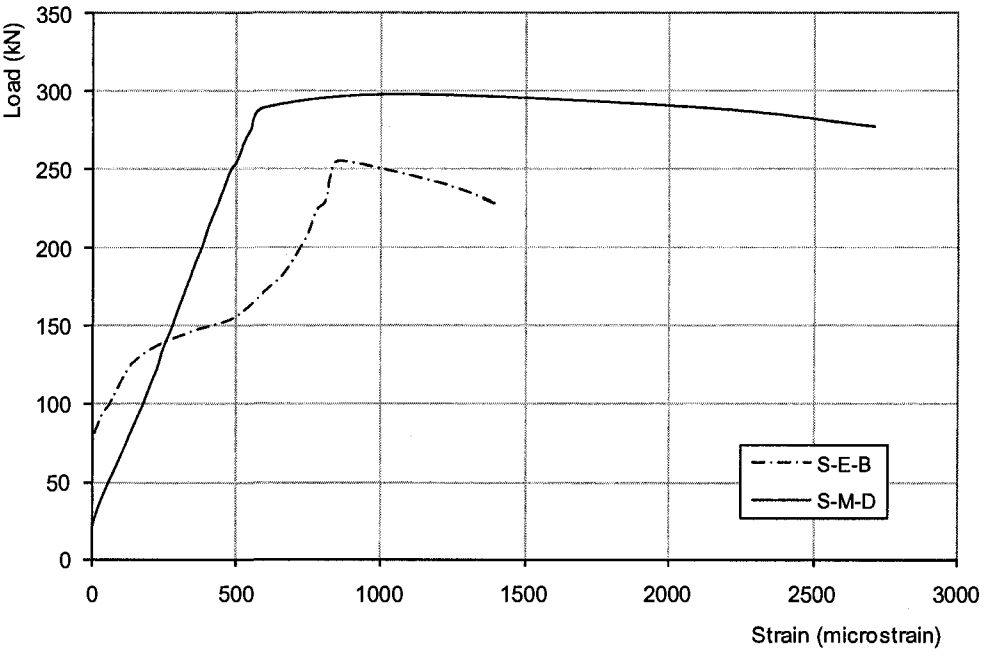

Figure 4.7. Load versus vertical strain in fibres of all the beams strengthened in shear

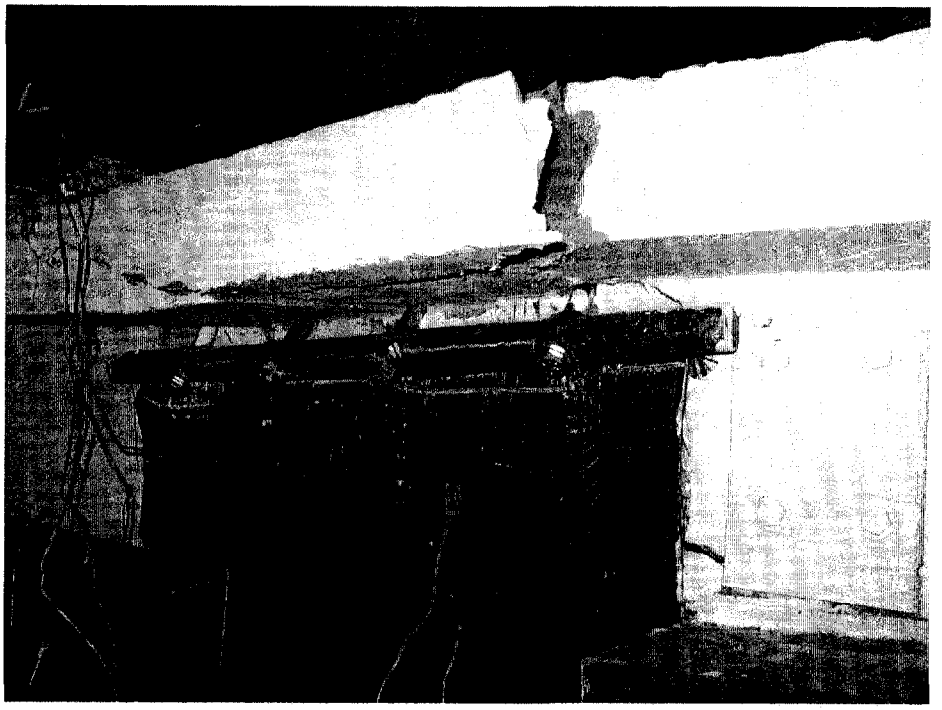

Figure 4.8. Effective CF strips in beam S-M-D (strengthened in shear)

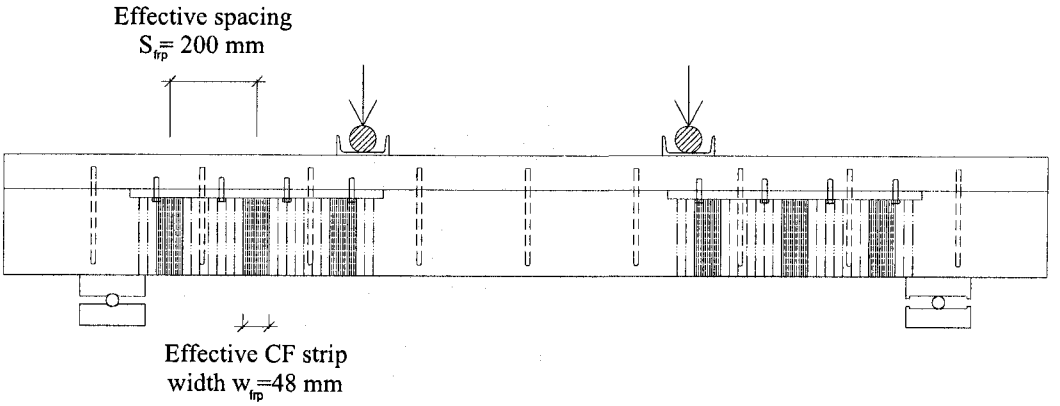

Figure 4.9. Effective CF strips in beam S-M-D (strengthened in shear)

CHAPTER 5

EXPERIMENTAL RESULTS FOR BEAMS STRENGTHENED IN FLEXURE

5.1. General

The results obtained from the tests performed on the four reinforced concrete T-beams with column stubs are discussed in this chapter. The T-beams were subjected to incremental increase of the load up to failure. During the test, the complete behaviour of each T-beam was monitored, including the strains in the steel reinforcements and in the CFRP sheet. In addition, the displacements at different locations along the T-beam's were recorded by LVDT. The crack patterns were manually traced.

The goal of this chapter is to evaluate the relative performance of beams strengthened with hybrid FRP / ductile anchorage system to those strengthened using conventional epoxy bonding application. References are made to specimens subject to similar test programs available in the literature. The experimental results include the load-deflection relationships, the strain along the CFRP sheets and the gain in strength for the strengthened T-beams.

5.2. Behaviour of control beam F-C-O

The control beam (F-C-O) with no strengthening system was the first beam that was tested in order to have a baseline for comparing the performance enhancement of different strengthening methods studied in this research. The control T-beam exhibited a conventional ductile flexural mode of failure in which the T-beam failed by yielding of

the steel reinforcement followed by crushing of the concrete in the constant moment region. During this test, flexural cracks first appeared in the mid span between the loading points as expected. These cracks became visible before the yielding load was reached. The control beam yielded at load of 62.6 kN. The ultimate moment of beam F-C-O was 45.9 kN.m corresponding to the ultimate load of 83.45 kN. The load-deflection curve for this beam is shown in Figure 5.1. The deflection used in the curves in this chapter is based on the deflection as measured by the LVDTs. The beam F-C-O continued to carry a significant load until the concrete has crushed on the top surface of the beam. This behaviour is attributed to the tightly spaced stirrups confining the concrete in the moment region. Figure 5.2 shows beam F-C-O after testing to a deflection over four times the deflection at the yield load. At this deflection the cover concrete has crushed and spalled away (Figure 5.3).

5.2.1 Strain in steel rebars

Figure 5.4 shows the strain in longitudinal reinforcement versus load at mid-span for the beam F-C-O. The control T-beam exhibited a conventional ductile flexural mode of failure in which the T-beam failed by yielding of the longitudinal reinforcement prior to crushing of the concrete in the constant moment region. The strain in the constant moment zone increased with a constant slope. The strain in the longitudinal bars remains constant in the moment span of the specimen. In the middle of the shear span, the strain is half of that in the constant moment zone. The longitudinal bars in the control beam (F-C-O) yielded at load of 62.6 kN. After the yielding point, strain in the constant moment-

zone increased at a higher rate with less improvement in the load. The strain gradually increased versus load until it failed at load 83.45 kN in a ductile manner.

5.2.2. Load-deflection relationship

Figure 5.1 shows the load versus the mid-span deflection of the control beam (F-C-O). From the figure, it can be seen that the control specimen failed in a ductile manner. The control beam had a yield displacement of 10.8 mm that corresponds to the load of 62.6 kN. The control specimen had a mid-span displacement of 44.86 mm when it reached its peak load capacity of 83.45 kN. Displacement ductility is defined as the ratio of the midspan deflection at the maximum load to the midspan deflection at general yield. The specimen F-C-O exhibited a ductile behaviour, with a displacement ductility of 4.15. The deflected shape of the beam is shown in Figure 5.2.

5.3. Behaviour of beam F-E-B

The FRP strengthening sheet was bonded using a common technique mainly for strength comparison purposes. Attention was paid to compare the preparation time required for of the epoxy bonded method and the hybrid FRP / ductile anchorage method. The bottom of the concrete was grinded until it got completely smooth.

Canadian Highway Bridge Design Code CSA-S6 (2006) and ISIS Canada (2006) divided the potential flexural failure modes for externally-strengthened reinforced concrete flexural members into four groups: (1) concrete crushing before yielding of the reinforcing steel; (2) steel yielding followed by concrete crushing; (3) steel yielding

followed by FRP rupture; and (4) debonding of the FRP reinforcement at the FRP/concrete interface.

During the test, hairline flexural cracks were visible in the constant moment region as the beam was loaded to near yielding. One flexural crack appeared on the outside of each load point shortly after the yield point was passed. As soon as shear cracks appeared in the shear spans close to the loading points, the beam failed suddenly. The CFRP sheet suddenly detached from the concrete beam and struck the floor. It is likely that the sheet delamination initiated at the end of the span near the shear cracks. Specimen F-E-B failed prematurely without warning by debonding of the CFRP sheet after yielding of the steel reinforcement (failure mode 4). After the CFRP sheet delaminated, the beam behaved as an unstrengthened control beam until the concrete crushed in compression in the moment span. The delaminated sheet had pieces of concrete, of a few millimeters thick, attached to it in several places. The attached concrete pieces made it difficult to ascertain whether the failure was initiated by a failure of the bond between the concrete and the adhesive or by a failure a few millimeters into the surface of the concrete. The beam yielded at a load of 72.5 kN and reached an ultimate load of 87.5 kN, resulting increases of 16 and 5 percent over the control beams respectively.

5.3.1. Strain in steel rebars

Figure 5.4 shows the strain in longitudinal reinforcement versus the load at mid-span for the beam F-E-B. The beam F-E-B T-beam exhibited a brittle flexural mode of failure in which the T-beam failed by yielding of the longitudinal reinforcement prior to

the CFRP sheet debonding. Upon the loading of specimen F-E-B, the strain in the mid-span increased with a constant slope along the load increment prior to longitudinal steel yield. The longitudinal bars in the beam F-E-B yielded at a load of 72.5 kN. After the yielding point strain in the mid-span, the strain increased at a higher rate with less improvement in the load until the FRP debonded. At this point the strain and the load jumped down suddenly in the longitudinal rebar. From this point the beam F-E-B continued with having the same behaviour of the control beam till the concrete crashed.

5.3.2. Strain in FRP

Figure 5.5 shows the strain along the principal fibres of the CFRP sheets versus the load at mid-span for the beam F-E-B. The strain in the mid-span increased with a constant slope along the load increment prior to the flexural concrete cracks (Load = 40 kN). Because of the CFRP sheet debonding, cracks resulted in less shear transfer points between the CFRP sheet and the concrete causing a slighter slope in the strain of CFRP versus the load diagram. After the longitudinal steel yielded the cracks opened up significantly, this led to more local debonding and slighter slope in the Figure 5.5 diagram. The maximum measured strain reached a strain of 4960 με which is 47.3% of the ultimate strain of the used CFRP (0.0105mm/mm) as provided by the supplier. The CFRP debonded at a load of 87.5 kN causing a brittle failure in the specimen F-E-B.

5.3.3. Load-deflection relationship

The load versus mid-span deflection relationship for the specimen F-E-B is shown in Figure 5.1. Specimen F-E-B that was strengthened with external epoxy bonding with

no external anchorage failed prematurely without warning by debonding of the CFRP sheet after yielding of the steel reinforcement.

The specimen F-E-B shows a slightly stiffer behaviour than the control beam, as shown in the Figure 5.1. The specimen F-E-B had a yield deflection of 9.91 mm that corresponds to the load of 72.5 kN. The F-E-B specimen had a mid-span displacement of 18.9 mm when it reached its peak load capacity of 87.5 kN. The first drop in the load-deflection diagram occurred when the FRP sheet detached from the concrete beam. The second drop in the same diagram occurred when the concrete in the moment span crushed. This beam had lower ductility than the control beam overall.

The specimen F-E-B exhibited a brittle behaviour due to the sudden debonding of the CFRP sheet, with a displacement ductility of 1.91. During the test, it was observed that the epoxy bonded CFRP sheet debonded very close the peak load attained. The debonding progressed from the midspan region toward one end of the beam. After the debonding of the CFRP sheet, the flexural behaviour of the T-beam followed that of the control. The deflected shape of the beam is shown in Figure 5.6.

5.4. Behaviour of beam F-M-U

The beam F-M-U which was strengthened with hybrid FRP / ductile anchor failed in a ductile manner by crushing of concrete in compression zone which was accompanied by excessive slip of the hybrid FRP / ductile anchor after yielding of the internal steel reinforcement and hybrid FRP / ductile anchor's steel link members.

In beam F-M-U, the total nominal resisting moment, $M_{n,\,total}$, of the strengthened beam is equal to the summation of the nominal resisting moment, $M_{n,\,orig.}$, of the control

beam (F-C-O) and added moment, ΔM, to the concrete beam due to the application of the hybrid FRP / ductile anchorage system.

$$M_{n,\,total} = M_{n,\,orig.} + \Delta M \tag{5-1}$$

$$\Delta M = A_{,links} \times jd \tag{5-2}$$

$$A_{links} \times f_{y,links} = \tfrac{3}{4} \times A_{FRP} \times f_{FRP,u} \tag{5-3}$$

Where $A_{,links}$ is the total cross-section area of the link members at each end; jd is the arm of the tension-compression couple; $f_{y,links}$ is the yield stress of the steel link members; A_{FRP} is the design area of the FRP sheet(s); and $f_{FRP,u}$ is the ultimate tensile strength of the FRP sheets. In equation (5-3), A_{links} were designed to ensure that failure would occur in steel link members and not in the FRP sheet. A factor of ¾ was arbitrarily chosen. It should be mentioned that due to the nature of the mechanism, there will be a small gap, δ, between the FRP sheet and the soffit of the beam, which is equal to half of the thickness of the plate that FRP sheets are wrapped around (Figure 5.7a). This gap will be closed as the beam deflects, as shown in Figure 5.7b. In this case, the FRP sheet will be experiencing tensile stresses that are transferred to the steel link members, which in turn transfer the stresses to the column stubs through the Hilti anchors.

Use of hybrid FRP / ductile anchors resulted in high amounts of ductility gained by the specimen F-M-U as well as high strength level. The small gap between the unbonded CFRP sheet and the soffit of the T-beam caused a rather beneficial behaviour of the system since the CFRP sheet did not fully contribute in low levels of load. As soon as the gap was closed and the internal steel was yielded, the strain in the CFRP sheet and the steel link members in the hybrid FRP / ductile anchorage system started to increase

while the strain in the longitudinal rebars dropped suddenly (Figure 5.4). Eventually, the specimen F-M-U failed in a ductile manner by crushing the concrete in compression zone which accompanied by excessive slip of the hybrid FRP / ductile anchor after yielding of the internal steel reinforcement and the hybrid FRP / ductile anchors' steel link members.

5.4.1. Strain in steel rebars

Upon loading of the F-M-U specimen, the strain in the longitudinal steel reinforcement started to increase. The strain in the tension rebars versus the load diagram (Figure 5.4) was similar to that in the control specimen at the early stages of loading, since the effect of the hybrid FRP / ductile anchorage system was negligible. As soon as the steel rebars yielded and the gap between the soffit of the T-beam and the CFRP sheet was closed, all the CFRP tensile capacity was brought into action (Load = 65 kN). After that, the full tensile effect of the CFRP sheet released a part of the tensile force from the longitudinal rebars, therefore the strain in the longitudinal steel reinforcement started to decrease. From the Figure 5.4, it can be seen that while the force increased from 65 kN to 90 kN, the strain in the longitudinal steel reinforcement decreased.

When the load is approximately 81 kN, a jump can be seen in the load without a noticeable change in the strain. This can be attributed to the yielding of the steel link member in hybrid FRP / steel ductile anchorage system. In this manner the steel link member in the hybrid FRP / ductile anchorage system acted like a filter for strain transfer to the longitudinal rebars by its yielding. The same phenomenon can be seen at the load equal of 90 kN. This could be caused by yielding the steel link member of the hybrid FRP / ductile anchorage system on the other end of the unbonded CFRP sheet. Eventually, the

F-M-U beam failed in a ductile manner by crushing the concrete in compression zone which accompanied by excessive slip of the hybrid FRP / ductile anchor after yielding of the internal steel reinforcement and hybrid FRP / ductile anchors' steel link members at the load of 100.77 kN.

5.4.2. Strain in FRP

As loading began on the F-M-U specimen, the strain in the FRP sheets started to increase in a slight manner since the hybrid FRP / ductile anchorage system was not fully in action (%35 of maximum strain of the CFRP material at 65 kN). The strain in the CFRP sheets versus the load diagram is shown in Figure 5.5. As the beam deflects (Load = 65 kN), the gap between the soffit of the T-beam and the CFRP sheet was closed, and the strain in the CFRP sheet increased with higher rate than the pre-yield loading. After that, the full tensile effect of the CFRP sheet released a part of the tensile force from the longitudinal rebars. From the Figure 5.5, it can be seen that while the force increased from 65 kN to 90 kN, the strain in the CFRP sheet reach from 35% of its ultimate strain capacity to 55% of its ultimate strain capacity.

When load was approximately 81 kN, the first set of steel tensile elements yielded and a reduction in strain increment speed in the CFRP could be seen. In this manner, the steel link member in the hybrid FRP / ductile anchorage system acted like a filter for strain transfer to the CFRP sheet fibres by its yielding. The same change in the increment speed of the strain in the CFRP sheet fibres can be seen at a load equal to 90 kN (67% of the ultimate strain of the CFRP sheet), which could be caused by yielding the tensile elements of the hybrid FRP / ductile anchorage system on the other end of the unbonded

CFRP sheet. Eventually the F-M-U beam failed at the load of 100.77 kN while the maximum strain in the CFRP sheet was 77% of the ultimate strain of the CFRP used in this test.

5.4.3. Strain in steel link members

Since the hybrid FRP / ductile anchorage system was not fully under tensile force in early stages of loading, the strain in the steel link member increased slowly. After yielding the steel due to higher deflections the gap was filled and the hybrid FRP / ductile anchorage system started the fully gain tensile force as shown in Figure 5.8.

To prevent a sudden CFRP failure and to add more ductility to the original ductility of the T-beam, steel link members were designed to yield before the CFRP sheet reaches its maximum tensile capacity. In this manner, the steel link members acted like a fuse for the system and hinder sudden failure by adding ductility to the system due to their capability to yield. A sudden change in the speed of strain increment of the internal longitudinal steel and the CFRP sheet could be seen when the steel link members yielded (Figure 5.4 and 5.5). Figure 5.8 shows the strain in one of the steel tensile elements versus the load.

5.4.4. Load-deflection relationship

The load versus mid-span deflection relationship for the specimen F-M-U is shown in Figure 5.1. The specimen F-M-U had a yield displacement of 9.69 mm that corresponds to the load of 65.02 kN. The F-M-U specimen had a mid-span displacement of 88.07 mm when it reached its peak load capacity of 100.77 kN.

The specimen F-M-U exhibited a ductile behaviour due to the effective presence of the hybrid FRP / ductile anchorage system, with a displacement ductility of 9.09. The deflected shape of the beam is shown in Figure 5.9.

5.5. Behaviour of beam F-M-B

The specimen F-M-B which was strengthened with epoxy-bonded CFRP along with the hybrid FRP / ductile anchors failed in a brittle manner by the CFRP sheet rupturing that was preceded by yielding of the steel reinforcement. The presence of the hybrid FRP / ductile anchors prevented debonding the CFRP sheet and hence the T-beam developed its full flexural capacity.

The bonded hybrid FRP / ductile anchored specimen, F-M-B, showed no signs of bond degradation at its failure just above the same load specimen F-E-B debonded. Specimen F-M-B did fail through the CFRP rupture because the tensile capacity of the CFRP sheet was attained.

Using the same system ductile anchorage system of F-M-U, yet bonding the CFRP with epoxy to the beam soffit, beam F-M-B showed an increase in the strength capacity of 27% compared to the control beam, but failed due to the rupture of CFRP due to the high strains arising from being bonded at the locations of crack growths in the flexure zone. Although anchoring the CFRP sheets, that are bonded to the beam, at the beams' ends eliminated the peeling off of the sheets, yet the CFRP sheet was subjected to high strains due to the growth of the flexural cracks, which resulted in a sudden rupture of the CFRP sheets (failure mode 2) without reaching high ductility levels in the beam.

5.5.1. Strain in steel rebars

Figure 5.4 shows the strain in longitudinal reinforcement versus the load at mid-span for the beam F-M-B. The beam F-M-B T-beam exhibited a sudden flexural mode of failure in which the T-beam failed by yielding of the longitudinal reinforcement prior to the CFRP sheet rupture. Upon loading of the specimen F-M-B, the strain in the mid-span increased with a constant slope along the load increment prior to the longitudinal steel yield. The longitudinal bars in the beam F-M-B yielded at a load of 75.45 kN. After the yielding point in the mid-span, the strain increased at a higher rate with improvement in the load until the FRP ruptured. The beam failed at the load of 105.75 kN.

5.5.2. Strain in FRP

Figure 5.5 shows the strain along the principal fibres of the CFRP sheets versus the load at mid-span for the beam F-M-B. The strain in the mid-span increased with a constant slope along the load increment prior to the flexural concrete cracks (Load = 20 kN). Due to the CFRP sheet local debonding, cracks resulted in less shear transfer points between the CFRP sheet and the concrete which caused a slighter slope in the strain of the CFRP versus the load diagram. After the longitudinal steel yielded, the cracks opened up noticeably. This led to more local debonding (evidenced by inspection) and slighter slope in the CFRP sheet strain versus the load at mid-span seen in Figure 5.5. The maximum measured strain in the CFRP reached a strain of 11600 με which is 110% of the ultimate strain of the used CFRP (0.0105mm/mm) as provided by the supplier. The CFRP ruptured at load of 105.75 kN which caused a brittle failure in the specimen F-M-B.

However, the anchoring mechanism of the epoxy-bonded FRP was successful in enabling the beam to reach the maximum flexural capacity of the FRP-rehabilitated beam by utilizing the full capacity of the provided CFRP sheet (that ruptured in the midspan of the beam).

5.5.3. Strain in steel link members

The presence of the anchorage system resulted that the CFRP sheet did not peel-off before its rupture. Therefore, the strain in the steel link members remained small during the loading time.

5.5.4. Load-deflection relationship

The load versus mid-span deflection relationship for the specimen F-M-B is shown in Figure 5.1. The specimen F-M-B was strengthened with the epoxy-bonded CFRP and the hybrid FRP / ductile anchors failed in a brittle manner by the CFRP sheet rupture that was preceded by yielding of the steel reinforcement. The beam F-M-B showed a slightly stiffer behaviour than the control beam, as shown in the Figure 5.1. The specimen F-M-B had a yield displacement of 10.41 mm that corresponds to the load of 75.45 kN. The F-M-B specimen had a mid-span deflection of 35.05 mm when it reached its maximum load capacity of 105.75 kN. The drop in load-deflection diagram occurred when the FRP sheet ruptured.

The specimen F-M-B exhibited a brittle behaviour due to the sudden rupture of the CFRP sheet, with a displacement ductility of 3.37. During the test, it was observed that the epoxy bonded CFRP sheet debonded very close to the peak load attained.

Debonding progressed from the midspan region toward one end of the beam.After the CFRP rupture, the test was stopped since the flexural behaviour of the T-beam would follow that of the control. The deflected shape of the beam F-M-B is shown in Figure 5.10.

5.6. Performance comparison of T-Beams strengthened in Flexure

The results obtained from the tests conducted on the four reinforced concrete beams with column stubs are discussed in this section. The intent of this discussion is to evaluate the relative performance of beams strengthened with hybrid FRP / ductile anchorage system to those strengthened using conventional epoxy bonding application. Table 5.1 shows a summary of the test results for the four tested beams. The load versus mid-span deflection relationship for all specimens is shown in Figure 5.1.

The control T-beam exhibited a conventional ductile flexural mode of failure in which the T-beam failed by yielding of the steel reinforcement followed by crushing of the concrete. Specimen F-E-B that was strengthened with external epoxy bonding with no external anchorage failed prematurely without warning by debonding of the CFRP sheet after yielding of the steel reinforcement (failure mode 4). Beam F-E-B had only 7% higher load capacity compared to the control beam F-C-O. The CFRP sheet debonded at a displacement ductility of 1.91, after which, the response of the beam was governed by the original RC section.

On the other hand, beam F-M-U strengthened using the unbonded hybrid FRP / ductile anchorage strengthening system resulted in about 21% increase in the load carrying capacity compared to that of the control beam. The beam showed a high

displacement ductility level that reached 9.09. The increase in strength and ductility were achieved by fully utilizing the capacity of the CFRP sheet through triggering yielding in the anchors' links and allowing the beam to crack and deflect without being restrained by bond with the CFRP sheet. Using the same system ductile anchorage system of F-M-U, yet bonding the CFRP with epoxy to the beam soffit, beam F-M-B showed an increase in the strength capacity of 27% compared to the control beam, but failed due to the rupture of CFRP at a low displacement ductility of 3.37 mainly due to the high strains arising from being bonded at the locations of crack growths in the flexure zone. Although anchoring the CFRP sheets, that are bonded to the beam, at the beams' ends eliminated the peeling off of the sheets, yet the CFRP sheet was subjected to high strains due to the growth of the flexural cracks, which resulted in a sudden rupture of the CFRP sheets (failure mode 2) without reaching high ductility levels in the beam.

Thus, the premature debonding and limited load capacity of F-E-B beam, and the FRP rupture with limited displacement ductility of beam F-M-B were successfully avoided in beam F-M-U that showed high load capacity and ductility.

From Table 5.1 it could be seen that the strengthening techniques used in F-E-B and F-M-B beams resulted in an increase in the load corresponding to the yielding of longitudinal reinforcement of the control beam by about 15% and 20%, respectively. On the other hand, the level of increase in the load corresponding to the yielding of longitudinal reinforcement in beam F-M-U was less than 5%. This could be attributed to the fact the strengthening mechanism of F-M-U comes in effect after the beam deforms and starts to strain the FRP sheets and the steel link members, which is not the case in the strengthening techniques of F-E-B and F-M-B where the FRP strains throughout the

increase in applied loads. The mid-span deflection at maximum load of the T-beam strengthened with unbonded hybrid FRP / ductile anchorage system was about 366% higher than that of specimen F-E-B, 151% higher than that of specimen F-M-B, and even 96% higher than that of the control.

Displacement ductility values for the four beams, defined as the ratio of the midspan deflection at the maximum load to the midspan deflection at the yield of longitudinal reinforcement, are shown in Table 5.1. From the table, it could be seen that beam F-M-U, which was strengthened with unbonded hybrid FRP / ductile anchorage method, had the most ductile behaviour, with a displacement ductility of 9.09, whereas the other strengthening methods resulted in displacement ductilities that are less than that of the control beam.

Figure 5.11 shows the load and displacement ductility capacities of the three strengthened beams in relation to those of the control beam. From the figure it could be seen that beam F-M-U that was strengthened using a ductile anchor system with unbonded FRP sheet was able to gain an increase in both; load carrying capacity and displacement ductility. This was not possible by the other two strengthening systems.

Table 5.1 Experimantal Results

Beam	Concrete compressive strength (MPa)	CFRP condition	Number of layers	Direction of Fibre alignment	External anchorage
F-C-O	32.0	---	---	---	---
F-E-B	37.1	wet-bonded	1	horizontal	---
F-M-U	39.0	wet-unbonded	1	horizontal	hybrid CFRP/ steel ductile anchor
F-M-B	39.2	wet-bonded	1	horizontal	hybrid CFRP/ steel ductile anchor

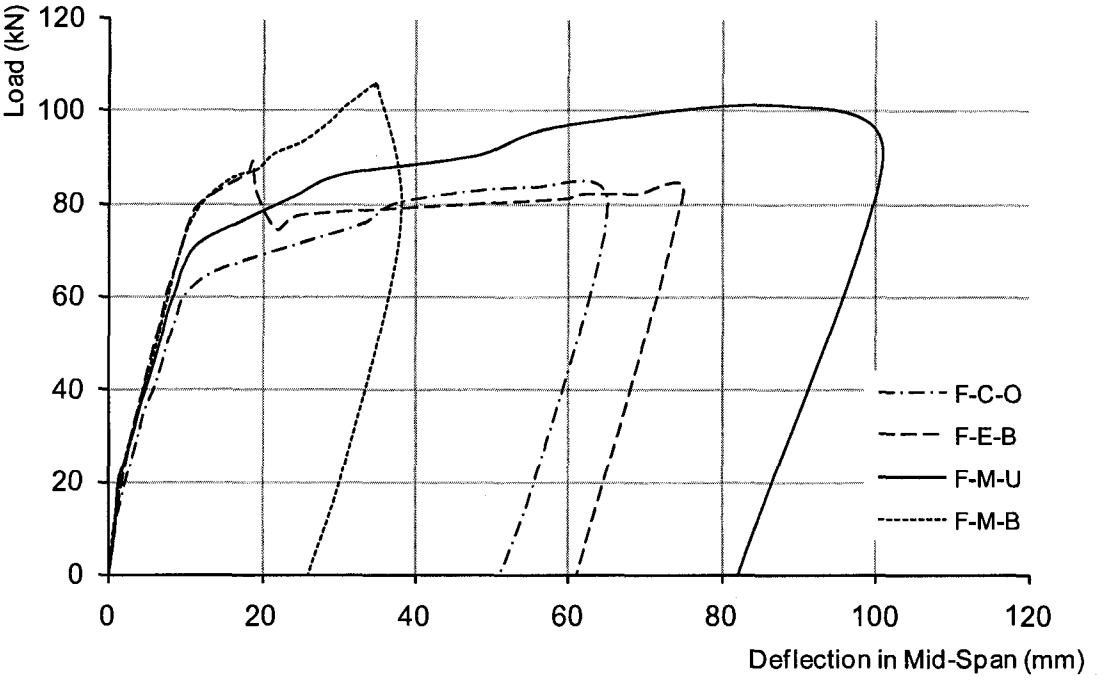

Figure 5.1. Load versus mid-span deflection of all the beams strengthened in flexure

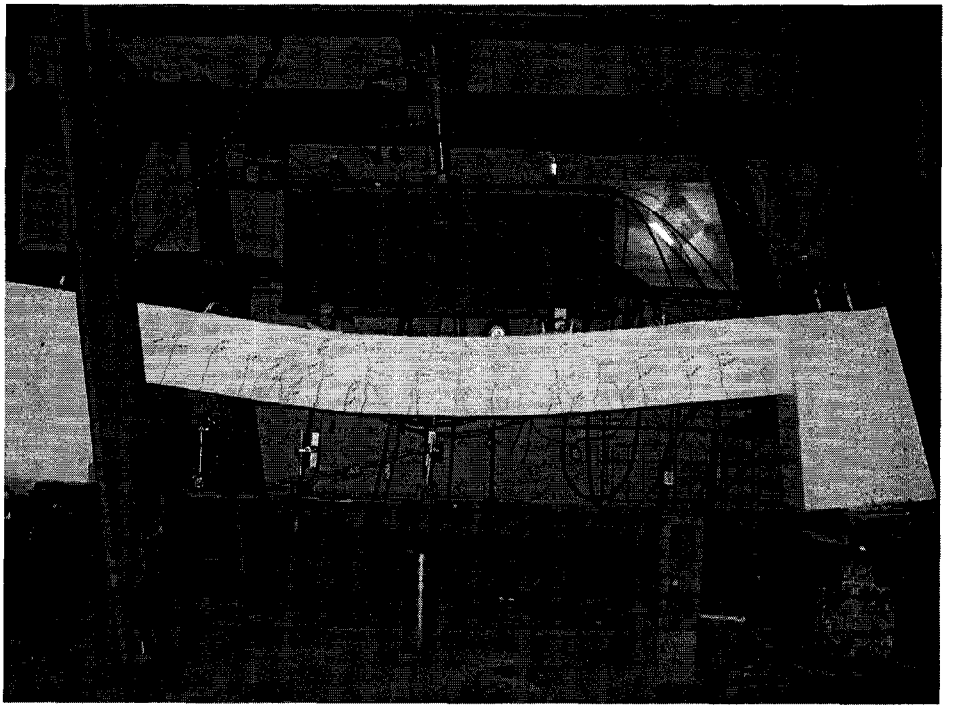

Figure 5.2. Beam F-C-O at maximum deformation

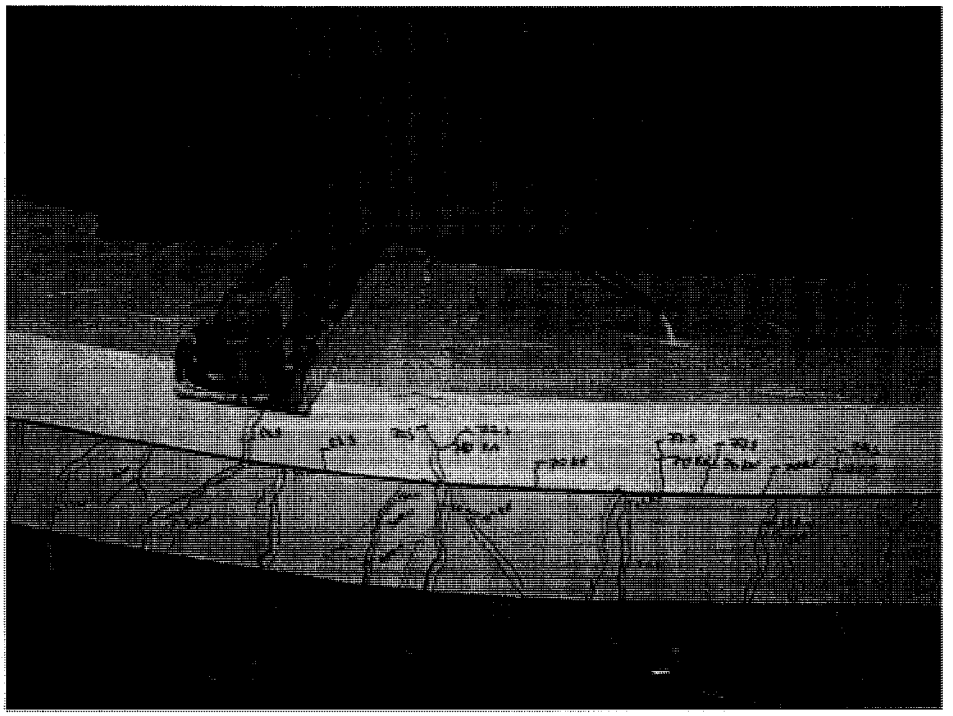

Figure 5.3. Cover concrete crushed in specimen F-C-O

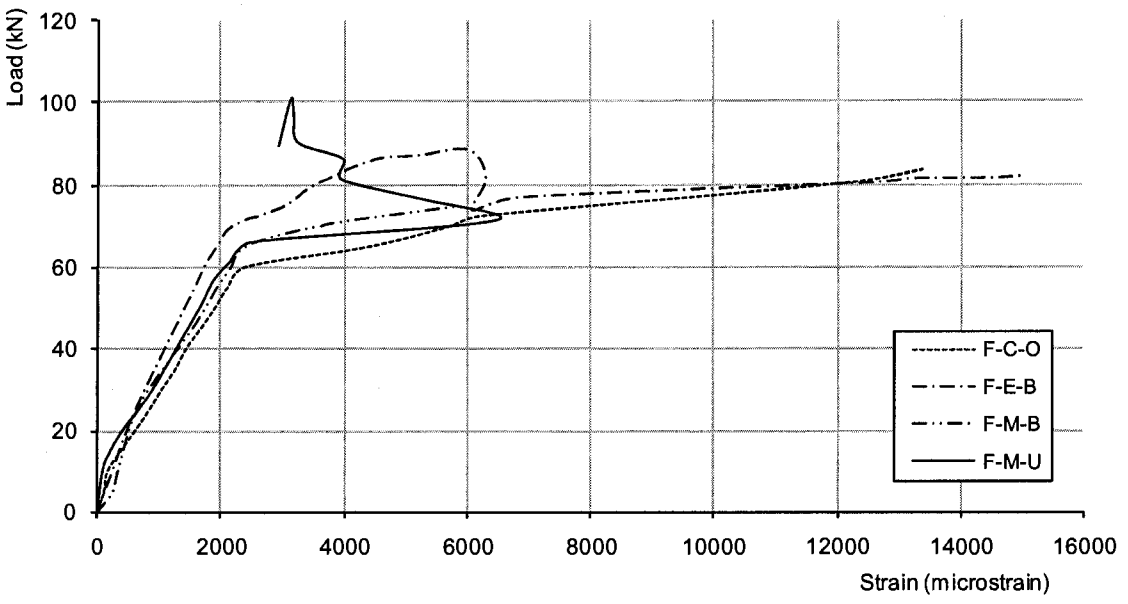

Figure 5.4. Load versus strain in flexural reinforcement in the mid-span of all the beams strengthened in flexure

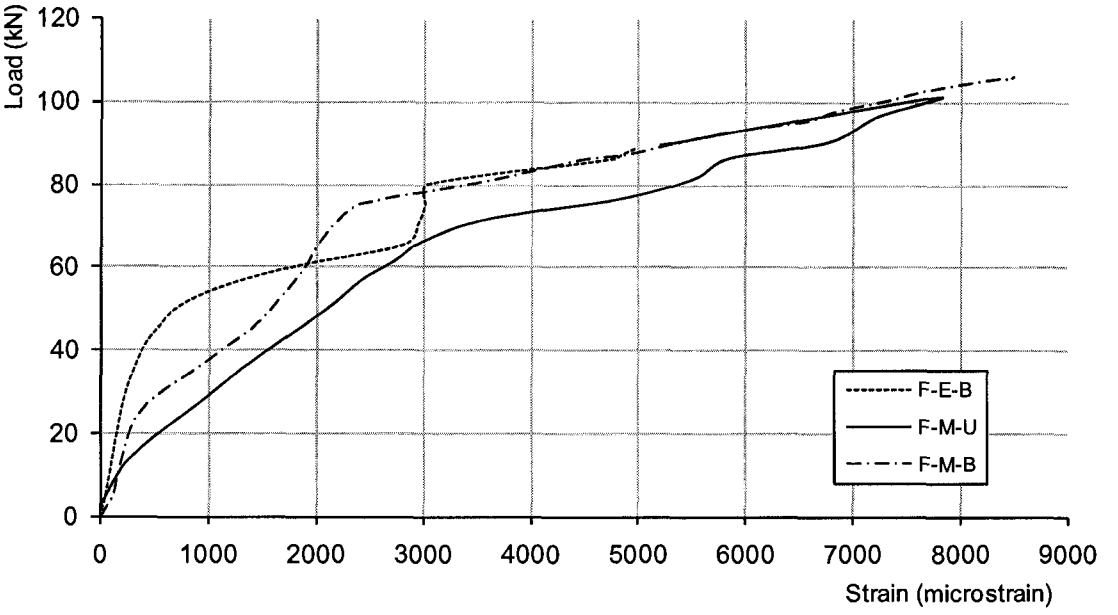

Figure 5.5. Load versus strain in CFRP sheet of all the beams strengthened in flexure

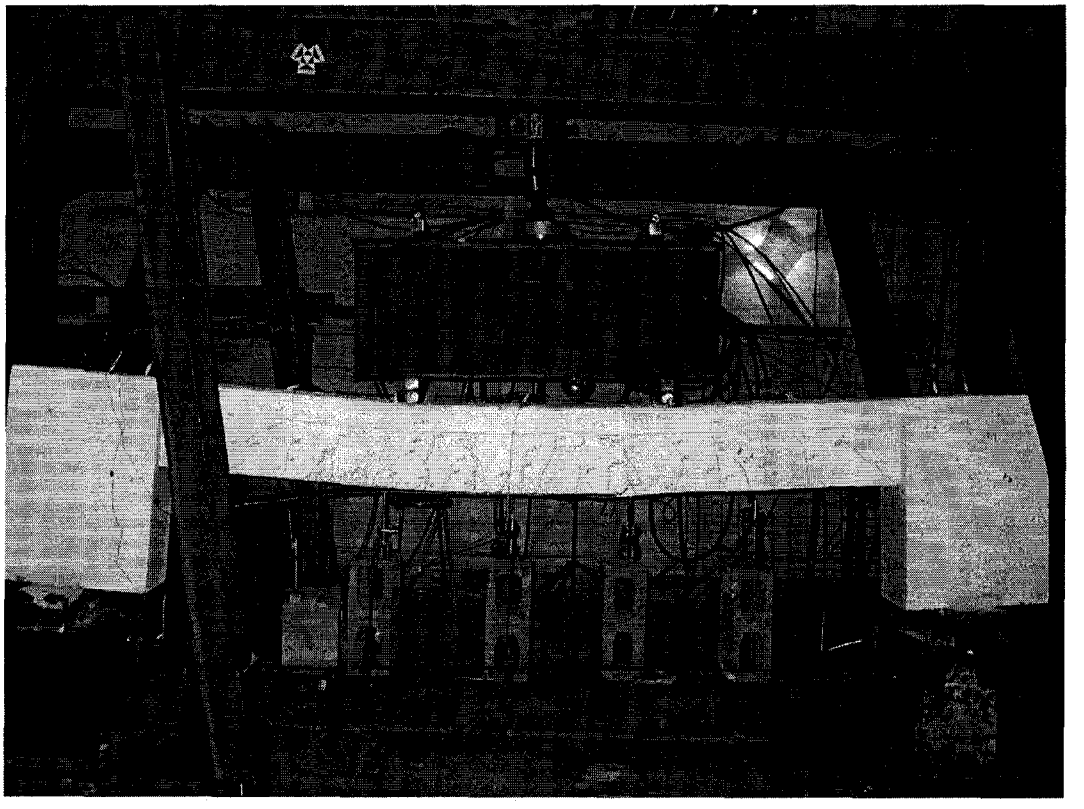

Figure 5.6. Deflected shape of the beam F-E-B

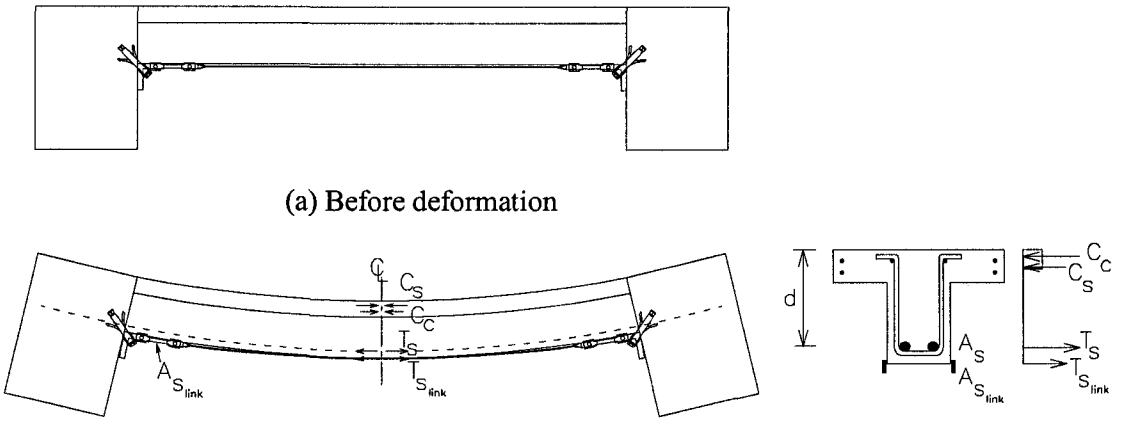

Figure 5.7. Simplified analysis of the proposed mechanism (beam F-M-U)

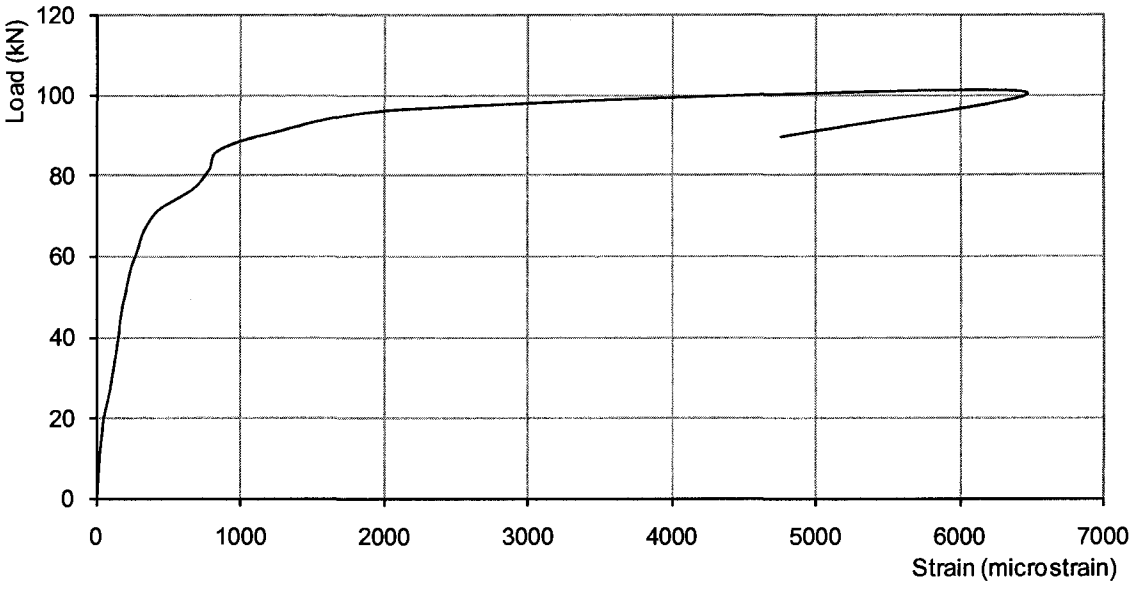

Figure 5.8. Load versus strain in steel link member of specimen F-M-U

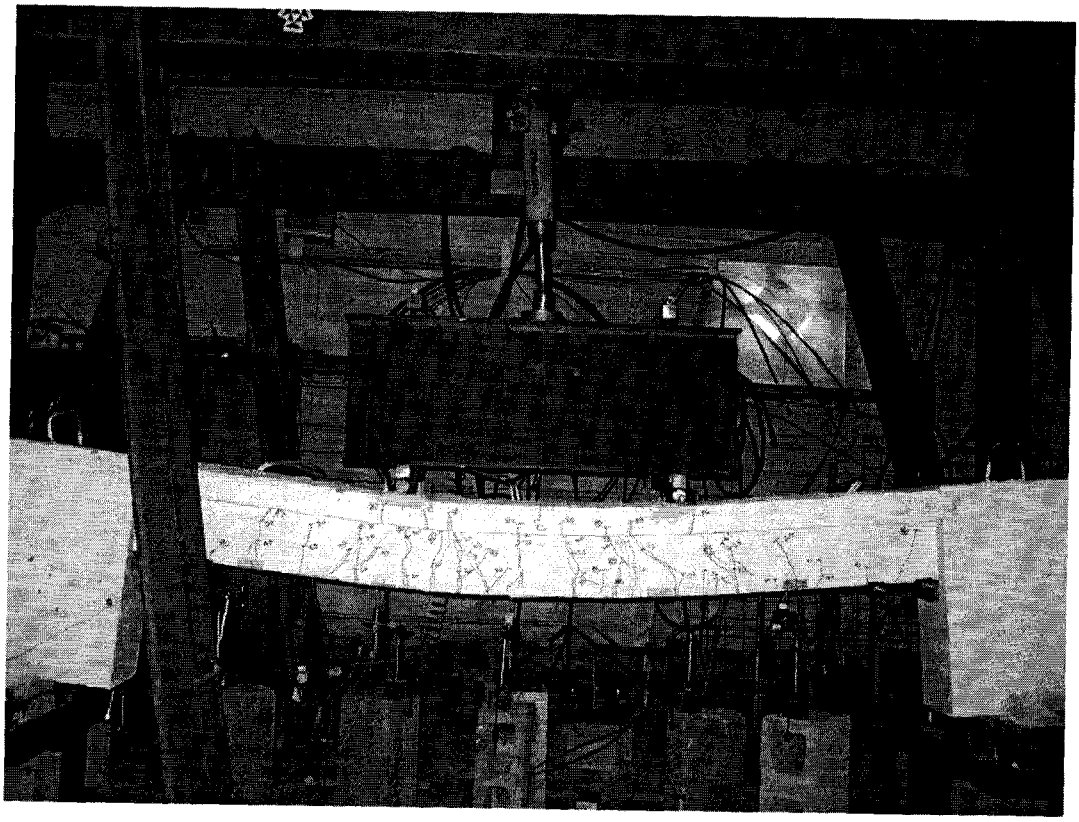

Figure 5.9. Deflected shape of the beam F-M-U

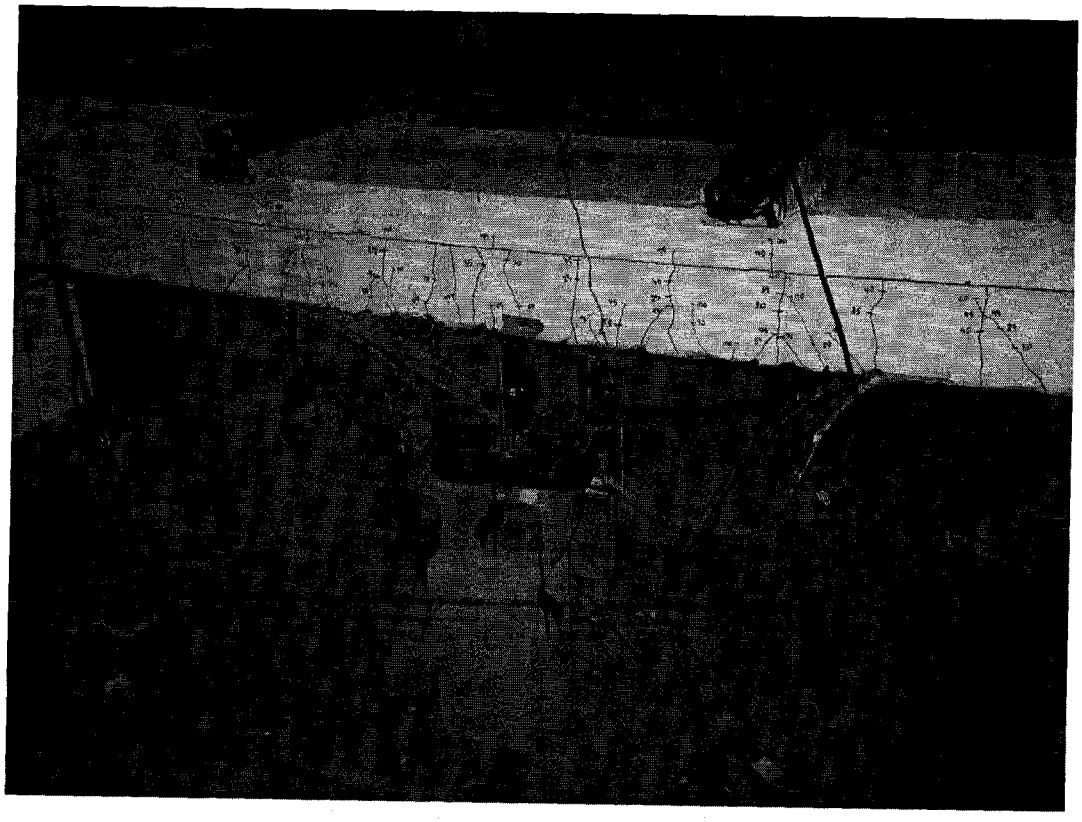

Figure 5.10. Deflected shape of the beam F-M-B

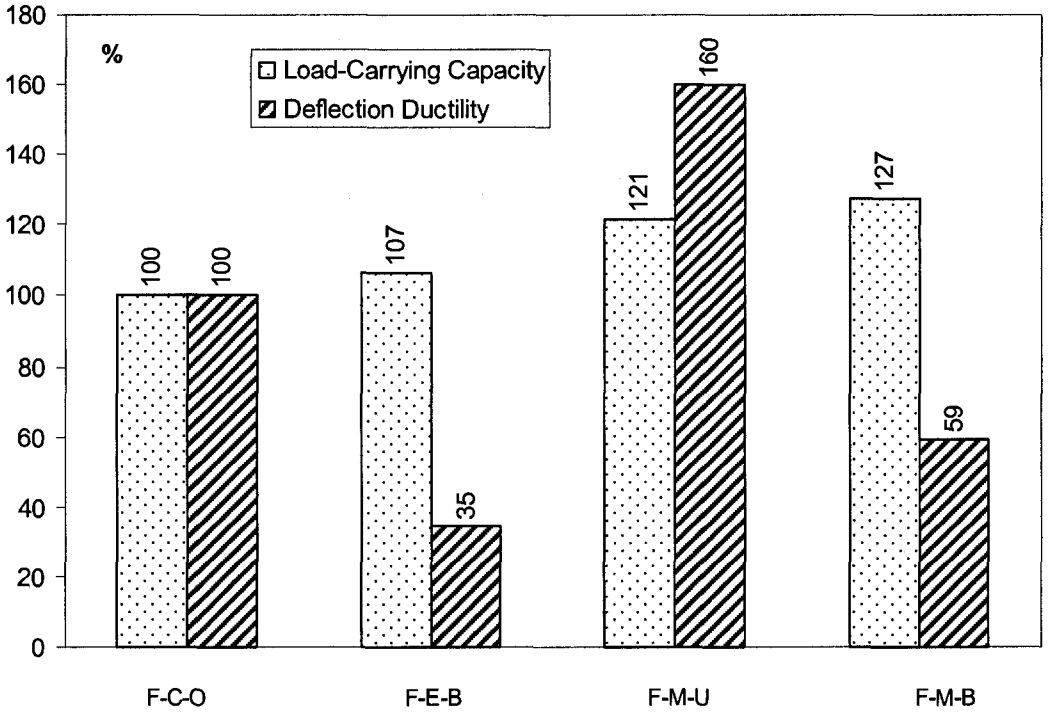

Figure 5.11. Load capacity versus deflection ductility of all specimens

CHAPTER 6

VERIFICATION OF ANALYTICAL MODELS

6.1. General

This chapter presents the predictions using the analytical models and compares the analytical results to the experimental ones. In this chapter, the control beam S-C-O and the beam strengthened in shear using epoxy-bonded FRP wrap, S-E-B, are analyzed using ISIS (2004) code equations. Beam S-M-D that is strengthened using mechanically anchored unbonded CF sheet is analyzed based on a truss behaviour assumption in the CFRP sheet that is analogous to the truss behaviour analysis of conventional steel shear reinforcement. On the other hand, the control beam F-C-O and the beam strengthened using epoxy-bonded CFRP sheet were analyzed using a numerical model of the Respose-2000® V.1.0.5 software (2008) to evaluate their force-deformation relationship. The suitability of using the Respose-2000 software in predicting the force-deformation relationship of beams F-M-U and F-M-B was examined by accounting for the contribution of the hybrid CFRP sheet (unbonded or bonded) / ductile anchor system to the original RC T-beam. Comparisons of the analytical predictions with the experimental results showed that the analytical models used were able to represent the behaviour of the tested beams with good accuracy.

6.2. Basis for numerical/analytical tool choice

The primary focus of this section was to construct a model that is capable of predicting the load carrying capacity and flexural response of reinforced concrete beams strengthened in flexure, tested in this research. The model was created using the commercially available software Response-2000® (2008). A 2D non-linear model of the RC T-beams was developed. The aim of the current model is to use simple models to represent concrete, steel and FRP. Response-2000 is a program that calculates the strength and ductility of a reinforced concrete cross-section subjected to shear, moment, and axial load. All three loads could be applied simultaneously, where the full load-deformation response is obtained based on the Modified Compression Field Theory (Vecchio and Collins, 1986).

Due to brittle mode of failure in the beams strengthened in shear, i.e. the beams did not reach and deform beyond their yielding load capacity, the load-deflection behaviour of the beams was not considered in this chapter. Analytical results for the three beam tested in shear was done using of the CSA A23.3-04 (2004) Design of concrete structures standard, and the ISIS (2006) (Intelligent Sensing for Innovative Structures) design guideline to predict the maximum shear strength of the beams.

6.3. Beams strengthened in shear

Due to the brittle nature of the failure in the beams strengthened in shear, the prediction of the beams' force-deformation response prior to failure was not considered. The goal is to predict the shear force capacity of each beam using analytical formulas provided by CSA A23.3-04 (2004) design code and ISIS (2006) design guidline.

6.3.1. Beam S-C-O

Beam S-C-O was the control T-beam in the group of the beams that were strengthened in shear. The analytical maximum shear resisting force of the beam S-C-O was calculated using CSA A23.3-04 code.

The nominal shear resistance, V_n, is determined by:

$$V_n = V_c + V_S \qquad (6.1)$$

Where V_c is the nominal shear resistance provided by the concrete mechanism, V_s is the nominal shear resistance provided by shear reinforcement.

The value of V_c is computed from:

$$V_c = \lambda.\beta.\sqrt{f_c'}.b_w.d_v \qquad (6.2)$$

Where λ is the factor to account for low-density concrete which is equal to 1.0 since normal-density concrete was used; β is the factor accounting for shear resistance of cracked concrete, f_c' is the specified compressive strength of concrete which is equal to 40.65 MPa for specimen S-C-O, b_w is the beam web width and d_v is the effective shear depth, taken as the greater of 0.9d (d is the distance from extreme compression fibre to centroid of longitudinal tension reinforcement) or 0.72h (where h is the overall height of the member).

The value of β is determined from the general method proposed in CSA A23.3-04 using the following equation:

$$\beta = \frac{0.4}{(1+1500\varepsilon_x)} \cdot \frac{1300}{(1000+s_{ze})} \qquad (6.3)$$

Where ε_x is the longitudinal strain at mid-depth of the member due to factored loads and s_{ze} is the equivalent value of s_z (crack spacing parameter dependent on crack

control characteristics of longitudinal reinforcement) that allows for influence of aggregate size. The longitudinal strain, ε_x, at mid-depth of the cross-section for non-prestressed sections is computed from:

$$\varepsilon_x = \frac{M_n / d_v + V_n}{2E_s A_s} \qquad (6.4)$$

Where V_n is the unfactored shear force; M_n is the unfactored moment, occurring simultaneously with V_n (i.e. at a distance d_v from the face of the support); E_s is the modulus of elasticity of reinforcement and A_s is the area of longitudinal reinforcement on the flexural tension side of the member.

s_{ze} the equivalent crack spacing parameter is calculated from:

$$s_{ze} = \frac{35 s_z}{15 + a_g} \qquad (6.5)$$

Where a_g is the specified nominal maximum size of coarse aggregate. Using the above equations β will be equal to 0.16 therefore:

$$V_c = 0.16\sqrt{f_c'} b_w d_v \qquad (6.6)$$

$$V_c = 0.16 \times \sqrt{40.65} \times 155 \times 224 = 35.4kN$$

The value of V_s is computed from:

$$V_s = \frac{A_v f_y d_v \cot\theta}{s} \qquad (6.7)$$

Where A_v is the area of shear reinforcement s; f_y is the specified yield strength of reinforcement and θ is the angle of inclination of diagonal compressive stresses to the longitudinal axis of the member (θ will be taken equal to 4\5°); s is the spacing of shear reinforcement measured parallel to the longitudinal axis of the member. Therefore V_s is equal to:

$$V_s = \frac{2 \times 100 \times 462 \times 224}{250} = 82.8kN$$

$$\therefore V_n = V_c + V_s = 35.4 + 82.8 = 118.2kN$$

6.3.2. Beam S-E-B

The beam S-E-B had U-shaped bonded CFRP jackets in its shear spans as external shear reinforcement. The jackets were made of single CFRP sheet with the fiber in the direction perpendicular to the longitudinal axis of the beam (90°). The maximum shear resisting force of the beam S-E-B was calculated using CSA A23.3-04 and ISIS 2006.

Using ISIS (2006), the nominal shear resistance, V_n, is determined by:

$$V_n = V_c + V_s + V_{frp} \qquad (6.8)$$

Where V_{frp} is the nominal shear resistance attributed to the FRP. V_c and V_s are calculated using the CSA A23.3-04 code. The value of f_c' for the beam S-E-B was 43.03 MPa. Therefore V_c and V_s are equal to:

$$V_c = 0.16 \times \sqrt{43.03} \times 155 \times 224 = 36.4kN$$

$$V_s = \frac{2 \times 100 \times 462 \times 224}{250} = 82.8kN$$

The value of V_{frp} is calculated using ISIS design guideline. V_{frp}, can be determined using the following expression, which is analogous to the equation used for the contribution of the internal reinforcing steel:

$$V_{frp} = \frac{A_{frp} E_{frp} \varepsilon_{frp} d_{frp} (\sin\beta + \cos\beta)}{s_{frp}} \qquad (6.9)$$

Where A_{frp} is the area of FRP shear reinforcement; E_{frp} is the FRP reinforcement modulus of elasticity; ε_{frp} is the strain in FRP reinforcement, d_{frp} effective depth to flexural FRP reinforcement and β is the angle between inclined FRP sheet and the longitudinal axis of the member (which is equal to 90°).

$$A_{frp} = 2t_{frp}w_{frp} \tag{6. 10}$$

In the above expressions, s_{frp}, w_{frp}, and β are the spacing, width and angle of the shear reinforcement to the longitudinal axis of the beam, respectively. For full surface (i.e. continuous) FRP shear reinforcement: $w_{frp} = s_{frp}$.

The effective depth of the FRP stirrups, d_{frp}, is taken as the distance from the free end of the FRP shear reinforcement underneath the flange to the bottom of the internal steel stirrups. For the rare case of a completely wrapped member, d_{frp} can be taken as the total height of the section.

The effective strain in the FRP, ε_{frpe}, is determined by applying a reduction factor, R, to the ultimate strain of the composite:

$$\varepsilon_{frpe} = R.\varepsilon_{frpu} \leq 0.004 \tag{6. 11}$$

The effective strain is limited to $\varepsilon_{frpe} \leq 0.004$ to ensure aggregate interlock in the concrete by preventing shear cracks from widening beyond acceptable limits. The reduction factor, R, is determined from an equation based on experimental data as follows:

$$R = \alpha\lambda_1 \left[\frac{f_c'^{2/3}}{\rho_{frp}E_{frp}}\right]^{\lambda_2} \tag{6. 12}$$

In the above expression, the reduction coefficient for effective strain, α, is equal to 0.8, and the experimentally derived parameters λ_1=1.35 and λ_2=0.30 for carbon FRPs (ISIS 2004). The FRP shear reinforcement ratio, ρ_{frp}, can be determined from:

$$\rho_{frp} = \left(\frac{2t_{frp}}{b_w}\right)\left(\frac{w_{frp}}{s_{frp}}\right) \tag{6. 13}$$

Therefore,

$$\rho_{frp} = \left(\frac{2\times 0.25}{155}\right) = 0.0032$$

$$R = 0.8\times 1.35\times\left[\frac{43.03^{2/3}}{0.0032\times 86900}\right]^{0.3} = 0.42$$

$$\varepsilon_{frpe} = R.\varepsilon_{frpu} \leq 0.004$$
$$\varepsilon_{frpe} = 0.42\times 0.0105 = 0.0044 \leq 0.004$$
$$\varepsilon_{frpe} = 0.004$$

A second limit is imposed on the effective strain in the FRP shear reinforcement to avoid failure by sudden debonding of the FRP reinforcement. Obviously, this limit does not apply to fully-wrapped specimens. The limiting strain in the FRP shear reinforcement to prevent debonding failure is described by:

$$\varepsilon_{frpe} = \frac{\alpha k_1 k_2 L_e}{9525} \tag{6. 14}$$

Where α = 0.8 and the parameters k_1 and k_2 are given by:

$$k_1 = \left[\frac{f_c'}{27.65}\right]^{2/3} \tag{6. 15}$$

$$k_2 = \frac{d_{frp} - n_e L_e}{d_{frp}} \tag{6. 16}$$

The parameter n_e in the above expression is the number of free ends of the FRP stirrup on the side of the beam (i.e., 1 for a U-wrap and 2 for side sheets). The effective anchorage length, L_e, can be determined using the following equation:

$$L_e = \frac{25350}{(t_{frp} E_{frp})^{0.58}} \qquad (6.17)$$

Using the above equations the effective strain ε_{frpe} can be calculated as below:

$$L_e = \frac{25350}{(0.25 \times 86900)^{0.58}} = 77.36mm$$

$$k_2 = \frac{170 - 1 \times 77}{170} = 0.547$$

$$k_1 = \left[\frac{43.03}{27.65}\right]^{2/3} = 1.34$$

$$\varepsilon_{frpe} = \frac{0.8 \times 1.34 \times 0.547 \times 77}{9525} = 0.0047$$

Therefore the effective strain in the FRP, ε_{frpe}, is limited to 0.004. As such, V_{frp}, can be calculated using the following expression:

$$V_{frp} = 2 \times 0.25 \times 86900 \times 0.004 \times 170 = 29.6kN$$

$$\therefore V_n = V_c + V_s + V_{frp} = 36.4 + 82.8 + 29.6 = 148.8kN$$

6.3.3. Beam S-M-D

The beam S-M-D was strengthened by the anchored U-shaped dry CF sheet system. The maximum shear resisting force of the beam S-M-D was calculated using CSA A23.3-04 (2004) and ISIS (2006).

Using ISIS (2004), the nominal shear resistance, V_n, is determined by:

$$V_n = V_c + V_s + V_{frp}$$

Where V_{frp} is the nominal shear resistance attributed to the CF. V_c and V_s are calculated using the CSA A23.3-04 code. The value of f_c' for the beam S-M-D was 42.5 MPa. Therefore V_c and V_s are equal to:

$$V_c = 0.16 \times \sqrt{42.5} \times 155 \times 224 = 36.2kN$$

$$V_s = \frac{2 \times 100 \times 462 \times 234}{250} = 82.8kN$$

In the calculation of V_{frp} , the formula provided by ISIS (2004) design guideline will be used. i.e.:

$$V_{frp} = \frac{A_{frp} E_{frp} \varepsilon_{frp} d_{frp} (\sin\beta + \cos\beta)}{s_{frp}}$$

Where A_{frp} is the area of CF shear reinforcement, E_{frp} is the dry fibre reinforcement modulus of elasticity, ε_{frp} is the strain in FRP reinforcement, d_{frp} effective depth to flexural reinforcement, β is the angle between inclined FRP stirrups and the longitudinal axis of the member (which is equal to 90°) and s_{frp} is the spacing of FRP shear reinforcement along the longitudinal axis of the member.

$$A_{frp} = 2t_{frp} w_{frp}$$

Although a continuous carbon fibre sheet was used in strengthening beam S-M-D, yet during the test it has been observed that the dry carbon fibres were significantly stretched in middle of the spacing of the internal steel stirrups in comparison to the fibres in other locations. This could be interpreted that the dry CF sheets are contributing to the shear capacity of the beam through the formation of a truss pattern, where the highest tensile stresses occurs at the middle of the spacing of the stirrups. This resulted in the

formation of CFR strips every 200 mm (at the middle of the spacing of the internal stirrups) each of them with approximately 48 mm width, based on test observations (Figure 6.1 and 6.2). Therefore in the analytical calculation of V_{frp}, it has been assumed that shear contribution of the FR sheet is gained from CF strips with 48mm width at 200mm spacing that reach their ultimate strain of dry CF, so V_{frp} can be calculated from:

$$V_{frp} = \frac{2 \times 0.127 \times 48 \times 230000 \times 0.017 \times 170}{200} = 40.5kN$$

Due to unbonded nature of the strengthening system used in the beam S-M-D, strain limitation to avoid failure by sudden debonding of the fibre reinforcement (i.e. limiting ε_{frpe}, to 0.004 as in beam S-E-B) need not to be checked. Consequently, V_n will be:

$$\therefore V_n = V_c + V_s + V_{frp} = 36.2 + 82.8 + 40.5 = 159.5kN$$

6.4. Comparison between experimental and analytical results for beams strengthened in Shear

Table 6.1 summarizes both the analytical predictions and the experimental results for the beams strengthened in shear. The degree of correlation between the predicted and experimental results is calculated as a ratio of predicted values to experimental values. As can be seen from the table, the shear strength analytical values are higher than the experimental failure loads upto 17% for the three tested beams. The proposed model for calculating the V_{frp}, and consequently V_n, for beam S-M-D showed a good correlation with the shear capacity reached during the test. Figure 6.3 compares the experimental results and analytical predicted results.

6.5. Beams strengthened in flexure

Load carrying capacity and flexural response of the beams strengthened in flexure is modeled using Response-2000 (2008) software. Response-2000 is a non-linear sectional analysis program which is designed to predict the load-deformation response of reinforced concrete sections subjected to bending moments, axial loads and shear forces (Figure 6.4). The analytical procedures in Response-2000 are based on traditional engineering beam theory, which assumes that plane sections remain plane and that the distribution of shear stresses across the section is defined by the rate of change of flexural stresses. When relating stresses and strains at various locations across the section, the program uses the Modified Compression Field Theory (Vecchio and Collins 1986). Engineering beam theory assumes that the response of a particular section depends only on the sectional properties and the values of the applied stress resultants (i.e. the moment, the axial load and the shear). That is, the theory is valid for analysis of the beams with flexural dominant behaviour. St. Venant's Principle implies that treating only the stress resultants will be appropriate for sections which are at least the depth of the member away from point loads or supports. Schlaich et al. (1987) introduced the terminology of B-regions and D-regions. A B-region is a portion of a member where the assumptions of engineering beam theory are accurate, while a D-region is a portion where the stress distributions are disturbed by the local effects of the applied loads, the supports, or other discontinuities. Sectional analysis is accurate in B-regions but not in D-regions.

Response-2000 uses a method to integrate the sectional behaviour for simple prismatic beam-segments. The first assumption in Response-2000 is the traditional engineering beam theory assumption that plane sections remain plane. The second

assumption is that there is no significant transverse clamping stress acting through the depth of the beam. This is also an appropriate assumption for beams that are of a similar length to that above and produces conservative results. That is, if there is transverse clamping, the real strength of the beam will be higher than that predicted by the program. The third assumption is that the Modified Compression Field Theory (MCFT) can be used for biaxial stress-strain behaviour throughout the depth of the beam. Using these three assumptions, the generally well known fibre model of sectional analysis is extended to include the effects of shear.

Response-2000 will calculate the full member behaviour for a prismatic section as well. This analysis will calculate an entire Moment-Shear interaction diagram and determine the load-deflection properties and crack diagram for the entire half span of the beam.

Figure 6.5a shows the stress-strain relationships of concrete in compression used to define the material properties of the non-linear model. In compression, the stress-strain curve is taken to be linear up to 60% of the compressive strength of concrete, after which a non-linear relationship represented by a parabola proposed by Vecchio and Collins (1986) is assumed. In tension, the stress-strain curve for concrete follows the model proposed by Bentz (1999).

Figure 6.5b shows the stress-strain relationships of the steel used in Response-2000 to define the material properties of the non-linear model. Values of elastic modulus, yield strength, rupture strain and ultimate strength are taken as 200,000 MPa, 462 MPa, 170 mm/m and 570 MPa, respectively.

Figure 6.6a shows the stress-strain relationship of the equivalent CFRP member used in Response-2000 model. Value of elastic modulus, rupture strain and ultimate strength is taken as 102,000 MPa, 10.5 mm/m and 1062 MPa.

6.5.1. Beam F-C-O

In the experimental program, all the beams were tested in 4-point bending. Similarly, in the computer models all the beams were loaded using 4-point loading systems. Figure 6.7 shows the comparison between the experimental load carrying capacity, numerical model load carrying capacity of the four beams strengthened in flexure taken from Response-2000 and code equations. Detailed calculation for the maximum load carrying capacity of the beam F-C-O using code equations is provided in appendix A.

The difference between the predicted load capacity using the Response-2000 model and the experimental load capacity for beam F-C-O is 5% (79.2 kN / 83. 45 kN). On the other hand, the difference between the predicted load capacities using the code equations and the experimental load capacity for beam F-C-O is 3% (85.8 kN / 83.45 kN).

The numerical model was used to predict the load-deflection behaviour of the beam F-C-O in order to compare the flexural behaviour of the beam with the experimental test results. The experimental and predicted load-deflection curves for the beam F-C-O are shown in Figure 6.8.

6.5.2. Beam F-E-B

Figure 6.7 shows the comparison between the experimental load carrying capacity, numerical model load carrying capacity of Beam F-E-B from Response-2000 model and code equations. Detailed calculation for the maximum load carrying capacity of the beam F-E-B is provided in appendix A. It is important to mention that Response-2000 does not have a model for FRP sheets, yet in this research, an equivalent FRP element was modeled using the available material library of the software. The equivalent element has a linear behaviour up to failure, where the stress values at yield and ultimate coincides to represent the ultimate strength of CFRP sheets. The stress in the CFRP sheet was limited according to ACI 440.2R-02 in order to model debonding behaviour of the CFRP sheet. Therefore ultimate stress in the CFRP sheet was taken as $0.9\sigma_{frp_u}$ (956 MPa), also the strain values at yield, strain-hardening, and ultimate coincides to represent the ultimate CFRP strain. The equivalent ultimate CFRP strain value was limited to $0.9\varepsilon_{frp_u}$ (9.45 mm/m). Detailed calculation for the CFRP ultimate strain limitation in the beam F-E-B is provided in appendix A.

The difference between the predicted load capacity using the Response-2000 model and the experimental load capacity for beam F-E-B is 3% (90.2 kN / 87. 5 kN). On the other hand, the difference between the predicted load capacities using the code equations and the experimental load capacity for beam F-E-B is 8% (94.3 kN / 87.5 kN kN).

The numerical model was used to predict the load-deflection behaviour of the beam F-E-B in order to compare the flexural behaviour of the beam with the

experimental test results. The experimental and predicted load-deflection curves for the beam F-E-B are shown in Figure 6.9.

6.5.3. Beam F-M-U

Figure 6.7 shows the comparison between the experimental load carrying capacity, analytical model load carrying capacity of the four beams strengthened in flexure taken from Response-2000 model and code equations. Detailed calculation for the maximum load carrying capacity of the beam F-M-U is available in appendix A. In order to model the hybrid CFRP sheet unbonded / ductile anchor system in the Response-2000 program accurately, an equivalent tensile rebar was used to represent both, the steel links and the CFRP sheet (of the hybrid unbonded CFRP sheet / ductile anchor system) such that the stress-strain properties of the equivalent tensile rebar simulate those of the hybrid unbonded CFRP sheet / ductile anchor system. The hybrid unbonded CFRP sheet / ductile anchor system consists of two steel links at the two ends, each with length equal to 100mm, and one CFRP sheet in the middle with length equal to 2200 mm. Figure 6.10 shows the characteristics of the equivalent tensile rebar used to represent the hybrid unbonded CFRP sheet / ductile anchor system.

In order to define the characteristics of the equivalent tensile rebar, three different points on its stress-strain relationship of the new material are considered:

At yield:

$$T_{link} = T_{frp} \quad \text{(Equilibrium)} \tag{6. 18}$$

$$f_y.A_{link} = \varepsilon_{frp}.E_{frp}.A_{frp} \Rightarrow \varepsilon_{frp} = \frac{f_y.A_{link}}{E_{frp}.A_{frp}} \tag{6. 19}$$

Also,

$$\Delta_{total} = 2\Delta_1 + \Delta_2 \quad \text{(Figure 6.12)} \tag{6. 20}$$

$$\varepsilon_{eq_1}(2L_1 + L_2) = 2\varepsilon_y L_1 + \varepsilon_{frp} L_2$$

$$\varepsilon_{eq_1}(2L_1 + L_2) = 2\varepsilon_y L_1 + (\frac{\varepsilon_y E_s}{E_{frp}} . \frac{A_{link}}{A_{frp}}).L_2$$

$$\therefore \varepsilon_{eq_1} = \varepsilon_y . \frac{2L_1 + \frac{E_s}{E_{frp}} . \frac{A_{link}}{A_{frp}} . L_2}{2L_1 + L_2} \tag{6. 21}$$

$$\varepsilon_{eq_1} = \varepsilon_y \times \frac{2\times 100 + \frac{200000}{102000} \times \frac{80}{38.5} \times 2200}{2400} = 3.91\varepsilon_y = 0.0078$$

And $$\sigma_{eq_1} = \frac{T_{link}}{A_{link}} = f_y \tag{6. 22}$$

Where T_{link} is tension force in the steel link member, T_{frp} is the tension force in the CFRP sheet, f_y is yield stress in the link member, A_{link} is the cross section area steel of the steel link member, ε_{frp} is the strain in the CFRP sheet, E_{frp} is the modulus of elasticity of CFRP sheet, A_{frp} is the area of the CFRP sheet, Δ_{total} is the total displacement caused by the force T, Δ_1 is the displacement of steel link member caused by a force T, Δ_2 is the displacement of CFRP sheet caused by the force T, ε_{eq_1} is the equivalent strain at yield point, ε_y is the steel strain at yield, E_s is modulus of elasticity of steel and σ_{eq_1} is the equivalent stress at yield point.

At strain hardening:

$$T_{link} = T_{frp} \quad \text{(Equilibrium)}$$

$$f_y . A_{link} = \varepsilon_{frp} . E_{frp} . A_{frp} \Rightarrow \varepsilon_{frp} = \frac{f_y . A_{link}}{E_{frp} . A_{frp}}$$

Also,

$$\Delta_{total} = 2\Delta_1 + \Delta_2$$

$$\varepsilon_{eq_2}(2L_1 + L_2) = 2\varepsilon_{sh}L_1 + \varepsilon_{frp}L_2$$

$$= 2\varepsilon_{sh}L_1 + (\frac{f_y}{E_{frp}}.\frac{A_{link}}{A_{frp}}).L_2$$

$$\varepsilon_{eq_2} = \frac{2\times 0.01\times 100 + \left[\frac{400\times 80}{102000\times 38.5}\right]\times 2200}{2400} = 0.0083$$

And $$\sigma_{eq_2} = \frac{T_{link}}{A_{link}} = f_y$$

Where ε_{eq_2} is the equivalent strain at strain hardening point, ε_{sh} is the steel strain at strain hardening point and σ_{eq_2} is the equivalent stress at strain hardening point.

At ultimate strain:

$T_{link} = T_{frp}$ (Equilibrium)

$$f_y.A_{link} = \varepsilon_{frp}.E_{frp}.A_{frp} \Rightarrow \varepsilon_{frp} = \frac{f_u.A_{link}}{E_{frp}.A_{frp}} = \frac{570\times 80}{102000\times 38.5} = 0.011 \simeq \varepsilon_{frpu}$$

Also,

$$\Delta_{total} = 2\Delta_1 + \Delta_2$$

$$\varepsilon_{eq_3}(2L_1 + L_2) = 2\varepsilon_u L_1 + \varepsilon_{frp_u}L_2$$

$$\varepsilon_{eq_3} = \frac{2\varepsilon_u L_1 + \varepsilon_{frp_u}L_2}{(2L_1 + L_2)} = \frac{2\times 0.17\times 100 + 0.011\times 2200}{2400} = 0.024$$

And $$\sigma_{eq_3} = \frac{T_{link}}{A_{link}} = f_u$$

Where ε_{eq_3} is the equivalent strain at ultimate point, ε_u is the ultimate steel strain, ε_{frp} is the ultimate CFRP strain and σ_{eq_3} is the equivalent stress at ultimate point.

Therefore, the calculated stress-strain relationship was used as input for the equivalent tensile rebar in the Response-2000 software. Figure 6.6b shows the stress-strain relationships of the equivalent material used in Response-2000 for beam F-M-U to define the material properties of the non-linear model.

The difference between the predicted load capacity using the Response-2000 model and the experimental load capacity for beam F-M-U is 1% (101 kN / 100.77 kN). On the other hand, the difference between the predicted load capacities using the code equations and the experimental load capacity for beam F-M-U is 2% (102.2 kN / 100.77 kN).

The numerical model was used to predict the load-deflection behaviour of the beam F-M-U in order to compare the flexural behaviour of the beam with the experimental test results. The experimental and predicted load-deflection curves for the beam F-M-U are shown in Figure 6.11.

6.5.4. Beam F-M-B

Figure 6.7 shows the comparison between the experimental load carrying capacity, numerical model load carrying capacity of Beam F-M-B from Response-2000 model and code equations. Detailed calculation for the maximum load carrying capacity of the beam F-M-B is provided in appendix A. It is important to mention that Response-2000 does not have a model for FRP sheets, yet in this research, an equivalent FRP element was modeled using the available material library of the software. The equivalent

element has a linear behaviour up to failure, where the stress values at yield and ultimate coincides to represent the ultimate strength of CFRP sheets (1062 MPa), and the strain values at yield, strain-hardening, and ultimate coincides to represent the ultimate CFRP strain (10.5 mm/m). As such, the model assumes perfect bond between CFRP sheet and concrete (provided by the anchoring system at the beam ends) and that the CFRP sheet would fail by rupture as it reaches its ultimate strain.

The difference between the predicted load capacity using the Response-2000 model and the experimental load capacity for beam F-M-B is 9% (97.2 kN / 105.75 kN). On the other hand, the difference between the predicted load capacities using the code equations and the experimental load capacity for beam F-M-B is 1% (104.4 kN / 105.75 kN).

The numerical model was used to predict the load-deflection behaviour of the beam F-M-B in order to compare the flexural behaviour of the beam with the experimental test results. The experimental and predicted load-deflection curves for the beam F-M-B are shown in Figure 6.12.

6.6. Comparison between experimental and analytical results for beams strengthened in Flexure

Figure 6.13 shows the experimental and analytical load-deflection relationship at mid-span of the four tested beams. The differences between the predicted load capacities using the analytical models and the experimental load capacities are all within 10% for the four tested beams in flexure. Table 6.2 shows the analytical and experimental load carrying capacity, P_{max}, for the four tested beams.

Table 6.1. Calculated and experimental shear strength (in kN) for beams strengthened in Shear

Beam	Shear Strength (kN)		Calc./Exp.
	Experimental	Calculated	
S-C-O	101 kN	118 kN	1.17
S-E-B	128 kN	148 kN	1.16
S-M-D	149 kN	159 kN	1.07

Table 6.2. Analytical and experimental load carrying capacity (in kN) for beams strengthened in Flexure

Beam	F-C-O	F-E-B	F-M-U	F-M-B
Design code results	85.8	94.3	102.2	104.4
Response-2000 results	79.2	85.6	101.0	97.2
Experimental results	83.5	87.5	100.8	105.7

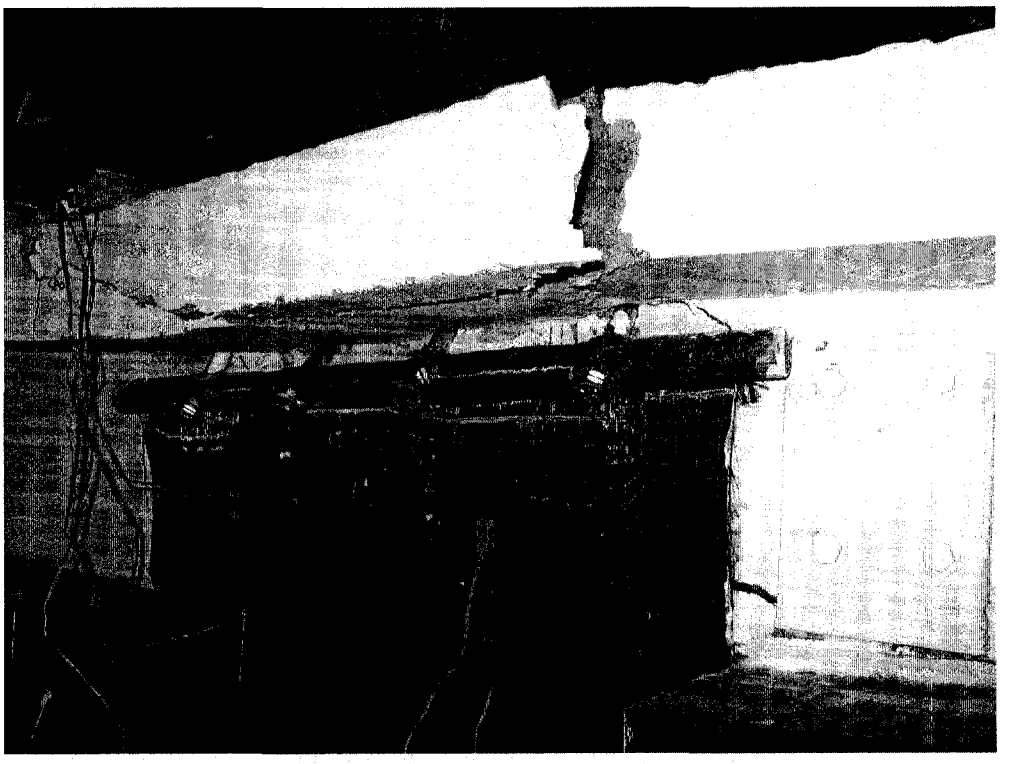

Figure 6.1. Effective CF strips in beam S-M-D (strengthened in shear)

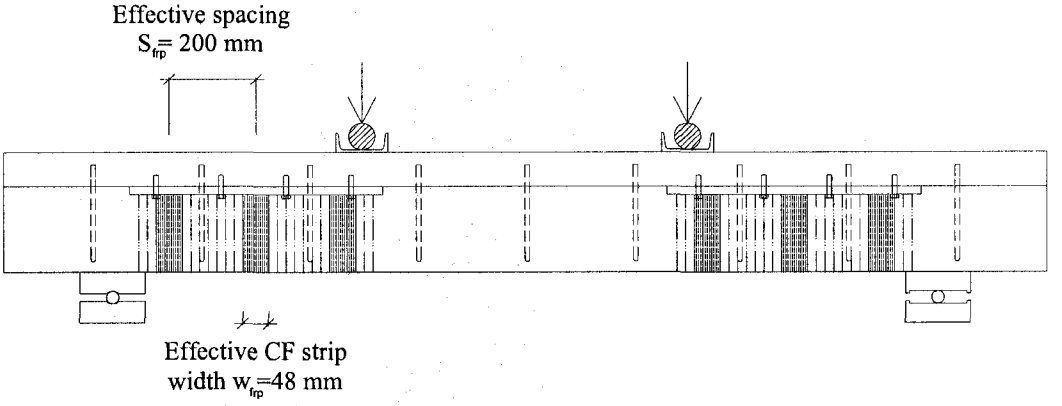

Figure 6.2. Effective CF strips in beam S-M-D (strengthened in shear)

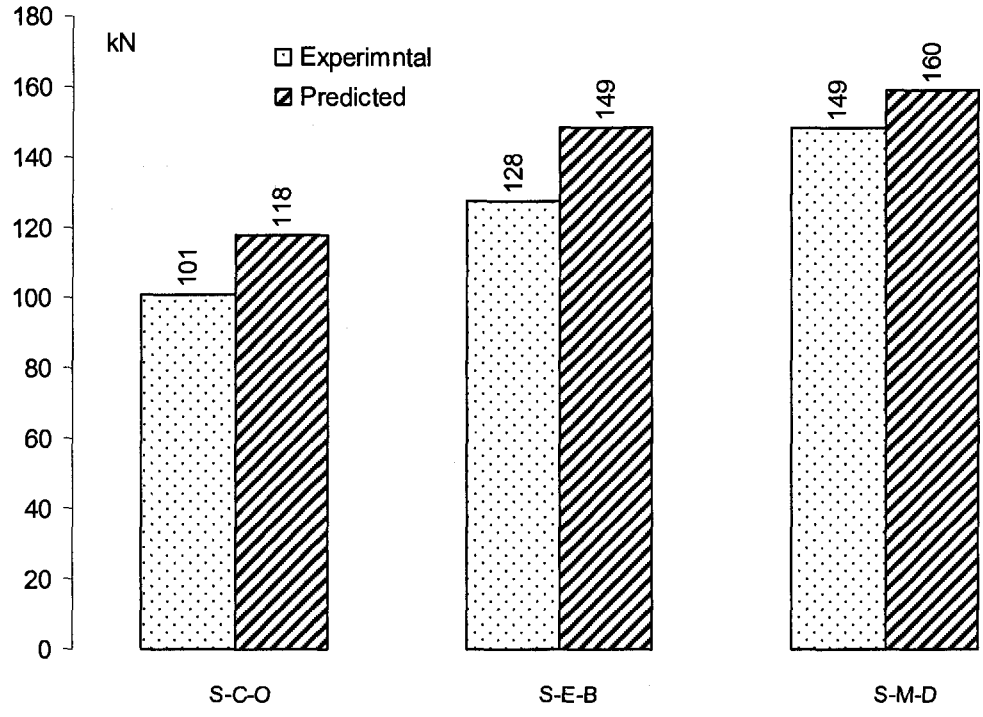

Figure 6.3. Comparison of experimental results and code predictions for beams strengthened in shear

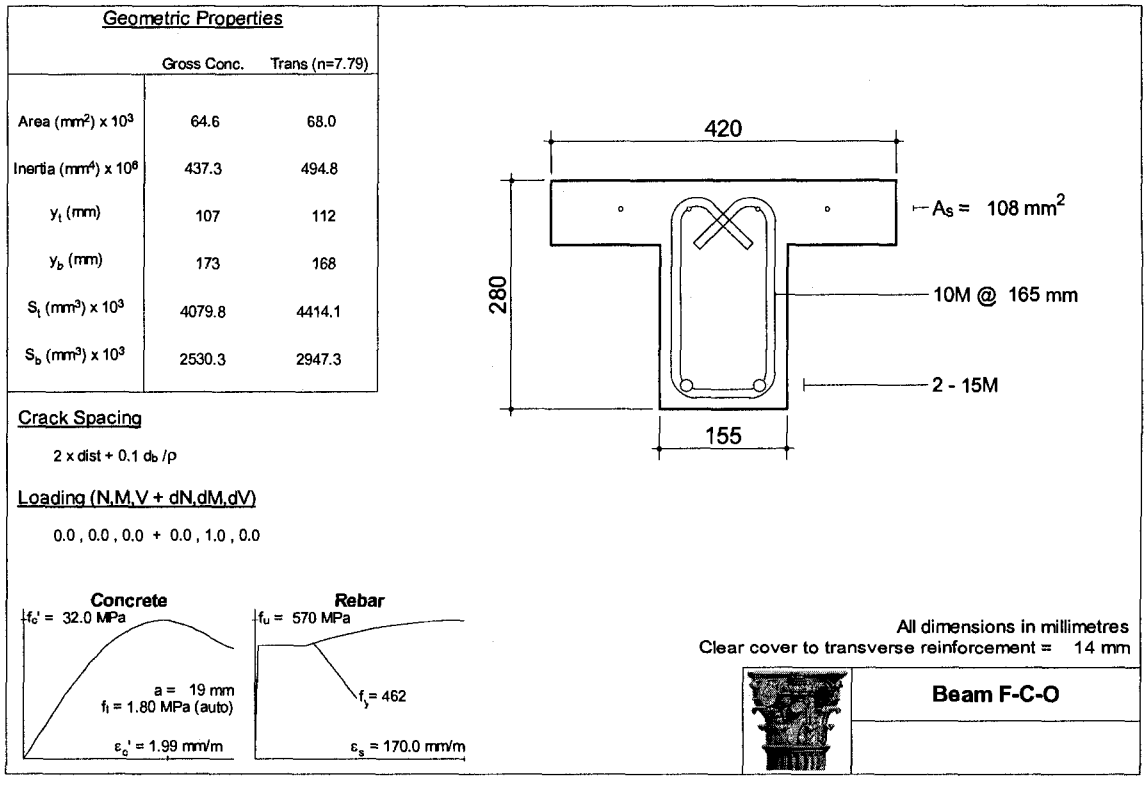

Figure 6.4. Response-2000 program geometric properties page (Bentz 2008)

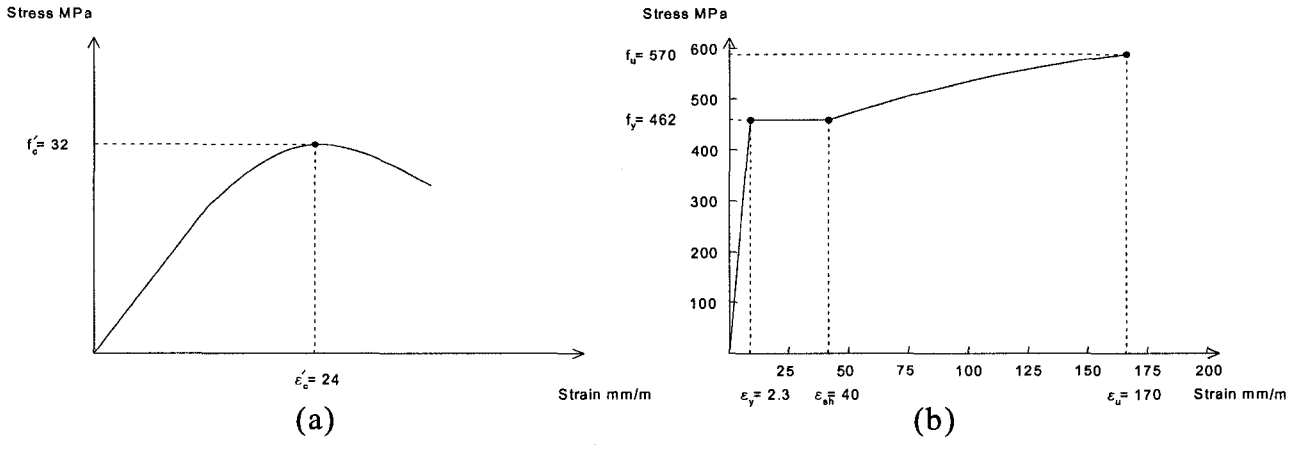

Figure 6.5. Stress-strain relationships of: (a) concrete in compression, and (b) steel used in Response-2000 model for beams strengthened in flexure

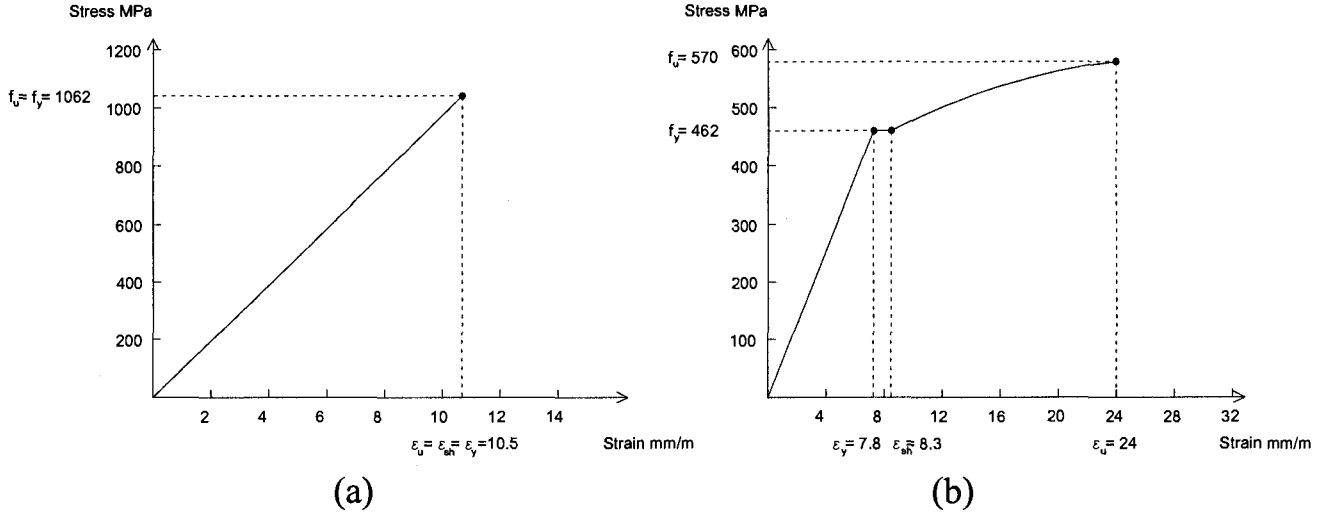

Figure 6.6. Stress-strain relationships of: (a) CFRP, and (b) equivalent tensile rebar in beam F-M-U used in Response-2000 model

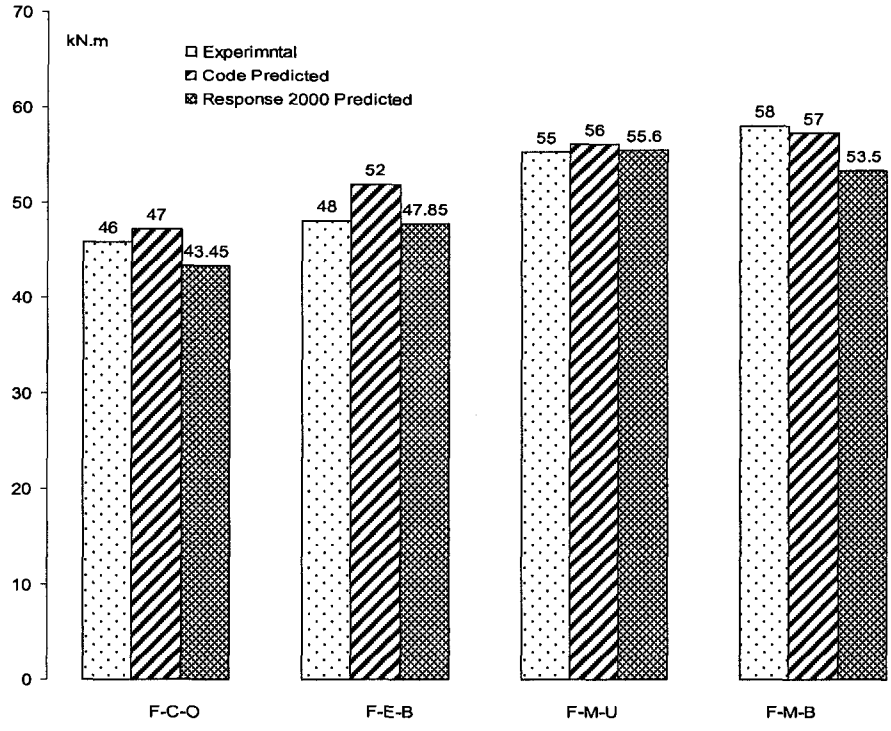

Figure 6.7. Comparison of experimental nominal moment and analytical predictions for beams strengthened in flexure

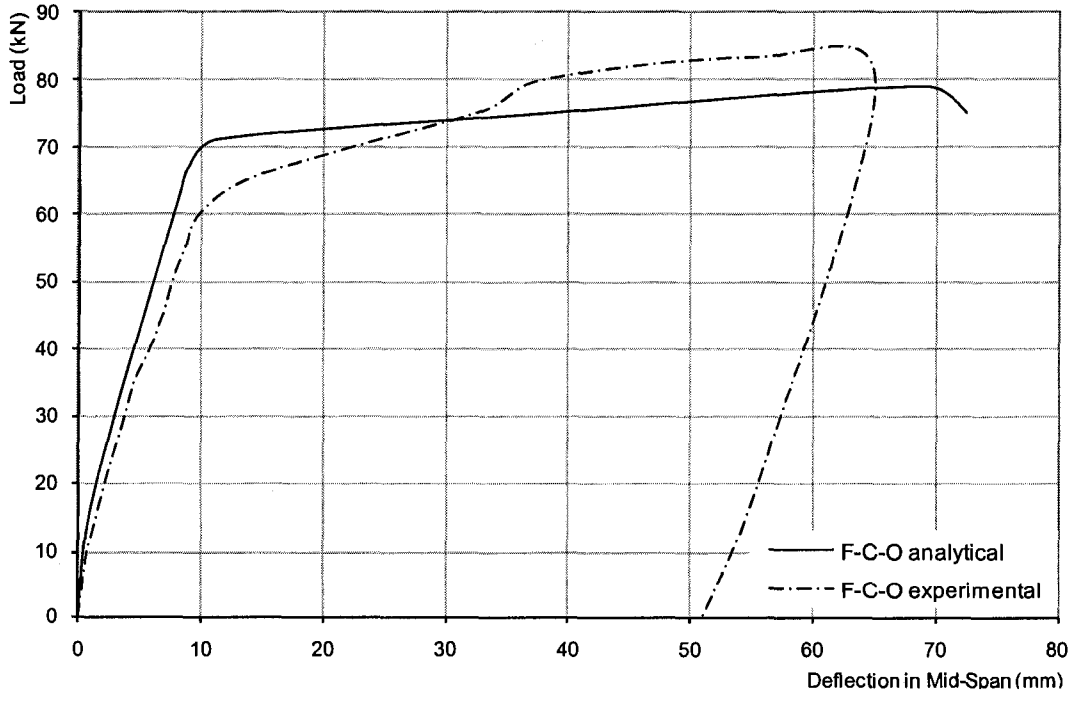

Figure 6.8. Analytical vs. experimental load-deflection relationship in mid-span of beam F-C-O

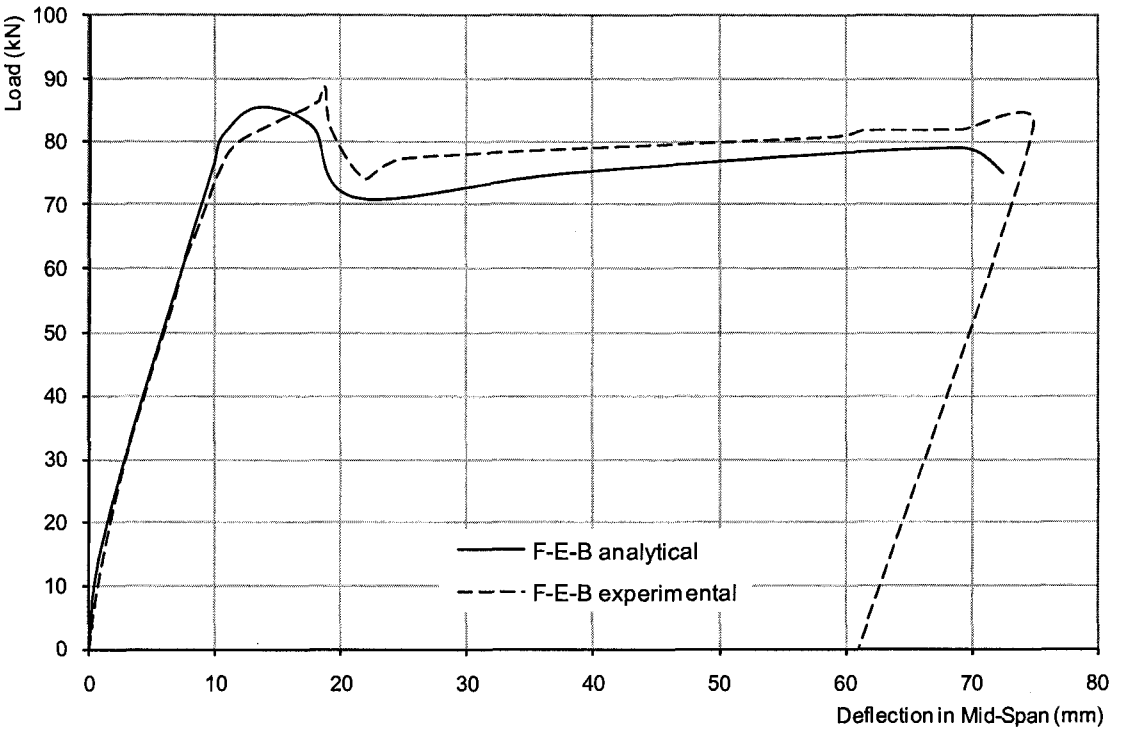

Figure 6.9. Analytical vs. experimental load-deflection in mid-span of beam F-E-B

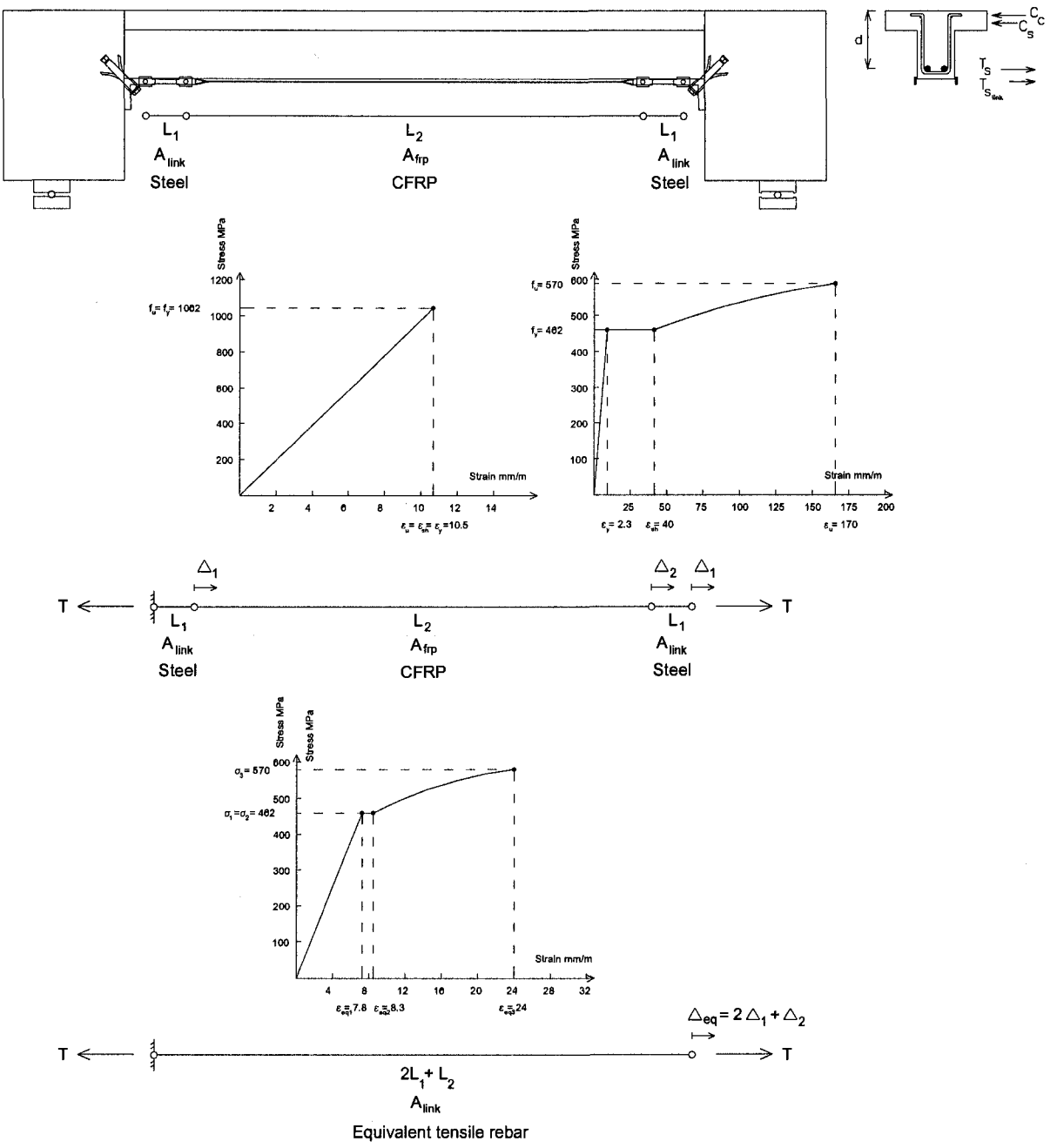

Figure 6.10. Equivalent tensile rebar to represent the hybrid unbonded CFRP sheet / ductile steel anchor system model

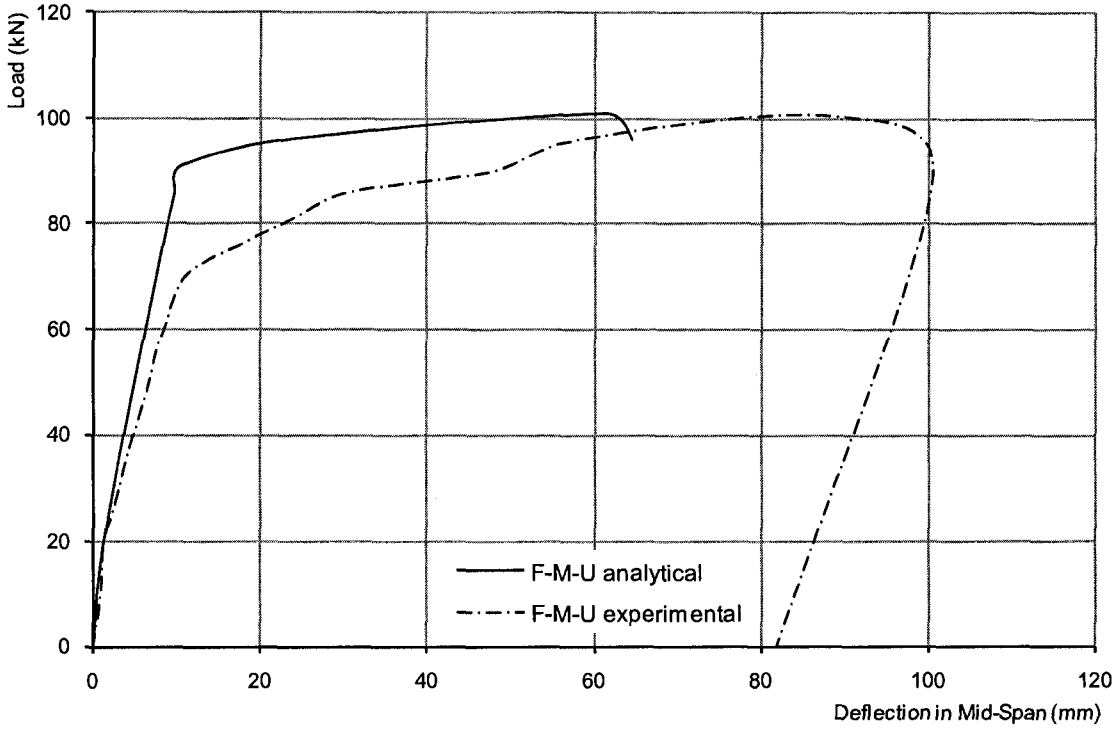

Figure 6.11. Analytical vs. experimental load-deflection in mid-span of beam F-M-U

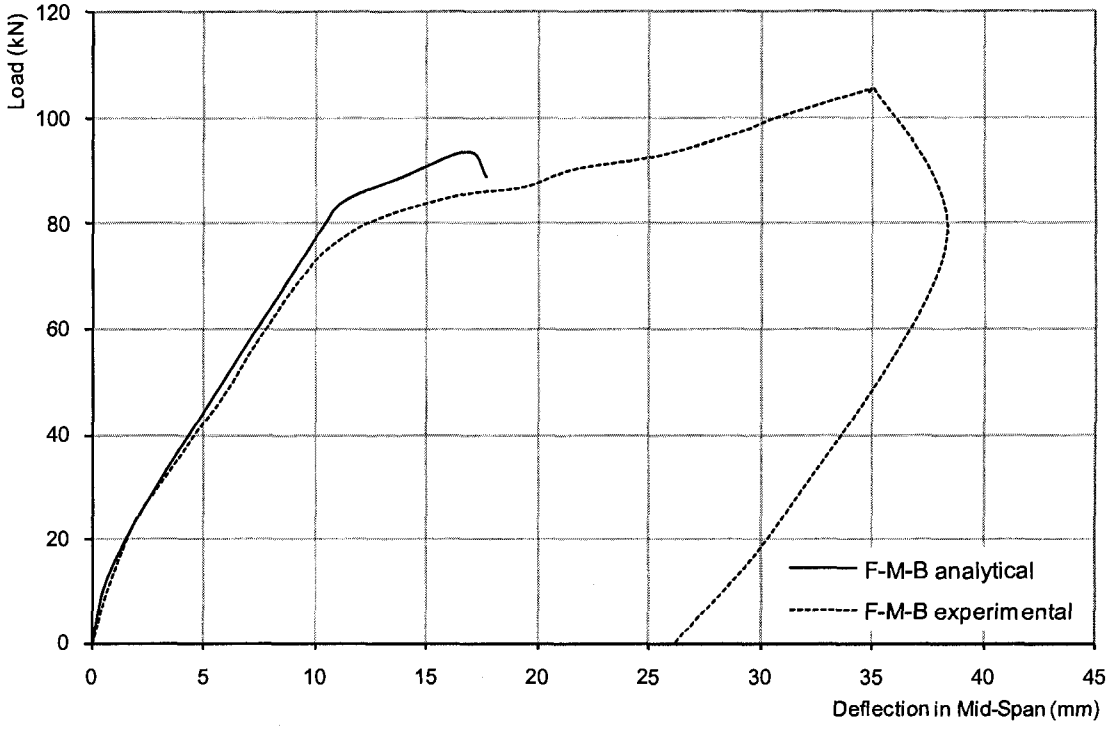

Figure 6.12. Analytical vs. experimental load-deflection in mid-span of beam F-M-B

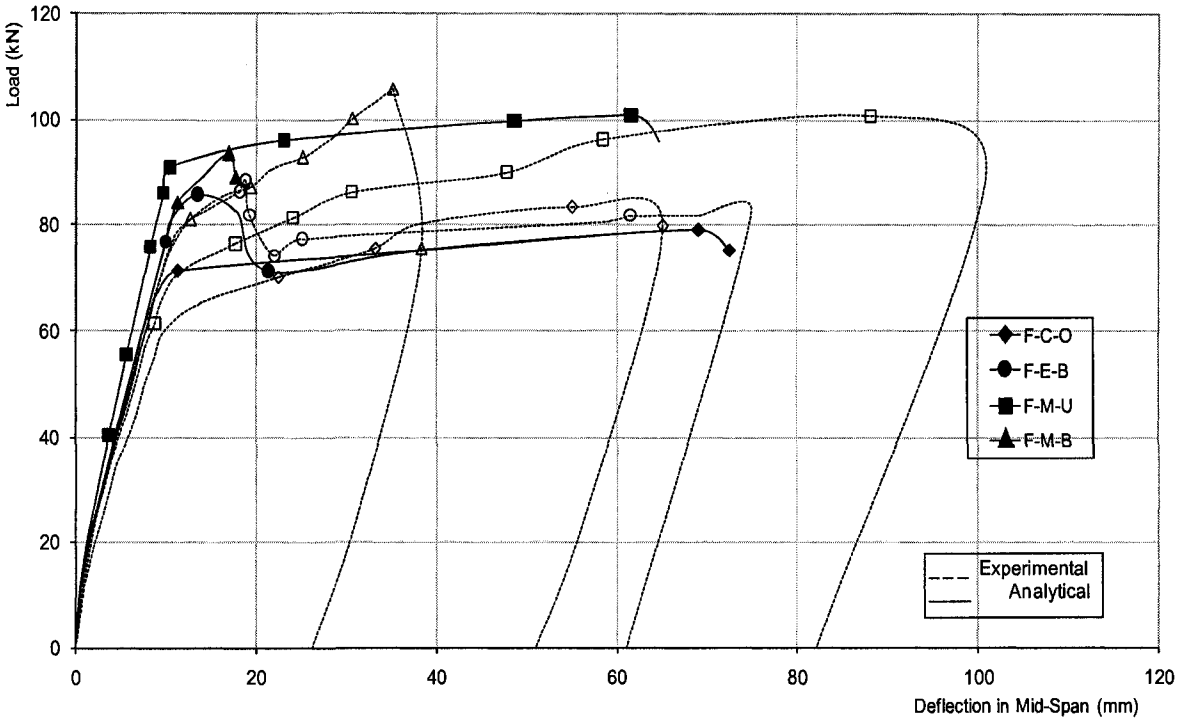

Figure 6.13. Experimental and analytical load-deflection at mid-span of the four beams strengthened in flexure

CHAPTER 7

CONCLUSIONS AND RECOMMENDATIONS

7.1 Summary

As an improvement to the current externally bonding method and mechanically-anchored unbonded method of strengthening reinforced concrete (RC) beams, new mechanically-anchored methods are developed to strengthen concrete beams in shear and flexure using dry carbon fibre (CF) and carbon fibre-reinforced polymer (CFRP) sheets, respectively. Two methods of strengthening T-section RC beams in shear and flexure are represented in this research. A total of seven RC T-beams were tested in order to evaluate the developed strengthening systems.

The first part of this research studies the feasibility and effectiveness of a new method of strengthening existing RC T-beams in shear by using mechanically-anchored unbonded carbon fibre sheets. Unlike conventional epoxy-bonding process for CFRP sheets, the studied CF anchorage system is not time consuming and does not need difficult surface preparation, high amount of adhesive application, or skilled workers, and on top of that eliminates the debonding of the CFRP sheets, which in turn, results in utilizing the full strength capacity of CF material.

Three RC T-beams with shear-span-to-depth ratio of 2.0 were tested under increasing monotonic load till failure. The pilot tests were done as a proof-of-concept of the effectiveness of the proposed method in increasing the shear capacity of the RC T-beams. The first T-beam which was tested as the control beam, failed in shear. The

second beam was strengthened by using a U-shaped CFRP sheet that was externally bonded to the web of the beam in the shear zones. The third beam was strengthened by using anchored U-shaped dry CF sheet. In this new strengthening method, dry CF sheets are wrapped around and bonded to two steel rods. Then the rods are anchored to the corners of the web-flange intersection of the T-beam with mechanical bolts. This makes a U-shaped dry CF jacket around the web which increases the shear strength of the T-beam using the privilege of higher tensile strength and module of elasticity of dry CF in comparison with wet (bonded) CFRP. It should be noted that, since dry CF sheet is exposed, similar to an epoxy-bonded FRP sheet, a protective cover could be utilized. Also, the anchors and anchor rod should be made of corrosion-resisting steel. The test results showed that the beam strengthened by the new mechanically anchored dry CF had about 48% increase in shear capacity as compared to the control beam and 16% increase in shear capacity as compared to the beam strengthened by CFRP epoxy-bonding method. Also, the beam strengthened by the new mechanically anchored dry CF sheet showed a potential increase in the displacement ductility of the beam through reaching its flexural yielding strength.

The second part of this research examines the effectiveness of a new hybrid fibre-reinforced polymer (FRP) sheet / ductile anchor system for increasing the flexural capacity and ductility of reinforced concrete (RC) beams. The privileges of this method on conventional FRP epoxy-bonding method for RC beams is that the studied hybrid FRP / ductile anchorage system is not time consuming and does not need difficult surface preparation, high amount of adhesive application, or skilled workers. It is also a solution for the problem of low ductility which results in brittle failure mode in conventional

methods of strengthening beams using epoxy-bonded FRP sheets. The proposed system leads to a ductile failure mode by triggering yielding to occur in the steel anchor system (steel links) rather than by rupture or debonding of FRP sheets, which is sudden in nature.

Four half-scale RC T-beams each connected to two column stubs were tested under four-point bending. One beam was used as the control beam (F-C-O). One beam was strengthened with conventional epoxy-bonding method (F-E-B). Two beams were strengthened with the new hybrid FRP sheet / ductile anchor system (unbonded, F-M-U, and bonded, F-M-B). The three retrofitted beams were strengthened using one layer of carbon FRP (CFRP) sheet. The results of the two beams that were strengthened with the new hybrid FRP sheet / ductile anchor system were compared with the results from the beam strengthened with conventional FRP bonding method and the control beam.

Beam F-E-B strengthened with conventional epoxy-bonding method had only 7% higher load capacity compared to the control beam F-C-O. The CFRP sheet debonded at a displacement ductility of 1.91, after which, the response of the beam was governed by the original RC section. On the other hand, beam F-M-U strengthened using the unbonded hybrid FRP / ductile anchorage strengthening system resulted in about 21% increase in the load carrying capacity compared to that of the control beam. The beam showed a high displacement ductility level that reached 9.09. The increase in strength and ductility were achieved by fully utilizing the capacity of the CFRP sheet through triggering yielding in the anchors' steel links and allowing the beam to crack and deflect without being restrained by bond with the CFRP sheet. Using the same ductile anchorage system of F-M-U, yet bonding the CFRP with epoxy to the beam soffit, beam F-M-B showed an increase in the strength capacity of 27% compared to the control beam, but

failed due to the rupture of CFRP at a low displacement ductility of 3.37 mainly due to the high strains arising from being bonded at the locations of crack growths in the flexure zone. Thus, the premature debonding and limited load capacity of F-E-B beam, and the FRP rupture with limited displacement ductility of beam F-M-B were successfully avoided in beam F-M-U that showed high load capacity and ductility.

7.2 Conclusions

From the outcomes of the experimental program on increasing the shear capacity of RC T-beams using new mechanically-anchored unbonded CF sheets, the following can be deducted:

1. The mechanically anchored dry CF jackets can increase the ultimate shear strength of RC T-beams and slightly improve the flexural stiffness.
2. The use of the mechanically anchored dry CF jacket eliminates the debonding of the CF jacket, and consequently results in a better utilization of the full capacity of the CF sheet.
3. The proposed strengthening method using mechanically anchored U-shaped dry CF sheets needs relatively less hard work and time consuming concrete surface preparation compared to conventional externally bonding methods.

From the outcomes of the experimental program on increasing the flexural capacity and ductility of RC beams using new hybrid FRP / ductile anchorage system, the following conclusions were drawn:

1. Externally-bonded CFRP strengthening system without end-anchorage increased the yield and the ultimate loads by about 16% and 5%, respectively relative to those of the control beam. The T-beam failed prematurely due to peeling off of the CFRP sheet. The T-beam mid-span deflection at ultimate load was 54% less than that of the control beam.
2. The presence of hybrid FRP / ductile anchorage in the externally-bonded CFRP system prevented early peel off of the CFRP sheet which enhanced the T-beam strength and ductility. The ultimate load of the T-beam strengthened with externally-bonded CFRP along with hybrid FRP / ductile anchorage was about 27% higher than that of the control T-beam whereas the mid-span deflection at ultimate load was 19% lower than that of the control.
3. Unbonded hybrid FRP / ductile anchorage strengthening system was effective in increasing the T-beam strength and the strength gain was 21% higher than that of the control beam and 13% higher than the strength of the beam rehabilitated using conventional externally-bonded CFRP.
4. The mid-span deflection at ultimate load of the T-beams strengthened with unbonded hybrid FRP / ductile anchorage system was 366% higher than that of the T-beam strengthened with externally-bonded CFRP without end-anchorage, 151% higher than that of the T-beam strengthened with externally-bonded along with hybrid FRP / ductile anchorage, and even 96% higher than that of the control.
5. Unbonded hybrid FRP / ductile anchorage system guarantees ductile failure in the strengthened concrete beams using hybrid CFRP sheet / steel anchor. The

specimen F-M-U, which was strengthened with unbonded hybrid FRP / ductile anchorage method, exhibited the most ductile behavior, with a displacement ductility of 9.09.

Comparisons of the analytical predictions using code formulas and available non-linear modeling software with the experimental results showed that the analytical models used were able to represent the behaviour of the tested beams with good accuracy.

7.3 Recommendations for Future Work

It should be mentioned that, although the results and performance of the RC beams strengthened with the proposed strengthening systems are promising, more tests has to be conducted in order to understand the system's behaviour for wide range of parameters and to develop design guidelines. In addition to the enhancement to the strength and ductility capacities of RC beams, the proposed rehabilitation system is expected to be more economic, faster in applying, and have reliable performance with less variability, yet in order to prove that, detailed assessment should be conducted.

Furthermore, to keep the attractive feature of corrosion-resistance of FRP, it is recommended that the steel rod and anchors are made of a non-corrosive alloy. Therefore it should be mentioned that more experimental studies should be done using the steel mechanism and anchors made of non-corrosive alloy.

The performance of FRP-rehabilitated RC T-beams under fatigue and torsional loading should be studied. Finally, the long-term performance and the durability performance of dry and wet CFRP composite materials exposed to environmental effects should be studied.

APPENDIX A

CALCULATIONS OF ANALYTICAL MODELS

In this appendix, analytical results for the four beam strengthened in flexure was done using latest version of CSA A23.3-04 (2004), ISIS Module 4 (2006) and ACI 440.2R-02 (2002) to verify the outputs of Response-2000 program for the beams strengthen in flexure.

A.1 Beam F-C-O

The beam F-C-O was the control T-beam in the group of the beams that were strengthened in flexure. The maximum moment resisting force of the beam F-C-O was predicted using CSA A23.3-04 code. According to CSA A23.3-04 code, maximum nominal moment (M_n) of the beam F-C-O is calculated as shown below:

From equilibrium (Figure A.1),

$T_s + T_s' = C$ (Assuming top steel is in tension) (A. 1)

$A_s f_s + A_s' f_s' = \alpha_1 . f_c' . b . \beta_1 . c$ (A. 2)

Assume $\varepsilon_s \geq \varepsilon_y$ and $\varepsilon_s' \geq \varepsilon_y$

ie $f_s = f_y$ and $f_s' = f_y$;

$\therefore \quad A_s f_y + A_s' f_y' = \alpha_1 . f_c' . b . \beta_1 . c$

$(400+107) \times 462 = 0.8 \times 34 \times 420 \times 0.885 \times c$

$c = \frac{234234}{10110} = 23.2mm$

Check $\varepsilon_s \geq \varepsilon_y$ where $\varepsilon_s = \frac{\varepsilon_c(d-c)}{c} = \frac{0.0035(260-23.2)}{23.2} = 0.0357 \geq 0.0024 ok$ (A. 3)

Check $\varepsilon_s' \geq \varepsilon_y$ where $\varepsilon_s' = \frac{\varepsilon_c(d'-c)}{c} = \frac{0.0035(35-23.2)}{23.2} = 0.0017 < 0.0024 \times$ (A. 4)

$$\varepsilon_s' < \varepsilon_y \Rightarrow f_s' = E_s\varepsilon_s' = E_s\frac{\varepsilon_c(d'-c)}{c} = 200000 \times \frac{0.0035(35-23.2)}{23.2} = 356MPa$$

$$A_s f_y + A_s' f_s' = \alpha_1 . f_c' . b . \beta_1 . c$$

$$c = \frac{A_s f_y + A_s' f_s'}{\alpha_1 . f_c' . b . \beta_1} = \frac{400 \times 462 + 107 \times 356}{0.8 \times 34 \times 420 \times 0.885} = 22.04mm \quad \text{(A. 5)}$$

$$M_n = T_s(d - \frac{\beta_1 c}{2}) + T_s'(d' - \frac{\beta_1 c}{2})$$

$$M_n = 184800 \times (260 - \frac{0.885 \times 22.04}{2}) + 38092 \times (35 - \frac{0.885 \times 22.04}{2}) \quad \text{(A. 6)}$$

$$M_n = (46.24 + 0.96) \times 10^6 N.mm = 47.2kN.m$$

Maximum applied load (P_{max}) $= \frac{M_n}{l_s} \times 2 = \frac{47.2}{1.1} \times 2 = 85.8kN$ (A. 7)

Where l_s, is the length of the shear span which is equal to 1.1 m.

A.2 Beam F-E-B

This specimen is strengthened in flexure using FRP external epoxy-bonding method. Specimen F-E-B failed prematurely without warning by debonding of the CFRP sheet after yielding of the steel reinforcement. The maximum moment resisting force of the beam F-E-B was predicted using ACI 440.2R-02 code. According to ACI 440.2R-02 code, a limitation should be placed on the strain level developed in the laminate, in order to prevent debonding of the FRP laminate. Cover delamination or FRP debonding can

occur if the force in the FRP cannot be sustained by the substrate. Equation (A. 8) gives an expression for a bond-dependent coefficient K_m.

$$K_m = \left\{ \begin{array}{l} \frac{1}{60\varepsilon_{fu}}(1-\frac{nE_f t_f}{360000}) \le 0.9 \, for: nE_f t_f \le 180000 \\ \frac{1}{60\varepsilon_{fu}}(\frac{90000}{nE_f t_f}) \le 0.9 \, for: nE_f t_f > 180000 \end{array} \right\} \quad \text{(A. 8)}$$

The term K_m, expressed in Equation (A. 8), is a factor no greater than 0.90 that may be multiplied by the rupture strain of the FRP laminate to arrive at a strain limitation to prevent debonding. The number of plies n used in this equation is the number of plies of FRP flexural reinforcement at the location along the length of the member where the moment strength is being computed.

$$nE_f t_f = 1 \times 86900 \times 0.25 = 21725 \le 180000$$

$$K_m = \frac{1}{60 \times 0.0105}(1-\frac{21725}{360000}) = 1.49 \le 0.9 \Rightarrow K_m = 0.9$$

$$\varepsilon_{frp_e} = K_m . \varepsilon_{frp_u} = 0.9 \times 0.0105 = 0.00945$$

Since the concrete stress has not reached its maximum strength, the rectangular stress block needs to be modified according to the stress level. Following formula are used as recommended by fib bulletin 14 (2001).

$$\alpha_1 = \left\{ \begin{array}{l} \frac{4-500\varepsilon_c}{6-1000\varepsilon_c} \, for: \varepsilon_c \le 0.002 \\ \frac{1000\varepsilon_c(3000\varepsilon_c - 4)+2}{1000\varepsilon_c(3000\varepsilon_c - 2)} \, for: 0.002 < \varepsilon_c \le 0.003 \end{array} \right\} \quad \text{(A. 9)}$$

$$\beta_1 = \left\{ \begin{array}{l} \varepsilon_c(425 - 70833\varepsilon_c) \, for: \varepsilon_c \le 0.002 \\ (1-\frac{1}{1765\varepsilon_c}) \, for: 0.002 < \varepsilon_c \le 0.003 \end{array} \right\} \quad \text{(A. 10)}$$

To solve for c, a loop is set up. The iterative loop exits when the equilibrium condition is satisfied.

For beam F-E-B, assuming c=60 mm will give α_1=0.786 and β_1=0.78 which satisfies the equilibrium condition.

$C_c + C_s = T_s + T_{frp}$ (top steel is in the compression zone) (A. 11)

Since debonding is the failure mode in specimen S-E-B, strain in the FRP is limited to $0.9f_{frp\,u}$ which is equal to 0.00945. Using the compatibility condition the strain in the steel and concrete can be calculated as below (Figure A.2):

$$\frac{\varepsilon_{frp_e}}{h-c} = \frac{\varepsilon_c}{c} \Rightarrow \frac{0.00945}{280-60} = \frac{\varepsilon_c}{60} \Rightarrow \varepsilon_c = 0.0025 < 0.0035$$ Concrete is not crushed

$$\frac{\varepsilon_{frp_e}}{h-c} = \frac{\varepsilon_s'}{c-d'} \Rightarrow \frac{0.00945}{280-60} = \frac{\varepsilon_s'}{60-35} \Rightarrow \varepsilon_s' = 0.001$$ Compression steel is not yielded

$$f_s' = E_s.\varepsilon_s' = 200000 \times 0.001 = 200MPa$$

Therefore, maximum nominal moment (M_n) of the beam F-E-B is calculated as below:

Assuming $\varepsilon_s \geq \varepsilon_y$

Check $\varepsilon_s \geq \varepsilon_y$ where $\varepsilon_s = \frac{\varepsilon_{frp_e}(d-c)}{h-c} = \frac{0.00945 \times (260-60)}{280-60} = 0.0085 \geq 0.0024$

Therefore maximum nominal moment (M_n) of the beam F-E-B is calculated as below:

$$M_n = A_s f_y (d - \frac{\beta_1 c}{2}) + A_{frp} f_{frp} (d_{frp} - \frac{\beta_1 c}{2}) + A_s' f_s' (d' - \frac{\beta_1 c}{2})$$ (A. 12)

$$M_n = 400 \times 462 \times (260 - \frac{0.78 \times 60}{2}) + 0.25 \times 155 \times 0.00945 \times 86900 \times (280 - \frac{0.78 \times 60}{2}) +$$

$$+107 \times 58 \times (35 - \frac{0.78 \times 60}{2}) = 51.9 \times 10^6 N.mm = 51.9kN.m$$

Maximum applied load (P_{max}) = $\frac{M_n}{l_s} \times 2 = \frac{51.9}{1.1} \times 2 = 94.3kN$

A.3 Beam F-M-U

The beam F-M-U which was strengthened with hybrid FRP / ductile anchor failed in a ductile manner by crushing the concrete in compression zone which was accompanied by excessive slip of the hybrid FRP / ductile anchor after yielding of the internal steel reinforcement and hybrid FRP / ductile anchor's steel link members.

In beam F-M-U, the total nominal resisting moment, $M_{n,\,total}$, of the strengthened beam is equal to the summation of the nominal resisting moment, $M_{n,\,orig.}$, of the control beam (F-C-O) and added moment, ΔM, to the concrete beam due to the application of the hybrid FRP / ductile anchorage system.

$$M_{n,\,total} = M_{n,\,orig.} + \Delta M \qquad \text{(A. 13)}$$

$$\Delta M = A_{s\,links} \times jd \qquad \text{(A. 14)}$$

$$A_{s\,links} \cdot f_y = \tfrac{3}{4} \times A_{FRP} \times f_{FRP\,U} \qquad \text{(A. 15)}$$

In equation A.15, A_{links} were designed to ensure that failure would occur in steel link members and not in the FRP sheet. A factor of ¾ was arbitrarily chosen. It should be mentioned that due to the nature of the mechanism, there will be a small gap, δ, between the FRP sheet and the soffit of the beam, which is equal to half of the thickness of the plate that FRP sheets are wrapped around (Figure A.3a). This gap will be closed as the beam deflects, as shown in Figure A.3b. In this case, the FRP sheet will be experiencing tensile stresses that are transferred to the steel link members, which in turn transfer the stresses to the column stubs through the Hilti anchors.

The maximum moment resisting force of the beam F-C-O was predicted using CSA A23.3-04 code. According to CSA A23.3-04 code, maximum nominal moment (M_n) of the beam F-M-U is calculated as below:

From equilibrium (Figure A.4),

$T_s + T_s' + T_{link} = C$ (Assuming top steel is in tension) (A. 16)

$A_s f_s + A_s' f_s' + A_{link} f_{link} = \alpha_1 . f_c' . b . \beta_1 . c$

Assume $\varepsilon_s \geq \varepsilon_y$, $\varepsilon_s' \geq \varepsilon_y$ and $\varepsilon_{link} \geq \varepsilon_y$

ie $f_s = f_y$, $f_s' = f_y$ and $f_{link} = f_y$

$\therefore \quad A_s f_y + A_s' f_y + A_{link} f_y = \alpha_1 . f_c' . b . \beta_1 . c$

$$c = \frac{A_s f_y + A_s' f_y + A_{link} f_y}{\alpha_1 . f_c' . b . \beta_1} = \frac{400 \times 462 + 107 \times 400 + 80.6 \times 462}{0.8 \times 34 \times 420 \times 0.885} = 26.85mm$$

Check $\varepsilon_s \geq \varepsilon_y$ where $\varepsilon_s = \frac{\varepsilon_c (d - c)}{c} = \frac{0.0035 \times (260 - 26.85)}{26.85} = 0.03 > 0.0024$

Check $\varepsilon_{s_{link}} \geq \varepsilon_y$ where $\varepsilon_{s_{link}} = \frac{\varepsilon_c (h - c)}{c} = \frac{0.0035 \times (280 - 26.85)}{26.85} = 0.033 > 0.0024$

Check $\varepsilon_s' \geq \varepsilon_y$ where $\varepsilon_s' = \frac{\varepsilon_c (d' - c)}{c} = \frac{0.0035 \times (35 - 26.85)}{26.85} = 0.001 < 0.0024$

$f_s' = E_s . \varepsilon_s' = 200000 \times 0.001 = 200MPa$

$$M_n = A_s f_y (d - \frac{\beta_1 c}{2}) + A_{link} f_y (h - \frac{\beta_1 c}{2}) + A_s' f_s' (d' - \frac{\beta_1 c}{2}) \quad \text{(A. 17)}$$

$$M_n = 400 \times 462 \times (260 - \frac{0.885 \times 26.85}{2}) + 80.6 \times 400 \times (280 - \frac{0.885 \times 26.85}{2}) +$$

$$+ 80.6 \times 200 \times (35 - \frac{0.885 \times 26.85}{2}) = 56.2 \times 10^6 N.mm = 56.2kN.m$$

Maximum applied load (P_{max}) $= \frac{M_n}{l_s} \times 2 = \frac{56.2}{1.1} \times 2 = 102.2kN$

A.4 Beam F-M-B

Specimen F-M-B was strengthened with the externally bonded FRP method using hybrid FRP / ductile anchorage system. Specimen F-M-B failed through the CFRP

rupture because the tensile capacity of the CFRP sheet was attained. By assuming full composite action between internal steel and external FRP reinforcement, a reinforced concrete section can fail by two main modes: concrete crushing or FRP rupture. Those failure modes can be predicted using the classic beam theory using following conditions:

- Compatibility condition: This condition states that the strain varies linearly along the section from the top fibre to the bottom fibre (Figure A.5).
- Equilibrium condition:

$C_c = T_s + T_s' + T_{frp}$ (Assuming top steel is in the tension zone) (A. 18)

Where $C_c = \alpha_1.f_c'.\beta_1.c.b$, $T_s = A_s f_s$, $T_s' = A_s' f_s'$ and $T_{frp} = A_{frp}.f_{frp}$.

The nominal moment capacity is:

$$M_n = A_s f_s (d - \frac{\beta_1 c}{2}) + A_{frp} f_{frp} (d_{frp} - \frac{\beta_1 c}{2}) + A_s' f_s' (d' - \frac{\beta_1 c}{2}) \quad \text{(A. 19)}$$

Due FRP rupture failure mode in the specimen F-M-B, stress in the FRP sheet is taken equal to FRP ultimate strain ($f_{frp_u} = 0.0105$).

$C_c = T_s + T_s' + T_{frp}$

$\alpha_1.f_c'.\beta_1.c.b = A_s.f_y + A_s'.f_y + A_{frp}.f_{frp_u}$ (Assuming $f_s = f_y$ & $f_s' = f_y$)

$0.8 \times 34 \times 0.885 \times c \times 420 = 400 \times 462 + 107 \times 462 + 155 \times 0.25 \times 1062$

$$c = \frac{400 \times 462 + 107 \times 462 + 155 \times 0.25 \times 1062}{0.8 \times 34 \times 0.885 \times 420} = 27.23mm$$

Check $\varepsilon_s \geq \varepsilon_y$ where $\varepsilon_s = \frac{\varepsilon_{frp}(d-c)}{h-c} = \frac{0.0105 \times (260 - 27.23)}{280 - 27.23} = 0.0096 \geq 0.0024$

Check $\varepsilon_s' \geq \varepsilon_y$ where $\varepsilon_s' = \frac{\varepsilon_{frp}(d'-c)}{h-c} = \frac{0.0105 \times (35 - 27.23)}{280 - 27.23} = 0.00032 < 0.0024$

$$f_s' = E_s.\varepsilon_s' = 200000 \times 0.00032 = 64MPa$$

$$M_n = 400 \times 462 \times (260 - \frac{0.885 \times 27.23}{2}) + 155 \times 0.25 \times 1062 \times (280 - \frac{0.885 \times 27.23}{2}) +$$

$$+107 \times 56 \times (35 - \frac{0.885 \times 27.23}{2}) = 57.47 \times 10^6 N.mm = 57.47kN.m$$

Maximum applied load (P_{max}) = $\frac{M_n}{l_s} \times 2 = \frac{57.47}{1.1} \times 2 = 104.49kN$

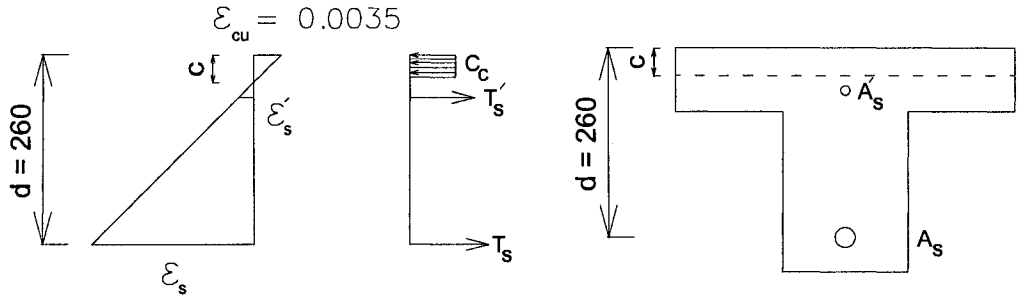

Figure A.1 Equilibrium and compatibility condition in the beam F-C-O

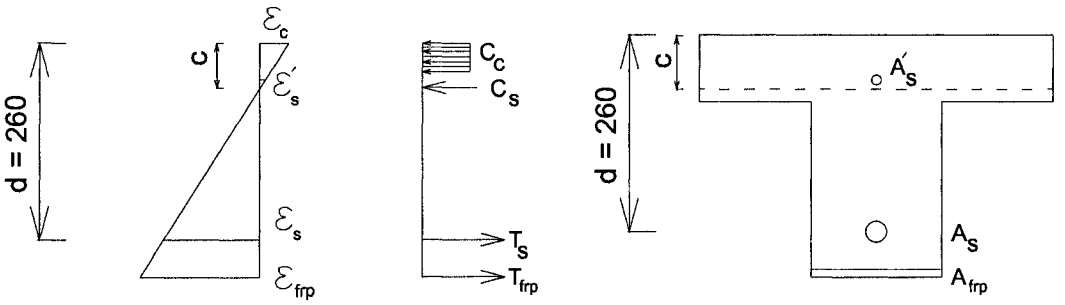

Figure A.2 Equilibrium and compatibility condition in the beam F-E-B

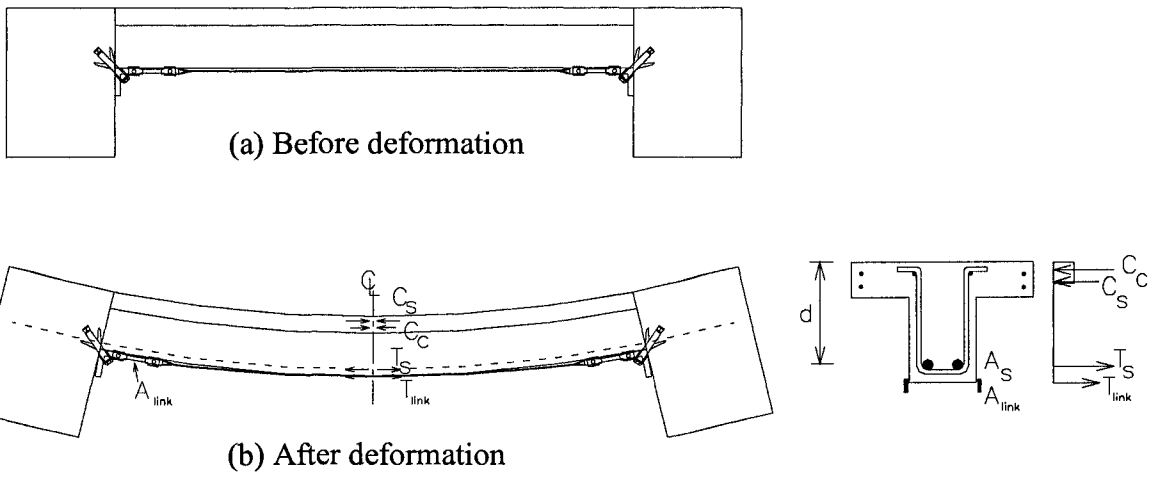

Figure A.3 Simplified analysis of the proposed mechanism in the beam F-M-U

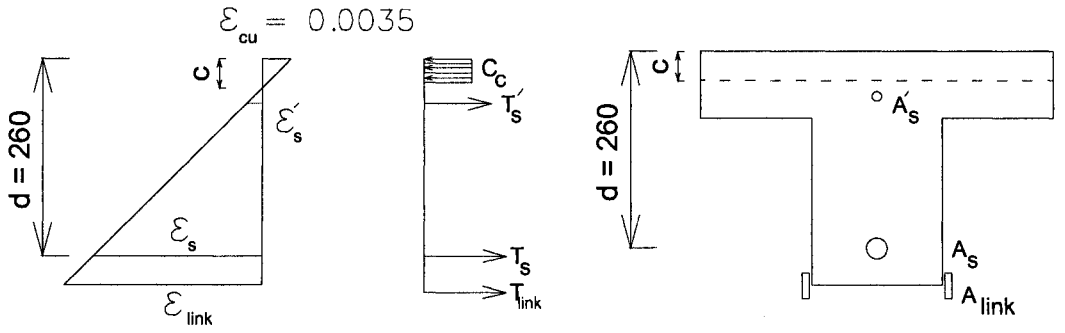

Figure A.4 Equilibrium and compatibility condition in the beam F-M-U

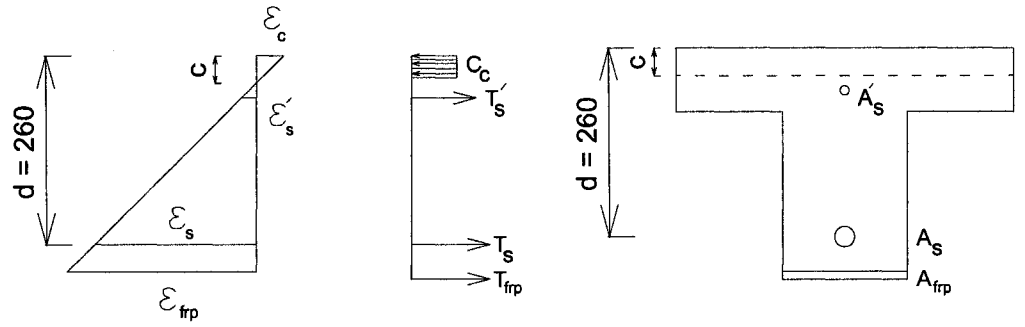

Figure A.5 Equilibrium and compatibility condition in the beam F-M-B

REFERENCES

AASHO. 1965. *Standard Specifications for Highway Bridges.* 9th ed. American Association of State Highway Officials. Washington, D.C., USA.

AASHTO. 2002. *Standard Specifications for Highway Bridges*, 17th ed. American Association of State Highway and Transportation Officials. Washington, D.C., USA.

ACI. 1968. *Manual of concrete practice.* Part 2, Committee 318-1R-68, American Concrete Institute, Detroit, USA.

ACI 440.2R-04. 2002. Guide for the design and construction of externally bonded FRP systems for strengthening concrete structures. ACI Committee 440, American Concrete Institute, Farmington Hills, Mich. , USA.

ACI 440.3R-04. 2004. *Guide for Test Methods for Fiber Reinforced Polymers (FRP) for Reinforcing and Strengthening Concrete Structures.* ACI Committee 440, American Concrete Institute, Farmington Hills, Mich. , USA.

Adhikary, B.B. and Mutsuyoshi, H. 2001. Behavior of concrete beams strengthened in shear with carbon-fiber sheets. *ACI Struct. J.* 8(3): 258–264.

Aidoo, J., Harries, K. A., and Petrou, M. F. 2004. Fatigue behavior of CFRP strengthened reinforced concrete bridge girders. *J. Compos. Constr.*, 8(6): 501–509.

Al-Sulaimani, G. J., Istem, A., Basunbul, A. S., Baluch, M. H., and Ghaleb, B. N. 1994. Shear repair for reinforced concrete by fiberglass plate bonding. *Am. Concr. Inst. Struct. J.* 91(3): 458–464.

Angelakos, D., Bentz, E. C. Khuntia, M. and Collins, M. P. 2002. Effect of concrete strength and minimum stirrups on shear strength of large members. *ACI Structural Journal* 99(2): 224-226

Arduini, M., and Nanni, A. 1997. Behavior of Pre-Cracked RC Beams Strengthened with Carbon FRP Sheets. *J. Compos. Constr.* 1(2): 63-70.

Bencardino, F., Spadea, G., and Swamy, R. 2002. Strength and ductility of reinforced concrete beams externally reinforced with carbon fibre fabric. *ACI Structural Journal*, 99(3): 163-171.

Bentz. 2007. www.ecf.utoronto.ca/~bentz/home.shtml. *Response-2000.* retreived September 2007.

Blaschko, M., and Zilch, K. 1999. Rehabilitation of concrete structures with strips glued into slits. *Proc., 12th Int. Conf. on Composite Materials*, Organization of the Int. Conf. on Composite Materials, Paris, CD-ROM.

Borowicz, D. T. 2002. *Rapid strengthening of concrete beams with powder-actuated fastening systems and fiber reinforced polymer (FRP) composite materials.* MS thesis, Dept. of Civil Engineering, Univ. of Wisconsin-Madison, Madison, Wisc. USA.

Brosens, K. and Van Gemert, D. 1997. Anchoring stresses between concrete and carbon fibre reinforced laminates. *Proc., 3rd Int. Symp. on Non-Metallic (FRP) Reinforcement for Concrete Struct.*, Japan Concrete Institute, Sapporo, Japan, 271–278.

Cao, S. Y. and Teng, J. G. 2005. Debonding in RC Beams Shear Strengthened with Complete FRP Wraps. *J. Compos. Constr.* 9(5): 417–428.

Chaallal, O. and Bousselham, A. 2004. Shear Strengthening Reinforced Concrete Beams with Fiber-Reinforced Polymer: Assessment of Influencing Parameters and Required Research. *ACI Struct. J.,*101(2): 219-227.

Chajes, M. J., Januszka, T. F., Mertz, D. R., Thomson, T. A., and Finch, W. W. 1995. Shear strength of RC beams using external applied composite fabrics. *ACI Struct. J.*, 92(3): 295–303.

CSA, *Canadian Highway Bridge Design Code* S6-06. 2006. Canadian Standards Association, Ontario, Canada.

CSA, *Design of concrete structures* A23.3-04. 2004. Canadian Standards Association, Ontario, Canada.

De Lorenzis, L., and Nanni, A. 2001. Shear strengthening of reinforced concrete beams with near-surface mounted fibre reinforced polymer rods. *ACI Struct. J.* 98(1): 60–68.

De Lorenzis, L., Rizzo, A. and La Tegola, A. 2002. A modified pull-out test for bond of near-surface mounted FRP rods in concrete. *Composites Part B: Engineering.* 33(8): 589-603.

Deniaud, C. and Cheng, J. J. R. 2003. Reinforced concrete T-beams, strengthened in shear with fiber reinforced polymer sheets. *J. Compos. Constr.*, 7(4): 302–310.

Dussek, I. J. 1980. Strengthening of Bridge Beams and Similar Structures by Means of Epoxy-Resin-Bonded External Reinforcement, *Transportation Research Record* 785, *Transportation Research Board,* 21-24.

Fanning, P. J., and Kelly, O. 2001. Ultimate response of RC beams strengthened with CFRP plates. *J. Compos. Constr.* 5(2): 122–127.

Fédération Internationale du Béton 2001. *Design and Use of Externally Bonded FRP Reinforcement (FRP EBR) for Reinforced Concrete Structures.* Progress Report of *fib* EBR Group, International Concrete Federation. (final draft).

Fyfe Company LLC. 2006. http://www.fyfeco.com. *Tyfo® SCH-11UP Composite using Tyfo® S Epoxy User's Guide.* retrieved Jan. 2006.

Hassan, T., and Rizkalla, S. 2003. Investigation of bond in concrete structures strengthened with near surface mounted carbon fiber reinforced polymer strips. *J. Compos. Constr.* 7(3): 248–257.

Higgins, C., Potisuk, T., Robelo, M. J.,Farrow W. C., McAuliffe T. K. and Nicholas B. S. 2007. Tests of RC Deck Girders with 1950s Vintage Details. *J. Brid. Eng.* 12(5): 621-631

Hilti (Canada) Corporation 2007. http://www.ca.hilti.com. *HSL heavy duty sleeve anchor.* retrieved Sep. 2007.

ISIS Canada. 2001a. *Reinforcing Concrete Structures with Fiber Reinforced Polymers.* Design Manual No. 3. The Canadian Network of Centers of Excellence on Intelligent Sensing for Innovative Structures. ISIS Canada Corporation, Winnipeg, Manitoba, Canada, 158.

ISIS Canada. 2006. *An Introduction to FRP Strengthening of Concrete Structures.* Design Manual No. 4. The Canadian Network of Centers of Excellence on Intelligent Sensing for Innovative Structures. ISIS Canada Corporation, Winnipeg, Manitoba, Canada.

Jones, R. et al. 1988. Plate separation and anchorage of reinforced concrete beams strengthened with epoxy-bonded steel plates. *The Struct. Engr.*, 66(5): 85–94.

Karbhari V. M. 2001. Material considerations in FRP rehabilitation of concrete structures *J. Materials Civ Eng.* 13: 2.

Khalifa, A., T. Alkhrdaji, A. Nanni, and S. Lansburg. 1999. Anchorage of Surface Mounted FRP Reinforcement. *Concrete International Design and Construction.* 21(10): 49-54.

Khalifa, A, and Nanni, A. 2000. Improving shear capacity of existing RC T-section beams using CFRP composites. *Cem. Concr. Compos.* 22(3): 165–174.

Klaiber, F. W. Dunker, K. F. Wipf, T. J. and Sanders, W. W. Jr., 1987. Methods of Strengthening Existing Highway Bridges, *NCHRP Research Report No. 293, Transportation Research Report Board.* 114.

Kotynia. 2005. *International Institute for FRP in Construction FRP Photo Competition* http://www.iifc-hq.org/photocompetition05/img/photos/PC05085.htm retrieved Jan. 2008.

Lamanna, A., Bank, L., and Scott, D. 2001. Flexural strengthening of reinforced concrete beams using fasteners and fiber-reinforced polymer strips. *ACI Structural Journal.* 98(3): 368-376.

Meier, U. 1992. Carbon fibre-reinforced polymers: Modern materials in bridge engineering. *Struct. Eng. Int. (IABSE, Zurich, Switzerland).*2: 7–12.

Mirza, S. M. and Haider, M. 2003. The State of Infrastructure in Canada: Implications for Infrastructure Planning and Policy. *A study prepared for Infrastructure Canada.*

Nanni, A. 1995. Concrete Repair with Externally Bonded FRP Reinforcement, *Concrete International*, 17(6). 22-26.

Oehlers, D. J., and Moran, J. P. 1990. Premature failure of externally plated reinforced concrete beams. *J. Struct. Engrg.* 116(4): 978–995.

Pham, H. and Al-Mahaidi, R. 2004. Assessment of available prediction models for the strength of FRP retrofitted RC beams. *J. Compos. Constr.* 66: 601-610.

Rabinovich, O. and Frostig, Y. 2000. Closed-form high-order analysis of RC beams strengthened with FRP strips. *J. Compos. for Constr.* 4(2): 65–74.

Ritchie, P. A., Thomas, D. A., Lu, L. W., and Connelly, G. M. 1991 External reinforcement of concrete beams using fiber reinforced plastics. *Am. Concr. Inst. Struct. J.* 88 (4): 490–500.

Roberts, T. M. 1989. Theoretical study of the behavior of RC beams strengthened by externally bonded steel plates. *Proc., Instn. Civ. Engrs.* (87): 39–55.

Saadatmanesh, H., and Ehsani, M. R. 1989. Application of fibrecomposites in civil engineering. *Proc., 7th ASCE Structures Congress*, ASCE, New York, 526–535.

Saadatmanesh, H. and Malek, A. M. 1997. Prediction of shear and peeling stresses at the ends of beams strengthened with FRP plates. *Proc., 3rd Int. Symp. on Non-Metallic (FRP) Reinforcement for Concrete Struct.*, Japan Concrete Institute, Sapporo, Japan, 311–318.

Schlaich, J. Schaefer, K. Jennewein, M. 1987. Toward a consistent design of structural concrete. *PCI Journal (Prestressed Concrete Institute).* 32(3): 74-150.

Sebastian, W. M. 2001. Significance of midspan debonding failure in FRP-plated concrete beams. *J. Struct. Eng.* 127(7): 792–798.

Sharif, A., Al-Sulimani, G. J., Basunbul, I. A., Baluch, M. H., and Ghaleb, B. N. 1994. Strengthening of initially loaded reinforced concrete beams using FRP plates. *ACI Struct. J.* 91(2): 160–168.

Soudki, K. El Maaddawy, T. Hamelin, J. Hrynyk and T. Schaus, L. 2005. Strengthening if one way reinforced concrete slabs with mechanically-anchored unbonded FRP strips. *33rd Annual General Conference of the Canadian Society for Civil Engineering.* CD - ROM.

Swamy, R. N., and Mukhopadhyaya, P. 1999. Debonding of carbon fibre reinforced polymer plate from concrete beams. *Eng. Structs and Bldgs.* 134(11): 301–317.

Täljsten, B. 2003. Concrete structures strengthened with near surface mounted reinforcement of CFRP. *Advances in Structural Engineering.* 6(3): 201-213.

Teng, J. G. De Lorenzis, L. Wang, B. Li, R. Wong, T. N. and Lam L. Debonding Failures of RC Beams Strengthened with Near Surface Mounted CFRP Strips. *J. Compos. for Constr.* 10(2): 92-105.

Triantafillou, T. C. 1998. Shear strengthening of reinforced concrete beams using epoxy-bonded FRP composites. *ACI Struct. J.* 95(2): 107–115.

Triantafillou, T. and Papanicolaou, C.G. 2002. Shear transfer capacity along pumice aggregate concrete and high-performance concrete interfaces. *Materials and Structures/Materiaux et Constructions.* 34(248): 237-245.

Vecchio, F. J. Collins, M. P. 1986. Modified Compression-field theory for reinforced concrete elements subjected to shear. *J. Am. Concr. Inst* 83(2): 219-231

Zhang, S. and Raoof, Z. 1995. Prediction of peeling failure of reinforced concrete beams with externally bonded steel plates. *Proc., Inst. of Civ. Engrs. Structs. and Build.* 110: 257–268.